



Republic of Iraq

Ministry of Higher Education & Scientific Research

University of Kerbala

College of Engineering

Mechanical Engineering Department

Solar Energy Harvesting Utilizing Photovoltaic–

Thermoelectric (PV-TEG) Integrated Hybrid System

A Thesis Submitted to the College of the Engineering/University of Kerbala
in Partial Fulfillment of the Requirements for the Master Degree in
Mechanical Engineering

Written By:

Walaa Nasser Abbas

Supervised By:

Asst. Prof. Dr. Mohammed Wahhab Aljibory

Asst. Prof. Dr. Hasan Talib Hashim

November 2022

Rabi' al-Thanii 1444

بِسْمِ اللَّهِ الرَّحْمَنِ الرَّحِيمِ

يَرْفَعِ اللَّهُ الَّذِينَ آمَنُوا مِنْكُمْ وَالَّذِينَ

أُوتُوا الْعِلْمَ دَرَجَاتٍ

صدق الله العلي العظيم

(المجادلة: من الآية 11)

EXAMINATION COMMITTEE CERTIFICATION

We certify that we have read the thesis entitled “ **Solar Energy Harvesting Utilizing Photovoltaic-Thermoelectric (PV-TEG) Integrated Hybrid System**” and as an examining committee, we examined the student “ **Walaa Nasser Abbas**” in its content and in what is connected with it, and that in our opinion it is adequate as a thesis for the degree of Master of Science in Mechanical Engineering.

(Supervisor)

Signature:

Name: Asst. Prof. Dr. Mohammed Wahhab
Aljibory

Date: / /2022

(Supervisor)

Signature:

Name: Asst. Prof. Dr. Hasan Talib
Hashim

Date: / /2022

(Member)

Signature:

Name: Asst. Prof. Dr. Mohammed Hassan
Abood

Date: / /2022

(Member)

Signature:

Name: Asst. Prof. Dr. Farhan Lafta
Rashid

Date: 30 / 11 /2022

(Chairman)

Signature:

Name: Prof. Dr. Haith Hasan Mohammed

Date: / /2022

Signature:

Name: Asst. Prof. Dr. Hayder Jabbar Kurji
Head of Department of Mechanical Engineering

Date: 5 / 12 /2022

Signature:

Name: Prof. Dr. Laith Shakir Rasheed
Dean of the Engineering College

Date: 5 / 12 /2022

Supervisor certificate

We certify that the thesis entitled “**Solar Energy Harvesting Utilizing Photovoltaic– Thermoelectric (PV-TEG) Integrated Hybrid System**” was prepared by **Walaa Nasser Abbas** under our supervision at the Department of Mechanical Engineering, College of Engineering, University of Kerbala as a partial of fulfilment of the requirements for the Degree of Master of Science in Mechanical Engineering.

Signature:



Asst. Prof. Dr. Mohammed Wahhab Aljibory

Date: / / 2022

Signature:



Asst. Prof. Dr. Hasan Talib Hashim

Date: / / 2022

Linguistic certificate

أقرار المقوم اللغوي

أشهد أنني قد اطلعت على رسالة طالبة الماجستير(ولاء ناصر عباس)
الموسومة بـ

**Solar Energy Harvesting Utilizing Photovoltaic–
Thermoelectric (PV-TEG) Integrated Hybrid System**

وقد قومتها من الناحية اللغوية والاسلوبية وبذلك تكون صالحة لأغراض
المناقشة مع توصيتنا بالأخذ بنظر الاعتبار تصحيح بعض الملاحظات اللغوية المؤشر
عليها

مع التقدير...

التوقيع:

أسم المقوم ولقبه العلمي: خبير عبد الامير جابر العواد-مدرس

التخصص العام: هندسة مدني

التخصص الدقيق: هندسة جيوتكنيكية

محل العمل: جامعه كربلاء

رقم الهاتف النقال: 07712375512

التاريخ : 2022/09/14

Abstract

Integrating photovoltaic and thermoelectric generators requires special attention, since both modules have a diametrically opposed relation with temperature. The TEG's conversion efficiency depends on attaining a high-temperature difference, whereas the PV needs a low temperature to produce high efficiency. So, correct and efficient integration of the photovoltaic cells with the thermoelectric modules is the main issue for enhancing the hybrid system's performance and increasing electrical power output. The methods to achieve this: include adopting an effective thermoelectric cooling system to ensure the maximum temperature is obtained and detecting the optimal number and appropriate distribution of the TEG modules that will cover the back surface of the PV model.

The present study included numerical simulation and experimental study to examine performance of (PV-TEG) a hybrid system. Firstly, a numerical and analytical study was conducted for the different hybrid system models with different numbers and distributions of the thermoelectric items at solar radiation of $1000 \text{ (W/m}^2\text{)}$, ambient temperature of 28°C , and wind speed of 0 (m/s) as a boundary conditions. All the hybrid system models were coupled by cold side of TEG modules, with heat exchanger (shell and tube) that water circulating through it. The main hybrid system models were four models: included S1 model (PV-204 items of TEG), S2 model (PV-94 items of TEG), S3 model (PV-85 items of TEG), and S4 model (PV-50 items of TEG) hybrid systems. The results showed that the (S4) model of a hybrid system was optimum model. To show the reliability degree of the software used in the current work and the accuracy of the numerical results of this thesis, the analytical results of PV/T system

performance were verified. By comparing these results with the results of previous studies in the same field and under almost the same conditions, the maximum difference that does not be more than 4 % and the smallest difference is 0.4 % between the results. So, it was concluded that the software was built correctly and gave acceptable results to a large degree.

Secondly, the optimum model (S4) hybrid system performance has been investigated in an indoor experimental study. The performance of the PV system and PV/T system were then experimentally and numerically put to comparison with that of the S4 model hybrid system. According to findings, showed that the PV-TEG (S4) model's output power was higher under identical operating conditions than that the photovoltaic panel and the PV/T system, respectively, by (36.94 %) and (16.8 %) numerically and 31.66 % and 16.5 % experimentally. Also, It can be seen that the average front surface of PV module in the PV-TEG (S4) hybrid system was higher by 4.5 % and 5.7 % than that PV/T system and lower by 29 % and 30 % than that the photovoltaic panel, numerically and experimentally, respectively. In addition to electrical efficiency (η_{el}) of the PV-TEG hybrid system were about (6.2 and 5.83) % in numerical and experimental tests, respectively and higher than that of the PV module and PV/T system.

The effect of the solar radiation on the hybrid system performance had studied at constant ambient temperature. The results showed an increasing hybrid system output power with increased solar radiation. The maximum obtained power regarding for the hybrid system was 39.4 W at solar radiation of 2000 (W/m^2).

Finally, a comparison has performed between the experimental and numerical outcomes of the current study, and a good agreement was noticed between them. The results showed that the difference percentage of the PV

module average front surface temperature (T_{sc}) in the PV panel, PV/T system, and PV -TEG hybrid system between numerical and experimental results were (2.9, 4.5, and 3.5) % respectively. At the same time, the difference percentage of the electrical output power (E_{el}) between numerical and experimental results in the PV panel, PV/T system, and PV -TEG hybrid system is (2.2, 6.3, and 6) %, respectively. This comparing result indicates that the current work was done according to what was planned and in a way that ensures that errors were avoided as much as possible. The results highlight that the integration of TEG modules with the PV panel as the S4 model hybrid system was the best solution for harvesting the solar radiation and converting the wasted heat in the PV into additional output power.

Undertaking

I certify that research work entitled “**Solar Energy Harvesting Utilizing Photovoltaic– Thermoelectric (PV-TEG) Integrated Hybrid System**” is my own work. The work has not been presented elsewhere for assessment. Where material has been used from other sources it has been properly acknowledged .

Signature:

Walaa Nasser Abbas

Date: / / 2022

Dedication

I Dedicate This Modest Effort

To my loyal teachers...

To my dear parents...

To my dear husband “Ali”...

To my children “ Jaafar, Farqed and Elias”

To my brothers and sisters...

To All Whom I Love...

Signature:

Walaa Nasser Abbas

Date: / / 2022

Acknowledgements

Praise and thank Allah who eased and quadrated us to accomplish this work. I would like to express my deepest thanks and sincere gratitude to my supervisors (Asst. Prof. Dr. Mohammed Wahhab Aljibory and Asst. Prof. Dr. Hasan Talib Hashim), guided me with all his expertise and science to accomplish this work correctly.

I submit my thanks and appreciation to my dear family for providing support while preparing this work.

I would also like to thank all who helped me accomplish this work.

Signature:

Walaa Nasser Abbas

Date: / / 2022

Table of Contents

Examination committee certification.....	iii
Supervisor certificate	iv
Linguistic certificate.....	v
Abstract.....	vi
Undertaking.....	viii
Dedication	x
Acknowledgements.....	xi
Table of Contents.....	xii
List of Tables	xvi
List of Figures	xvii
List of Abbreviations	xxi
List of Symbols.....	xxii
Chapter One: Introduction	1
1.1 Generally.....	2
1.2 Photovoltaic Cell	6
1.2.1 Photovoltaic cell technology types	6
1.2.2 Main parts of photovoltaic module.....	8
1.3 Thermoelectric (TE) device	9
1.3.1 Effectuated parameters on the thermoelectric generator performance.	10
1.3.2 Applications of thermoelectric generator	13
1.3.3 Advantages and disadvantages of thermoelectric generator.	13
1.3.4 The popular type of thermoelectric generator.	13
1.4 Photovoltaic- Thermoelectric Generator (PV-TEG) hybrid system.....	14
1.4.1 Hybrid system integration methods.....	15
1.5 Aim of the research	17

Chapter Two: Literature Review	18
2.1 Introduction.....	19
2.2 Experimental investigations.....	19
2.3 Theoretical/ Numerical investigations.....	25
2.4 Numerical simulation and experimental investigations	30
2.5 Summary	30
2.6 Scope of the present work.....	30
Chapter Three: Mathematical Model, Numerical Simulation, and Models	
Optimization.....	44
3.1 Introduction	45
3.2 Mathematical model.....	45
3.2.1 Physical model description and operation	45
3.2.2 Assumption	47
3.2.3 Governing equations	808
3.3 Numerical simulation.....	50
3.3.1 Geometric domain.....	80
3.3.2 Mesh generation.....	80
3.3.3 Setup and solution.....	80
3.3.3.1 Boundary conditions and operating parameters	60
3.3.3.2 Solution method and checking for convergence	61
3.3.4 Flow chart of computational model	80
3.4 Data reduction.....	64
3.5 Models optimization	68
3.6 Summary	66
Chapter Four: Experimental Work	67
4.1 Introduction	68
4.2 The experimental rig.....	68

4.2.1 The components of experimental rig.....	72
4.2.2 Measurement Instrumentations.....	80
4.3 Design Considerations.....	83
4.4 Test rig building.....	84
4.5 Tests procedures	86
4.6 Calibration.....	89
4.7 Repeatability	90
Chapter Five: Results and Discussion	92
5.1 Introduction	93
5.2 Numerical results.....	93
5.2.1 Temperature distribution contour	93
5.2.2 Electrical power and efficiency of tested systems.....	105
5.2.3 Validation of numerical results with previous work	107
5.3 Experimental results	108
5.3.1 Temperature measurements	108
5.3.2 Electrical measurements	109
5.3.2.1 Electrical power and efficiency calculation	112
5.4 Comparison of the results.....	114
5.4.1 The temperature of photovoltaic module.....	114
5.4.2 Electrical output power and efficiency	114
5.4.3 The influence of solar radiation (G)	116
Chapter Six: Conclusions and Recommendations.....	121
6.1 Conclusion.....	122
6.2 Recommendations for future research.....	124
References.....	125
Appendices.....	1
Appendix-A	2

Thermoelectric modules (TEG) Performance test results	2
Appendix-B	6
Calibration of Instruments	6
Data Logger and Thermocouples Calibration	6
TES 132 Data Logger and Solar meter Calibration	9
Appendix-C	11
Sample of Results	11
Different number of thermoelectric modules	11
Data reduction calculations	13
Appendix-D	14
Uncertainty Calculation	14
Flow meter	14
Output power	16
Appendix-E.....	17
Pupleshed Researches	17

List of Tables

Table 1-1: Datasheet of most using thermoelectric modules.....	14
Table 2-1: A gain power for each type of Hybrid System at 1000 (W/m ²) irradiation.....	31
Table 2-2: The parameters of the (m-Si)PV/TEG hybrid system components	31
Table 2-3: Side length and number of junctions of the thermoelectric generator (TEG) samples investigated.....	35
Table 2-4: Summary of Literatures Review.....	36
Table 3-1: Geometrical dimensions of the PV Panel, TEG module, and the heat exchanger smyste.....	52
Table 3-2: Mesh settings.....	57
Table 3-3: Thermo physical properties of the simulated PV-TEG system.....	60
Table 3-4: Boundary conditions in detail.....	61
Table 3-5: Specific parameter are used in the calculations.....	64
Table 4-1: Electrical and technical data of PV module at STC.....	79
Table 4-2: Electrical and technical data of TEG module.....	79
Table 4-3: Test Conditions.....	83
Table 5-1: The average temperature on the PV surface in each PV only, PV/T system and (S1, S2, S3, S4) hybrid systems.....	105
Table 5-2: The output power and the overall electrical efficiency in the PV, PV/T and (S1, S2,S3, S4) hybrid system models.....	106
Table 5-3: The Experimental results of temperatures for PV only, PV/T and PV-TEG systems.....	109
Table 5-4: The Experimental results of electrical characteristics for PV only, PV/T and PV-TEG systems.....	110

List of Figures

Figure 1-1: The annual average solar radiation on earth.....	3
Figure 1-2: Global cumulative PV installation until 2030.....	3
Figure 1-3: Basic structure of hybrid solar cells.....	5
Figure 1-4: Some of PV cells technologies.....	7
Figure 1-5: Layers of a typical crystalline silicon PV module.....	9
Figure 1-6: Schematic of a thermoelectric.....	10
Figure 1-7: Relation between ZT of the Thermoelectric module materials and temperature.....	11
Figure 1-8: Typical heat sinks are used with thermoelectric module.....	12
Figure 1-9: Schematic diagram of the splitting spectrum method.....	16
Figure 1-10: Schematic diagram of directcoupling method of PV and TEG in hybrid system.....	17
Figure 2-1: Illustration of prototype panel layer TEG and cooling system.....	20
Figure 2-2: Optical image of prototype PV-TE hybrid circuit.....	21
Figure 2-3: Photographs of Parabolic Trough Concentrator, CPV/T-TEG collector receiver with out cover, and CPV/T-TEG collector receiver with cover.....	22
Figure 2-4: Structure and photograph of the PV–TEG coupling device.....	23
Figure 2-5: A photo of the back solar panel with TEG and fan cooling.....	25
Figure 2-6: Schematic diagrams of PV–TEG hybrid system with three kinds of cooling methods investigated in this paper.....	28
Figure 2-7: Structural diagram of two systems: PV only and PV-TEG.....	29
Figure 2-8: Schematic of PV-TEG hybrid system.....	32
Figure 2-9: Schematic of the experimental set up.....	34
Figure 3-1: Simulated PV-TEG Hybrid System.....	46
Figure 3-2: Illustrates the energy pathway for the simulated PV-TEG.....	47
Figure 3-3: The 3D geometric model of photovoltaic system.....	53

Figure 3-4: The 3D geometric model of photovoltaic/thermal (PV/T) system, (a) extruded view and (b) PV/T assembled.....	53
Figure 3-5: 3D Geometric model of : (a) S1, (b) S2, (c) S3, and (d) S4 PV-TEG Hybrid System.....	54
Figure 3-6: Schematic of the generated 3D mesh of (a) PV/T system, (b) S1, (c) S2, (d) S3 and (e) S4 models (PV –TEG) hybrid systems.....	57
Figure 3-7: Convergence history to solve discrete conservation equations.....	62
Figure3-8: The schematic diagram of flow chart of steps of computational model.....	63
Figure 3-9: PV -TEG control volume.....	64
Figure 4-1: Schematic diagram of the PV/T-TEG integrating system.....	69
Figure 4-2: Photographs of experimental Rig; (a)Front view and (b)Side view.....	70
Figure 4-3: PV module.....	74
Figure 4-4: Thermoelectric module.....	74
Figure 4-5: Aluminum sheet.....	74
Figure 4-6: Heat exchanger manufacture stages.....	75
Figure 4-7: Solar simulator.....	77
Figure 4-8: Iron structure with slider part.....	77
Figure 4-9: Bench.....	77
Figure 4-10: Glass wool.....	78
Figure 4-11: Thermal grease.....	78
Figure 4-12: Wooden enclosure.....	78
Figure 4-13: Temperature Recorder Type Lutron BTM-4208SD.....	81
Figure 4-14: Thermocouple Type k.....	81
Figure 4-15: Solar Module Analyzer Type PROVA 200A.....	82
Figure 4-16: Solar Meter Type TES132.....	82
Figure 4-17: Flow Meter Type ZYIA.....	82

Figure 4-18: Digital Multimeter Type TMT 46001.....	82
Figure 4-19: Temperature distribution on heat exchanger surface with 7(l/min) volume flow rate at solar radiation 1000 (W/m ²).....	83
Figure 4-20: Schematic diagram of locations of thermocouples connection on the: (a) PV module, (b) heat exchanger, and (c) Aluminum plate (thermal absorber) Schematic diagram of the PV/T-TEG integrating system.....	85
Figure 4-21: Arrangement the TEG items on the back surface of the thermal absorber.....	88
Figure 4-22: Details of experimental rig parts.....	89
Figure 4-23: Calibration of the Water Flow meter.....	90
Figure 5-1: Temperature distribution on the front surface of PV cells in the PV system only.....	95
Figure 5-2: Temperature distribution on the top surface of : a) PV panel and (b) heat exchanger in the PV/T system.....	96
Figure 5-3: Temperature distribution on the: a) top surface of PV panel, (b) TEG modules hot side, (c) TEG modules cold side, and (d) top surface of heat exchanger in the (S1) model PV-TEG hybrid system.....	97
Figure 5-4: Temperature distribution on the: a) top surface of PV panel, (b) TEG modules hot side, (c) TEG modules cold side, and (d) top surface of heat exchanger in the PV-TEG hybrid system (S2) model	99
Figure 5-5: Temperature distribution on the: a) top surface of PV panel, (b) TEG modules hot side, (c) TEG modules cold side, and (d) top surface of heat exchanger in the PV-TEG hybrid system (S3) model.....	101
Figure 5-6: Temperature distribution on the: a) top surface of PV panel, (b) TEG modules hot side, (c) TEG modules cold side, and (d) top surface of heat exchanger in the PV -TEG hybrid system (S4) model.....	103
Figure 5-7: The electrical power of each PV, PV/T, and PV -TEG (S4) model hybrid system in a numerical test	107

Figure 5-8: Comparison between the numerical results are obtained by the present study and those in the previous study [69].....	108
Figure 5-9: The electrical output power of three systems (PV only, PV/T, and PV - TEG) in an experimental test	113
Figure 5-10: The electrical efficiency of three systems (PV only, PV/T, and PV - TEG) in an experimental test	113
Figure 5-11: Numerical and experimental results of average front surface temperature of the PV in the PV panel, PV/T system, and PV -TEG Hybrid system.....	115
Figure 5-12: Numerical and experimental results of electrical output power of the PV panel, PV/T system, and PV -TEG hybrid system	115
Figure 5-13: Numerical and experimental results of electrical efficiency of the PV panel, PV/T system, and PV -TEG hybrid system	116
Figure 5-14: Influence of solar radiation G on the PV cell temperature in PV only system, PV/T and PV –TEG and temperature difference between both sides of TEG, numerically	118
Figure 5-15: Influence of solar radiation G on the PV cell temperature in the PV only system, PV/T and PV -TEG and temperature difference between both sides of TEG experimentally	119
Figure 5-16: Influence of solar radiation G on the output power in PV only system, PV/T and PV -TEG, numerically	119
Figure 5-17: Influence of solar radiation G on the output power in the PV only system, PV/T and PV –TEG, experimentally.....	120

List of Abbreviations

Abbreviation	Description
ANSYS	Analysis System
a-Si	Amorphous silicon
Bi ₂ Te ₃	Bismuth Telluride
CPV	Concentrated photovoltaic
c-Si	Crystalline silicon
EVA	Ethylene Vinyl Acetate
FVM	Finite Volume Method
HS	Heat Sink
m-Si	Mono-crystalline silicon
p-Si	Poly-crystalline silicon
PV	Photovoltaic
PV/T	Photovoltaic and thermal collector
PV -TEG	Photovoltaic thermoelectric generator hybrid system
TE	Thermoelectric
TEG	Thermoelectric generator
TPT	Tedlar Polyester Tedlar

List of Symbols

Latin Symbols		
Symbol	Description	Units
A_{pv}	The area of solar panel	m^2
A_{TE}	The area of thermoelement	m^2
C_p	Specific heat	$J\ kg^{-1}\ K^{-1}$
D	Diameter of pipe	m
E	Electrical power	W
E_{el}	Total electrical power	W
G	Solar Radiation	$W\ m^{-2}$
h_{conv}	Heat transfer coefficient	$W\ m^{-2}\ K^{-1}$
I_{mp}	Current at maximum point	A
K	Thermal conductivity	$W\ m\ K^{-1}$
L_{TE}	The thermo element length	m
m	Mass	kg
M	Number of thermoelectric module	-
N	Number of thermo element pair	-
P_m	Electrical power at maximum power point	W
Q	Heat transfer	W
T_{amb}	Ambient temperature	$^{\circ}C$
T_c	Cold side temperature of TEG	$^{\circ}C$
T_h	Hot side temperature of TEG	$^{\circ}C$
T_{in}	Input water temperature	$^{\circ}C$
T_{out}	Output water temperature	$^{\circ}C$
T_{sc}	Average front surface temperature of PV	$^{\circ}C$
ΔT	Temperature difference	$^{\circ}C$
V	Water velocity	$m\ s^{-1}$
v	Wind speed	$m\ s^{-1}$
V_{mp}	Voltage at maximum power point	V
V_{oc}	Open circuit voltage	V
Z	Figure of merit	K^{-1}

Greek Symbols		
Symbol	Description	Units
α_c	Absorptivity coefficient of the PV cell	
α	Seebeck coefficient	(V/K)
ε	Emissivity	---
τ_g	Transmittance coefficient of the glass	---
η	Efficiency	(%)
η_0	Efficiency at standard conditions	(%)
η_{pv}	Electrical efficiency of Photovoltaic panel	(%)
η_{el}	Total electrical efficiency	(%)
β_0	Photovoltaic temperature coefficient	K ⁻¹
β_c	The packing factor	---
ρ	Density	kg/m ³
ρ	Electrical resistivity	$\Omega \cdot m$
μ	Dynamic viscosity	N.s.m ⁻²

Chapter One: Introduction

Chapter One Introduction

1.1 Generally

Sustainability is difficult to provide everyone access to clean, renewable power. This is due to the vital importance of getting this energy, particularly electrical energy, in people's daily lives. The studies (International Energy Agency, 2019) indicated that in 2018, approximately 860 million people lacked electricity. Between 2017 and 2040, the demand for all forms of energy is expected to rise by 20%, with a substantial growth (60%) in electricity use [1].

As well as the increasing environmental pollution concerns due to fossil fuel emissions and depletion prompted the world to pay more attention to the use of renewable energy. Renewable energies are derived from the Earth's natural resources, such as wind, sun, and tidal wave energy. Also, these energy resources that are freely available on Earth and have no harmful emissions effects. Its use will ensure the preservation of traditional energy sources and at the same time, its application protects the environment from pollution. Most renewable energy originates from the sun, the dominant thermal energy source [2].

The sun offers a continuous source of about 1.2×10^{15} terawatts, much more than the power consumed globally [3]. The sun provides us with free energy, but it must be transformed into forms that can be put to good use, like electricity or heat. Figure (1-1) illustrates the location of Iraq, which is close to the Sunbelt, and the annual average incident solar radiation is high enough to make solar energy a suitable source of power generation. Iraq must increasingly rely on renewable energy sources to lessen environmental damage and address a peak load electricity shortfall [4].

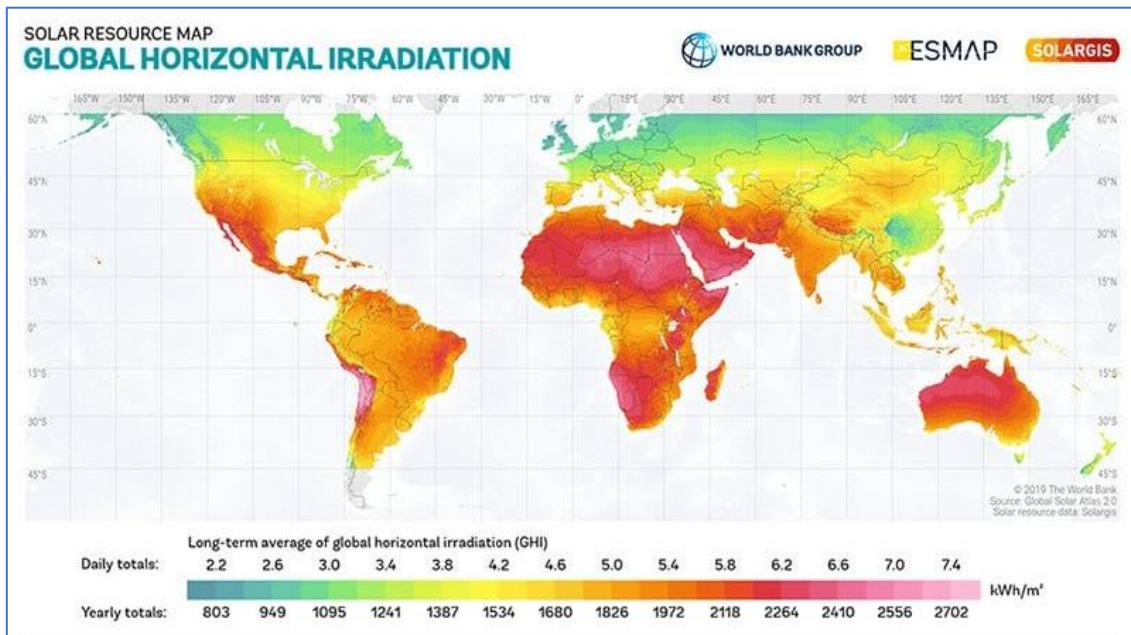


Figure 1-1: The annual average solar radiation on earth [4]

Given its ability to function under diffuse radiation, solar cells are one of the most rapidly emerging renewable energy technologies today and will play a significant role in the future. Global energy production with PV modules reached 227 GW in 2015, and installed capacity was projected to exceed 500 GW in 2020. In addition, the share of photovoltaic modules is expected to be 16% of total energy production in 2050 [5]. Figure (1-2) shows global cumulative PV installation until 2030, a significant increase in Asia.

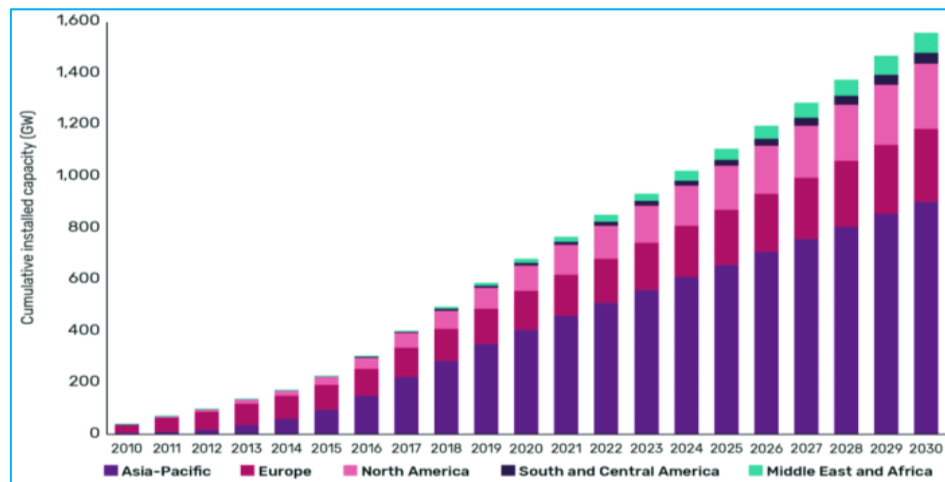


Figure 1-2: Global cumulative PV installation until 2030 [5]

Photovoltaic technology has been developing quickly, and studies have shown that [6] [7]:

- Less than 20% of solar energy could be converted into electricity while the rest is dissipated as unused heat.
- PV cells respond to changed climatic conditions, such as clouds, dust, wind, and ambient temperature.
- The temperature of the PV cell affects its performance, where the PV cell efficiency drops about (0.4-0.65) % at a temperature rise of one °C.

Based on the upper list, the operating temperature of the solar cell can be maintained at an acceptable level by using various thermal management devices for a cooling PV module, such as passive or active cooling techniques. The system is then referred to as a combined photovoltaic and thermal (PV/T) system [8].

PVT systems produce a higher total energy output (thermal energy + electrical energy) than photovoltaic and thermal systems employed alone. However, since the PVT systems majorly generate low-grade thermal energy. So, it becomes necessary to find a device capable of converting thermal energy directly into electrical power, such as a thermoelectric (TEG) module [9].

Increasing the valuable energy from the PV module is possible by using a combined photovoltaic-thermoelectric (PV-TEG) hybrid system, where the integrated of the thermoelectric (TEG) module with the PVT system will improve the high-grade electrical energy output, as shown in figure (1-3) [10].

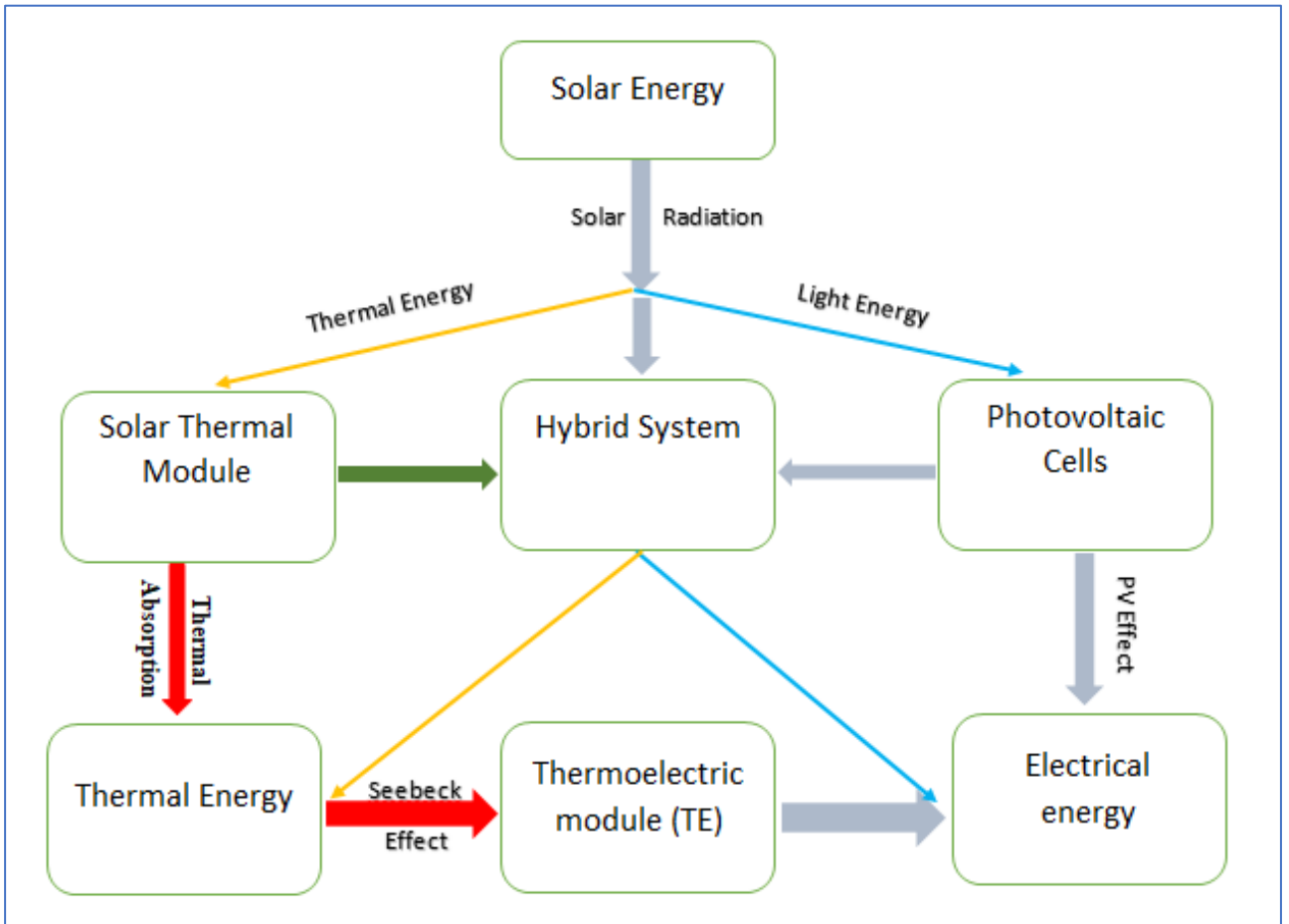


Figure 1-3: Basic structure of hybrid solar cells.[10]

1.2 Photovoltaic cell

The word "photovoltaic" comes from the Greek word "photovoltaic." The terms "photo" and "voltaic" refer to light and electricity, respectively. The technology of converting sunlight (visible range) directly into electricity without fuel is known as photovoltaic PV or solar cell [11].

The rest of the solar energy (especially infrared radiation) is frequently lost as heat distributed through the cell. Edmond Becquerel, a French physicist, 1839 discovered that some materials create small quantities of electric current, when they are exposed to light. The n-type region and the p-type region are two oppositely doped layers that make up a PV cell. Only high-energy photons may discharge electrons in a solar cell, allowing an electrical circuit to function. A PV cell's efficiency is limited because it operates within a narrow band of the solar spectrum (400-1100 nm), which only has enough energy to excite electrons [12].

The energy required to excite charge carriers depend on the band gap of material (1.12 eV for Silicon). The most common material used in solar cells is silicon, and Bell Telecom invented the modern solar cell in 1954 [13].

1.2.1 Photovoltaic cell technology types

Many types of PV cell technology are in the market today; they are classified into three generations, depending on the primary material. Some PV Cells technologies are shown in figure (1-4) [14]:

- First Generation or Crystalline Silicon technology includes:
 - 1- Mono-crystalline Silicon (m-Si).
 - 2- Poly- crystalline Silicon (p-Si).

- Second Generation or Thin-film PV technology generally includes:
 - 1- Amorphous silicon (a-Si).
 - 2- Cadmium-Telluride (CdTe).
 - 3- Copper-Indium Gallium- Selenide (CIGS).
- Third Generation or Multi-junction cell technology includes:
 - 1- Copper Indium-Selenide (CIS) and Copper-Indium Gallium-Selenide (CIGS) which arrange in layers as one cell and have the highest efficiency of about 37%
 - 2- Dye-Sensitized Solar Cell (DSSC).
 - 3- Perovskite Solar Cell.
 - 4- Organic PV Cell and Concentrated photovoltaic system (CPV).

Crystalline silicon cells are the most commercial, and their cost reductions continue through improvements in manufacturing processes, where it forms about (80-85) % of the market share, while thin-film cells with a share of (10 to 15) %. The efficiency of crystalline Silicon modules ranges (from 14 to 20) %, while for thin film modules, it ranges (from 6 to 11) % [15].

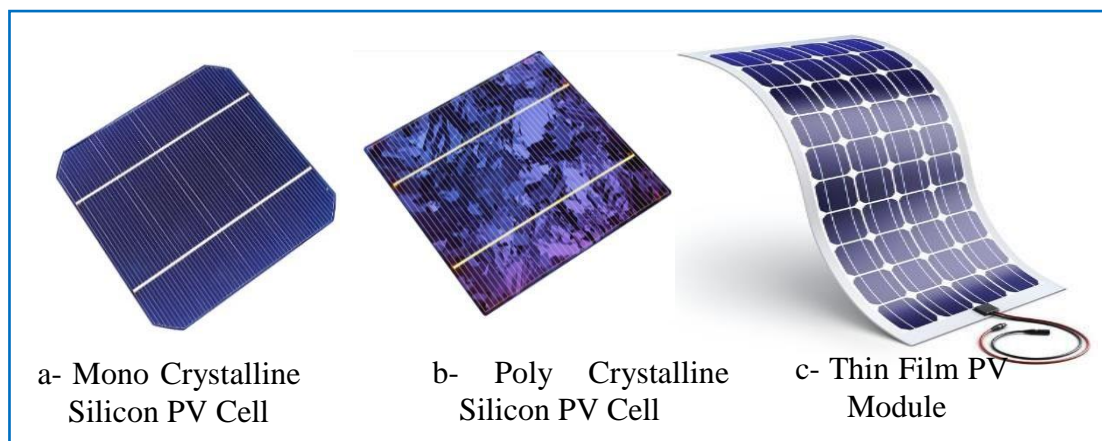


Figure 1-4: Some PV Cells Technologies [14]

*

Many PV cells can be linked in parallel, series to boost output current, voltage, or both to make a PV module. A typical PV module comprises several tiny PV cells encased in a single flat rigid structure to protect the sensitive cells and accompanying cables from the harsh environment in which they are deployed [4].

1.2.2 Main parts of photovoltaic module

The main parts of the PV module structure are as follows [16]:

- The front surface is typically a glass cover with high transmission and low reflection capacity for the concerned sunlight. Low-iron glass is commonly used because it is "affordable, strong, stable, clear, impervious to water and gases, and has good self-cleaning qualities."
- Encapsulant is a fragile film applied to PV cells' front and rear surfaces as Ethyl Vinyl Acetate (EVA). It should have a strong link between the PV module's layers, be stable at various operating temperatures, and be transparent with low thermal resistance.
- Photovoltaic (PV) cells are fragile, with a metallic contact grid on the front surface that generates electricity.
- The rear surface is a thin, low-thermal-resistance layer that coats the back of the module. Tedlar (thin polymer sheet) or glass is used in its construction. A typical crystalline silicon solar module's layers are shown in figure (1-5).

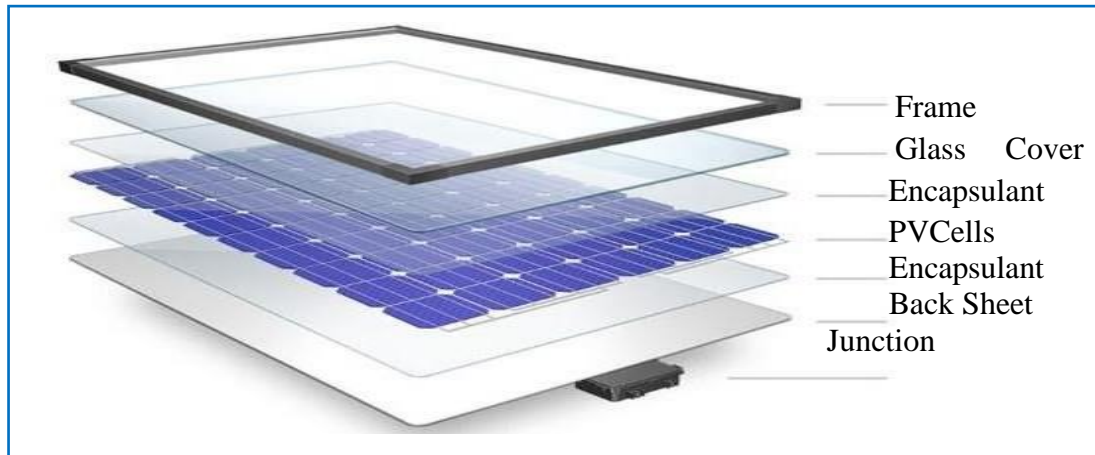


Figure 1-5: Layers of a Typical Crystalline Silicon PV Module [16]

1.3 Thermoelectric (TE) Device

Thermoelectric power sources are characterized by the conversion of heat into electricity by the Seebeck effect, then are called (TEG) or vice versa by the Peltier effect, then are called TE cooler as shown in figure (1-6) [17]. The working part of a thermoelectric generator is the electron. Thus a TEG produces no noise, is environmentally friendly, and has no moving parts [18]. TE generators are as reliable as PV and could work for 10 to 30 years on average without significant technical problems [19].

The basic structure of thermoelectric (TEG), or the basic building block, consists of n-type and p-type semiconductor thermoelements connected electrically in series by a conducting strip (usually copper or aluminum). The module consists of a number of the primary building connected electrically in series but thermally in parallel and sandwiched between two ceramic plates [20].

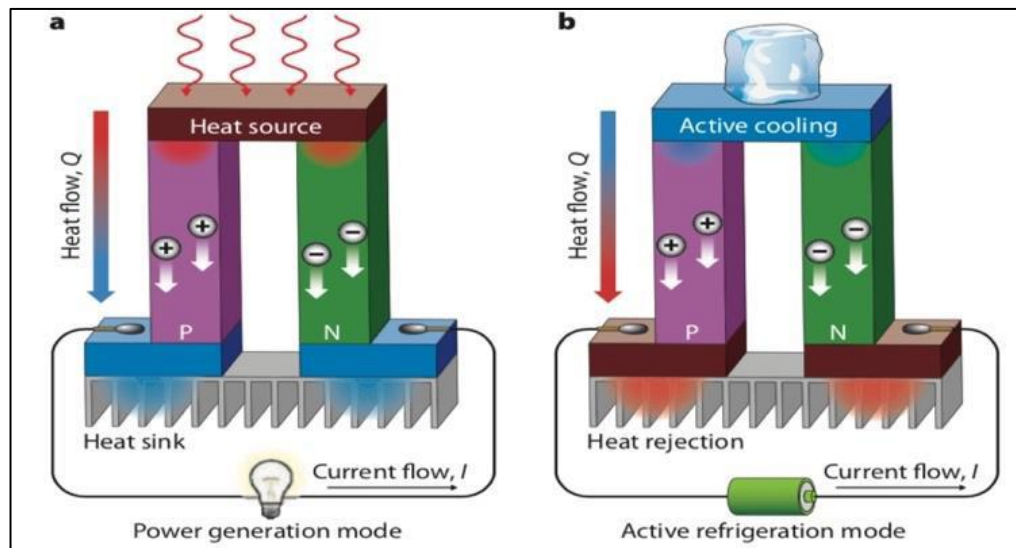


Figure 1-6: Schematic of a thermoelectric (a) generator and (b) more excellent [17]

1.3.1 Effected parameters on the thermoelectric generator performance

➤ Thermoelectric materials

Modern thermoelectric converters are made of semiconductors, which have better conversion efficiency and output power than metal alloys. The implementation of the thermocouple junction is complicated by the fact that semiconductors are generally nonductile crystalline solids. Electrical conductivity, Seebeck coefficient, and thermal conductivity are three intrinsic material qualities that define the quality of thermoelectric materials used for generating electric power via the Seebeck effect or cooling (refrigeration) via the Peltier effect [21].

Electrical current is passed in both the power generation and cooling modes. Hence materials with high electrical conductivity are advantageous. Since a significant produced voltage per unit temperature gradient is wanted, a significant Seebeck coefficient is required, according to the dimensionless parameter called the figure of merit (Z) [22]:

$$Z = \frac{\alpha^2}{\rho \cdot K}$$

1-1

Where α is the Seebeck coefficient, ρ is the electrical resistivity, and k is the thermal conductivity.

Finally, TE materials must have a low thermal conductivity since a temperature difference across the material must be maintained [23]. Bismuth telluride (Bi_2Te_3) is utilized for low-temperature (500 K) power generation according to a classification system based on the operating temperature range. For mid-temperature (500-800 K) power generation, materials found on group tellurides such as PbTe, GeTe, and SnTe are employed. Finally, high-temperature (> 800 K) power generation uses silicon-germanium alloys, as shown in figure (1-7) [24].

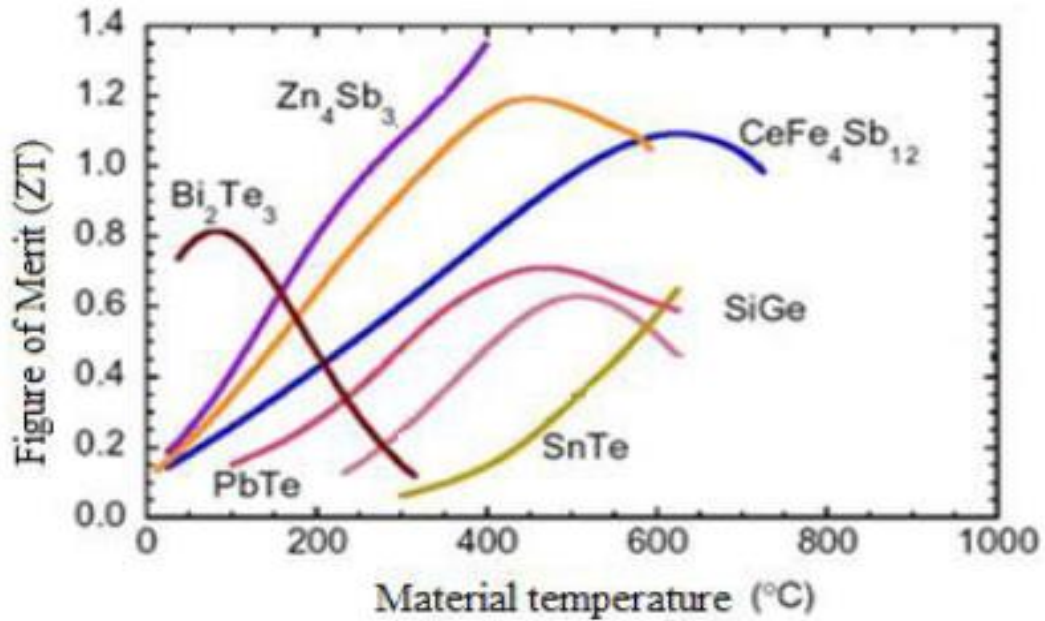


Figure 1-7: Relation between ZT of the Thermoelectric module materials and temperature [24]

➤ **Thermoelectric geometry**

Thermoelectric geometry can be involved the thermoelement length l , the thermoelement cross-sectional area A , and the number of the thermocouples (N). The effect of thermoelectric material properties on its performance, so the conversion efficiency of a thermoelectric module versus the length of thermoelements for different temperature differences. A long thermoelement is required to obtain higher conversion efficiency, while a relatively shorter thermoelement is needed to get a larger power output, especially if the heat source is inexpensive or essentially free, such as in the case of waste heat recovery or energy harvesting [18]

➤ **Heat exchanger**

Heat exchangers are required to extract heat from heat sources. They then dissipate a heat into the ambient environment to establish a temperature difference across a thermoelectric device. With rising temperature differences across it, a thermoelectric device's power output and conversion efficiency both grow significantly by depending upon coolant type; the most popular types of cooling devices used with thermoelectric are heat sink (fins type), heat exchanger as water cooling block, and fan, as shown in figure (1-8) [25].



(a) Heat sink (fins)

(b) Water cooling block

(c) Fan

Figure 1-8: Typical heat sinks are used with Thermoelectric modules (a) heat sink (fins type), (b)heat exchanger (water cooling block), and (c) Fan [25] .

1.3.2 Applications of thermoelectric generator

Thermoelectric generators have a wide range of applications, such as:

- Wasted heat recovery for automobiles [26].
- Wearable sensors [27].
- Micro power generation [28].
- Wireless sensor network [29].
- Solar thermoelectric system [30].
- Harvesting the wasted heat from Photovoltaic in the application of hybrid PV-TEG system [31][32].

1.3.3 Advantages and disadvantages of thermoelectric generator.

➤ **Advantages** [33] [20]:

- Solid-state devices that do not need any fluids for fuel or cooling.
- Have no moving parts.
- Operating in severe environments.
- More reliable.
- Do not require maintenance for long periods.
- Environmentally friendly

➤ **Disadvantages** [34] [35]:

- TEG materials have scarce elements, which make them costly compounds.
- The typical efficiency of TEG is very low, around 5-8%.

1.3.4 The popular type of thermoelectric generator.

Most types of thermoelectric modules available commercially, that were made of Bismuth-Telluride materials with different specifications and dimensions. Thermoelectric module can be categorized according for their

specifications, such as the maximum temperature at the hot end of the thermoelectric or the temperature difference between the two TEG sides. Table (1-1) below shows the properties of most using thermoelectric modules.

Table 1-1: Datasheet of most using thermoelectric modules

TEG module type	Parameter	Value
TGM199-1.4–2.0 [36]	Number of thermocouples	199
	Internal resistance	3.7 Ω
	Hot side temperature	200 $^{\circ}\text{C}$
	Maximum temperature difference	170 $^{\circ}\text{C}$
	Dimensions (L * W * H)	40 * 40 * 4.4 mm
ZT4-12-F1-4040-TA-W8 [37]	Number of thermocouples	127
	Internal resistance	3.56 Ω
	Hot side temperature	50 $^{\circ}\text{C}$
	Maximum temperature difference	71.7 $^{\circ}\text{C}$
	Dimensions (L * W * H)	40 * 40 * 4.8 mm
TEC1-12706 [38] [8]	Number of thermocouples	127
	Internal resistance	2.3 Ω
	Maximum temperature difference	75 $^{\circ}\text{C}$
	Dimensions (L * W * H)	40 * 40 * 4.2 mm

1.4 Photovoltaic- Thermoelectric (PV-TEG) hybrid system

Integrating thermoelectric devices into photovoltaic systems can improve PV's overall performance by allowing more effective temperature

control. When thermoelectric generators are coupled with PV, depending on the PV-TEG integration method, the TEG can use the PV's waste heat to generate some electrical energy if it is adequately cooled and the temperature difference [1].

Furthermore, suppose the system is constructed correctly. In that case, integrating thermoelectric generators into PV could improve the overall hybrid system's performance [8].

1.4.1 Hybrid system integration methods

Incorporating photovoltaic and thermoelectric systems allow for greater utilization of the solar spectrum. PV transforms the sun spectrum's ultraviolet and visible parts (200–800nm) into energy, whereas TEG converts the infrared range (800-3000nm) into electricity [39]. Spectrum splitting and direct coupling integration are the most used PV-TEG integration methods:

➤ Spectrum splitting method

Solar spectrum splitting systems have attracted interest due to their complete utilization of solar energy in a wide wavelength range, as well as their ability to reduce the PV operating temperature [40]. A splitting technique that contained a splitter system, a concentrator system, PV cells, a TEG, and cooling systems, as shown in figure (1-9). These systems divide the solar spectrum into two areas, the light area and the heated room, by a splitter at a specific wavelength (cut-off wavelength). The PV and TEG work separately to convert solar energy into electricity; the TEG does not cool the PV or use the PV's waste heat for energy conversion. Furthermore, the equipment for the spectrum splitting technique is more expensive [41].

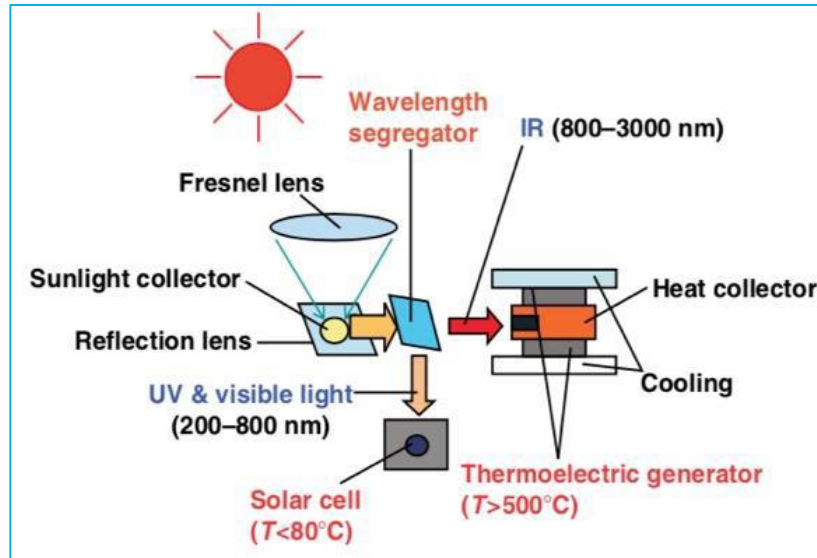


Figure 1-9: Schematic diagram of the splitting spectrum method [41].

➤ Direct integration method

In the direct coupling system, The PV and TEG are directly coupled and put in a parallel arrangement as a single system, as shown in figure (1-10). The PV is placed directly above the TEG, and a heat sink is attached to the bottom of the TEG, for the PV absorbs the shorter wavelengths while the TEG absorbs the longer wave length. This method involved two integration ways: the first involved using thermal paste between the PV and TE. In contrast, the other way to connect the PV and TEG thermally is by using a thermal concentrator (a copper or aluminum plate) [42]. The second way of direct integration is proposed because the metal plate ensures heat transfer rapidly from PV into TEG and allows the ensuing electrical connection to be in series or parallel [8] [43].

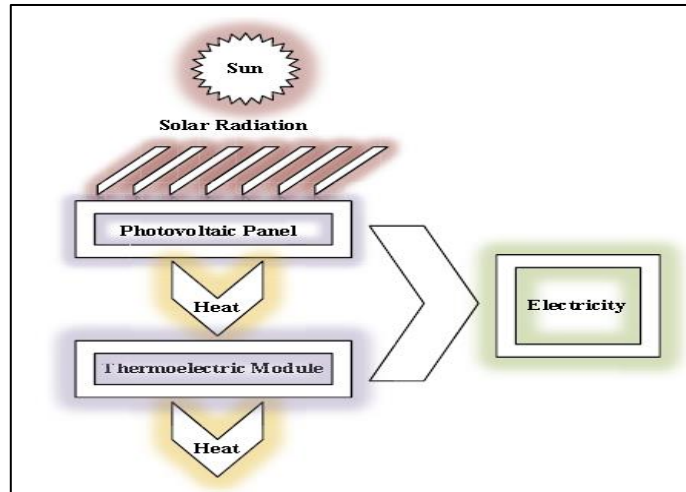


Figure 1-10: Schematic diagram of Direct Coupling method of PV and TEG in hybrid system [43]

1.5 Aim of the research

The main aims of the work in this thesis are:

- To investigate the possibility of increasing the benefit of solar energy by integrating thermoelectric modules with solar cells as a PV- TE hybrid system.
- Harnessing a waste heat recovery in photovoltaic cells (PV) by using thermoelectric (TEG) to generate more electric power.
- Evaluation of the hybrid system's potential as a promising future renewable energy technology through experimental and numerical investigation of its performances.

Chapter Two: Literature Review

Chapter Two

Literature Review

2.1 Introduction

A great number of researchers have investigated and proposed several methods for boosting the amount of solar energy and recovering wasted heat in PV cells. To generate additional output power, thermoelectric (TEG) directly is connected with photovoltaic as (PV-TEG) hybrid systems. Some researchers had done the tests under an indoor environment, which are featured by simplicity and controlling the operation condition, but others made their experiments under outdoor exposure. This review will be classified into the experimental, theoretical and numerical simulation, and numerical simulation/ experiment investigations.

2.2 Experimental investigations

Wang et al. (2011) [44] experimentally investigated the performance of a novel photovoltaic–thermoelectric (PV–TEG) hybrid system in the USA. The new model composed of a series-connected dye-sensitized solar cell prototype (DSSC), a solar selective absorber (SSA) and a TEG. The total efficiency of 13.8 % was achieved in the hybrid system whereas the efficiency of PV alone 9.39% under boundary condition such as 1000 (W/m²) solar radiation and 25°C ambient temperature.

Daud et al. (2012) [45] developed a hybrid system for utilizing solar radiation and heat from the sun as source of electricity generation by using polycrystalline silicon cells and TEG module with

a liquid cooling systems, as shown in figure (2-1) in the laboratory of University Technology PETRONAS Perak, Malaysia. The dimension area of PV panel was 0.1875 m^2 that was integrated with 4 items of TEG modules. The results showed that the efficiency of PV thermal can be increased to up to 0.79 % without cooling system and 1.84 % with integration of cooling system from traditional PV panel at 600 W/m^2 of solar radiation. Also, the results showed that at 868 W/m^2 solar radiations, prototype panel and TEG with liquid cooling system can improve efficiency up to 3 % compared with PV only.

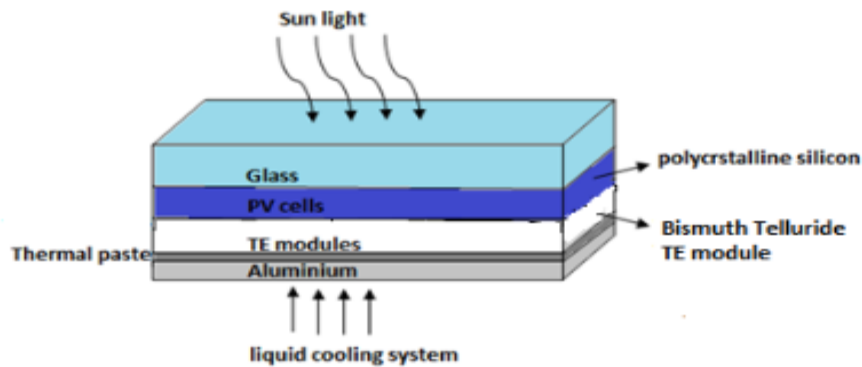


Figure 2-1: Illustration of prototype panel layer, TEG and cooling system [45]

Park et al. (2013) [46] performed the optimization of a hybrid PV-TEG system via lossless coupling in the indoor environment at China. The hybrid system consisted of crystalline silicon cell (c-Si), the TEG module, solar simulator (Xe arc lamp), thermal conductive paste between the hybrid system components and passive heat sink was based down the TEG as shown in figure (2-2). The obtained results indicated that thermal efficiency increased from 12.5 % to 16.3% and the electrical power increased by 30%. Also this result is based on the 15 degrees Celsius temperature difference between two sides of the thermoelectric module and $1000 \text{ (W/m}^2\text{)}$ solar radiation intensity.

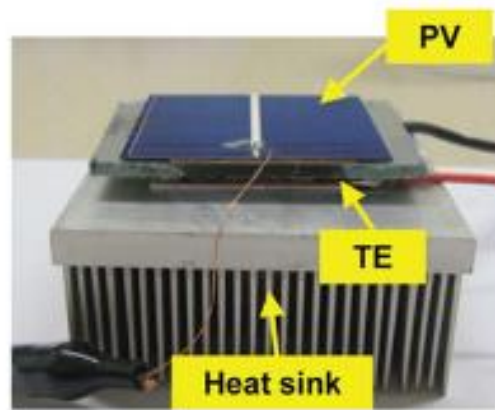


Figure 2-2: Optical image of prototype PV-TE hybrid circuit [46].

Mohsenzadeh et al. (2017) [38] proposed a new structure for parabolic trough photovoltaic/thermal collector with thermoelectric (CPV/T-TEG). Experimentally investigated its thermal and electrical performances in outdoor environment at Iran. This hybrid system consists of the receiver of concentrator contains a triangular channel; an outer surface covered with 8 photovoltaic cells in series type of Mono-Si, 20 items of thermoelectric modules TEG (TEC1-12706) type, and one-axis solar tracker as shown in figure (2-3).

Performance evaluation of this combined heat and power system that showed daily average electrical and thermal efficiencies can reach 4.83% and 46.16%, respectively comparison with the photovoltaic- only system.

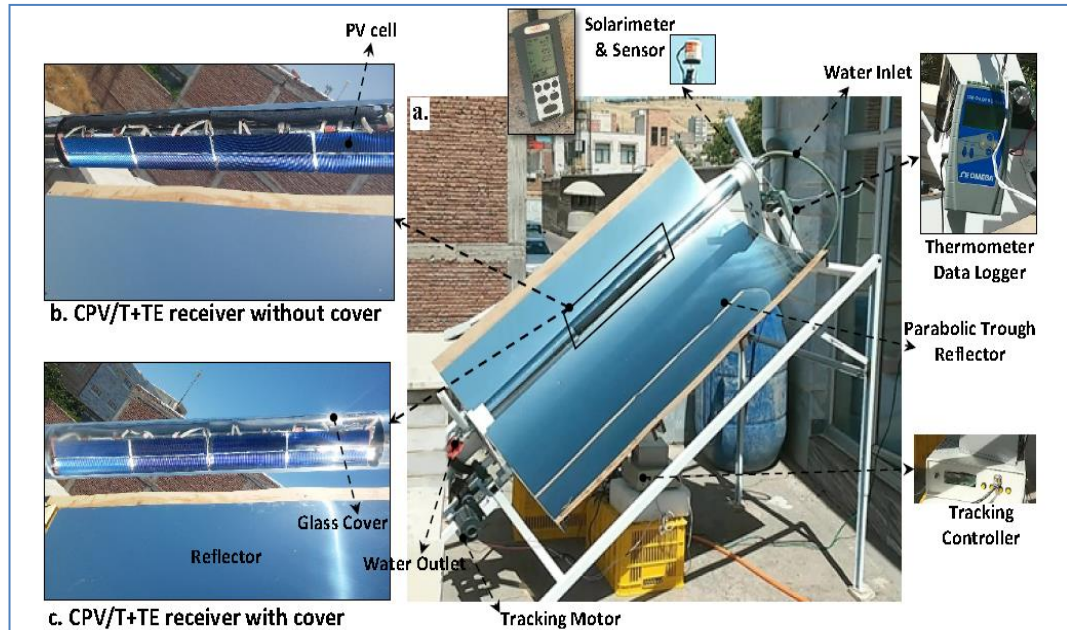
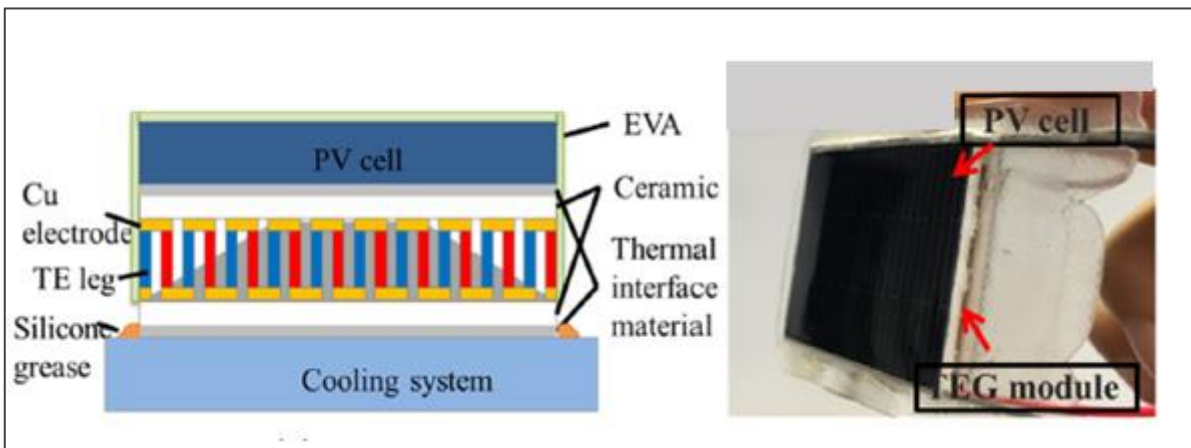


Figure 2-3: Photos of (a) parabolic trough concentrator which is oriented towards the earth's polar axis with the E-W sun tracker, (b) CPV/T-TEG collector receiver without cover, and (c) CPV/T-TEG collector receiver with cover [38].

Haiping et al. (2018) [47] performed an outdoor experiment of a novel low concentrating photovoltaic/thermal–thermoelectric generator (LCPV/T-TEG) hybrid system in Beijing- Chain. The system mainly consists of a compound parabolic concentrator, a double-glazing PV panel, the TEG, and a micro-channel heat pipe array. The TEG modules is designed to be associated with the cold side of heat pipe array. Which acts as the cooling method of the LCPV/T system to improve PV efficiency instead of directly adhering to the backplane of the PV panel. The results showed that the daily average thermal efficiency was 45.0%, the daily average PV electrical efficiency was 11.8%. While the daily average TEG electrical efficiency was 0.23%. So, the daily average overall efficiency reached 57.03%.

Liu et al. (2020) [48] fabricated PV- TEG coupling device by combining mono- crystalline silicon prototype and bismuth telluride TEG with thermal interface materials. The performance of a novel system was compared with pure photovoltaic cell under different irradiation, and cooling conditions in the indoor environment at China, as referred in figure (2-4). As the results indicated that TEG adoption can effectively reduce the overheating of the photovoltaic, improve the performance of the photovoltaic, and harness the wasted heat to generate electricity. Also, the results showed that using the thermal interface material enhances solar energy consumption and reduces the thermal contact resistance in the PV- TE coupling device. The power generated by the solar cell has increased by at least 14% and the power generation by TEG has increased by at least 60% due to the reduced resistance of heat to contact.



(a) Structure of the PV-TEG hybrid system

(b) Photograph of the PV-TEG hybrid system

Figure 2-4: (a) Structure of the PV-TEG coupling device (b) Photograph of the PV-TEG coupling device [48].

Shittu et al. (2020) [49] Presented for the first time a detailed experimental study of a photovoltaic-thermoelectric with a flat micro-channel heat pipe and water cooling. The experiment was carried out in a laboratory at the University of Hull, United Kingdom in April by using a solar simulator and the insulation layer on the backside of the flat plate-micro-channel heat pipe. The results shown the hybrid system provided an enhanced performance, where the efficiencies of the photovoltaic thermoelectric-micro channel heat pipe, with and without insulation . Also, notice that of the photovoltaic only after 1 h were 11.98%, 12.19% and 11.94% respectively. The photovoltaic temperature in the hybrid system with an without insulation (62.2 °C and 61.9 °C respectively) was lower than that in the photovoltaic only system (67.9 °C) after 1 h .Also, the average power output of the hybrid system increased from 1.86 W to 3.92 W when the solar radiation increased from 500 (W/m²) to 1000 (W/m²).

Omar et al. (2020) [50] presented modified system consist of Monocrystalline PV solar plate which faces the solar radiation from the top .In addition to 12 unit of (TEC1-12706) TEG modules were attached on the back side of the PV plate, as shown in figure(2-5). The experimental study was conducted, outdoor conditions in Egypt to include enhancement of temperature difference through the TEG module by applying two arrangements of thermoelectric devices in the back of PV solar plate with forced convection fans cooling system. Comparison was made between the obtained results from the present modified (PV/TEG) system and the traditional PV system. The results referred the efficiency increases to reach about 26.6 % by using PV/TEG system, while it was 17.56 % in the absence of TEG system at symmetric case arrangement. In contrast, the

efficiency of PV/TEG system increases to reach to 27.2 %, while it was 18 % in the absence of TEG system at unsymmetrical arrangement case.

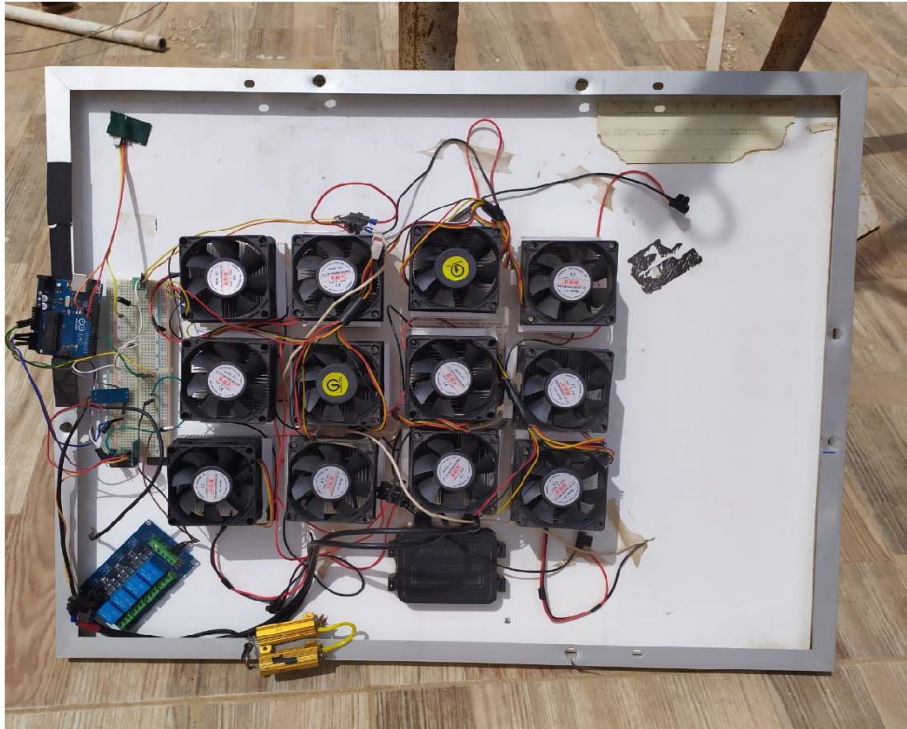


Figure 2-5: A photo of the back solar panel with TEG with fan cooling [50].

2.3 Theoretical/ Numerical investigations

Sark et al. (2011) [51] proposed a PV/TEG hybrid system by attaching thermoelectric generators (Bi₂Te₃) to the back of PV (Multi – Crystalline silicon) modules using the direct coupling method to enhance electrical performance of PV cells. Efficiency calculations based on an idealized model showed that by employing present day thermoelectric materials with figure of merits (Z) of 0.004 K^{-1} at 300 K could lead to efficiency enhancements of up to 23% for roof integrated PV/TEG modules. The results obtained also showed that by using the annual irradiance and temperature profiles of Malaga and Utrecht, the annual energy of these cities could increase by about 14.7% and 11%

respectively.

Najafi and K. A. Woodbury (2013) [52] modeled a combined the PV (Mono- crystalline silicon) that dimensions (120 cm *52.7 cm*3 cm) with 36 TEG (Bi₂Te₃) modules as a hybrid system. TEG units are attached to the back side of PV by its hot side and heat sink by its cold side. The effect of parameters on the hybrid system performance, such as air flow speed and solar radiation were studied. The air flowed into the air channel at a speed of 2 m/s and temperature of 27 (°C) through the heat sink fins. Also, the solar irradiance varied from 600 to 2800 (W/m²), a The results showed that at 2800 (W/m²) solar irradiance the considered PV- TEG system produced 145 W by the PV panel and 4.4 W by the TEG modules. For another case at solar irradiance 600 (W/m²) and T, the percentage of power generated by the TEG were found to be 1.84% of the total generated electricity by the PV panel.

Hashim et al. (2016) [25] developed a theoretical model for the optimization of thermoelectric generators in a hybrid PV-TEG system in the United Kingdom. The model could efficiently determine the optimum TEG geometry for maximum power output. It consists of an amorphous silicon PV cell on the top of (TEC1-12706) TEG module via a copper plate. In the study, heat exchanger with water and copper plate were used as the cooling system and thermal concentrator respectively. The effect of cross section area of TEG on the hybrid system performance were studied at ambient temperature of 25 (°C), solar radiation of 1000 (W/m²), and air speed of 0 (m/s). Results showed that the power output of the solar cell will decrease when integrated with a TEG because the operating temperature of the solar cell was increased due to a large thermal

resistance across the TEG. However, the power reduction in the solar cell (2 mW) will be compensated by the power generation by TEG (5.2 mW). As a result, the total power output P_{tot} of the hybrid system increased to 163 mW for operation in ambient atmosphere. For a solar cell with a cross-sectional area of 40 mm², the total efficiency increased from 10% to 10.2% for a TEG with the optimal length l_{TE} of 2 mm. So, the results referred that the power output of TEG modules with a smaller cross-sectional area than that of the PV was higher than those with a larger cross-sectional area. Also, operating the hybrid system in vacuum could enhance its performance.

Yin et al. (2017) [53] investigated, theoretically the performance of a hybrid PV/TEG system using three different cooling methods in the China, as shown in figure (2-6). Natural cooling, forced air-cooling and water-cooling were compared and the influence of optical concentration ratio, water velocity and thermal contact resistance were studied. In addition, the hybrid systems using four different PV types with dimension (30 mm* 30 mm) including, mono crystalline silicon, polycrystalline silicon, amorphous silicon and polymer cell were investigated to determine the best performing PV. Results showed that water-cooling was more effective for hybrid systems than natural cooling and forced air-cooling, especially highly concentrated systems. In addition, they argued that crystalline silicon and polycrystalline silicon PV were suitable for hybrid PV/TEG systems at low concentration.

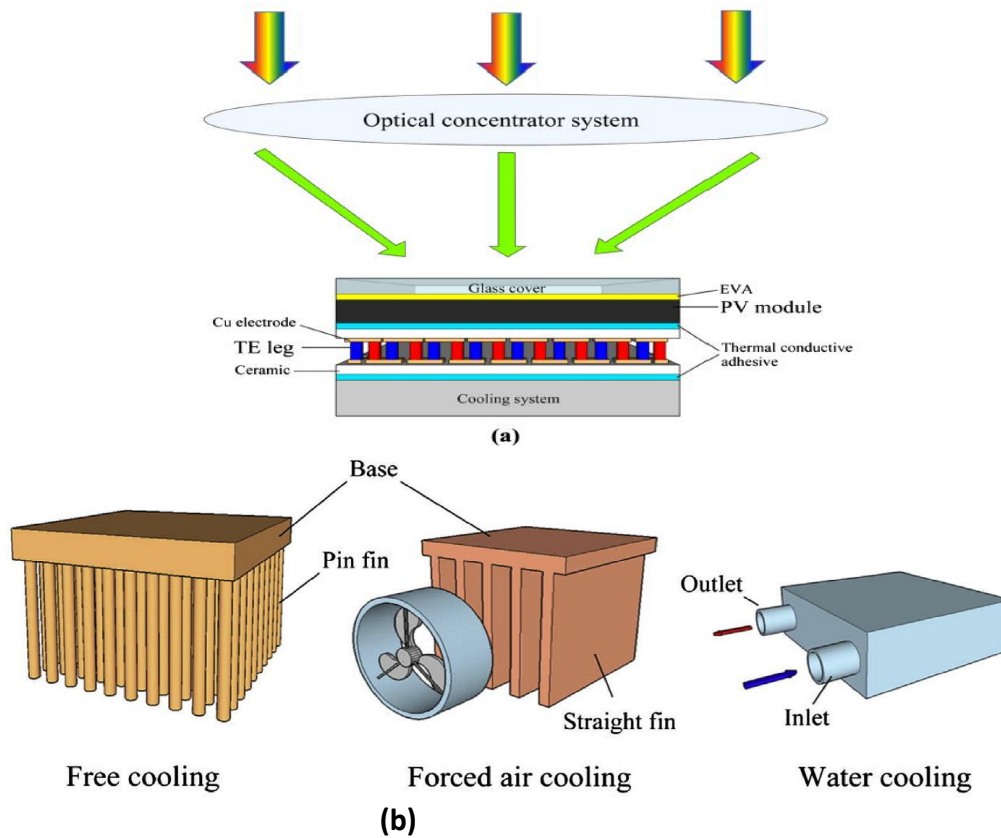


Figure 2-6: (a) Schematic diagrams of PV-TEG hybrid system; (b) three kinds of cooling methods investigated in this paper [53].

Soltani et al. (2018) [54] presented a non-dimensional model of a tri-generation unit consisting parabolic trough solar collector, integrated with (Crystalline silicone) solar cell and thermoelectric type (TEC1-12706). A set of functions were coded in the MATLAB software, in order to obtain the effects of solar irradiance and ambient temperature on the performance of the system and analyze the thermal and electrical power of the hybrid device. Results have reflected some improvements on the electrical efficiency by placing thermoelectric module and solar cell on the lateral area of the absorber tube. Furthermore, an electrical power of 22.714W could be reached at the solar irradiation of 998 W/m^2 , the maximum amount of thermal power (240 W) is attained at 1:30 p.m.,

by increasing the solar irradiance and the maximum amount of thermal efficiency is about 57 %.

Gu et al. (2019) [55] presented a mathematical model of the hybrid PV-TE system and developed it based on thermal resistance theory for PV panel, heat sink, and thermoelectric generator (TEG). The electric and thermal performance of the hybrid system was obtained by iterative calculating temperature, which was a link of electricity and heat coupling generation of the system. Meanwhile, various heat losses and weather conditions were taken into account during the numerical simulation, and the PV alone is taken as a reference for comparison as shown in figure (2-7). Results indicated that higher concentration ratio and smaller temperature coefficient of PV cells are ideal for designing the PV-TE hybrid system that the PV-TE still produces 1.24–2.85 % higher electricity than PV alone although the cell temperature in PV-TE is higher. Also the authors found that reducing thermal resistance of the cooling system with TE by using gel layer was the most effective way to improve the efficiency of the hybrid system.

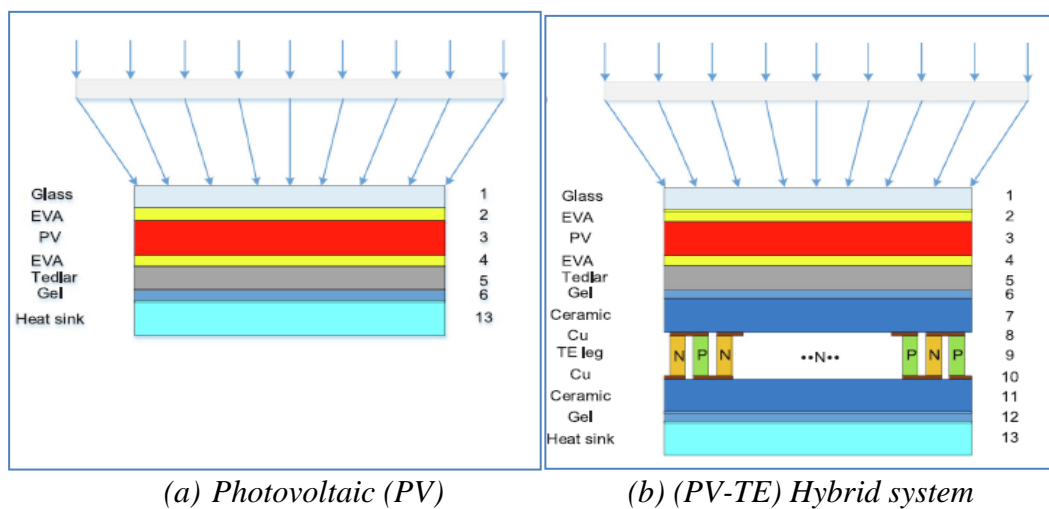


Figure 2-7: Structural diagram of the two systems (a) PV- only; (b) PV-TEG [55].

2.4 Numerical simulation and experimental investigations

Cotfas et al. (2016) [32] carried out their work in the indoor environment in Romania. They studied experimentally and theoretically the performance of three type of the PV-TEG hybrid systems in Romania. They built using prototype of m-Si, p-Si, a-Si photovoltaic cells, Bi₂Te₃ thermoelectric element and Aluminum as heat sink with cooling water. The important parameters, such as the short circuit current, the open circuit voltage, the maximum power, and the efficiency of the photovoltaic cell. The internal resistance of the thermoelectric element were determined at different illumination levels and temperatures for both of the PV-TEG hybrid system components. The result referred to the m-Si/ Bi₂Te₃ hybrid system is the best solution as shown in Table (2-1). Using the PV/TEG hybrid system, the temperature of the photovoltaic cell at 1000 (W/m²) irradiance was for m-Si 32.5 °C, p-Si 33.1 °C, and a-Si 35.7 °C.

The temperature difference increases proportionally with the irradiance grow. The highest temperature difference was obtained for mSi/Bi₂Te₃ hybrid system. The I-V characteristics of the photovoltaic cell (m-Si) in a function of the irradiance are presented Table (2-2). The short circuit current increases proportionally with irradiance for both the photovoltaic cells. The open circuit voltage remains quasi constant because the decreasing caused by the temperature increasing is compensated by the increase in irradiance.

Table 2-1: A gain power for each type of hybrid system at 1000 (W/m²) irradiation [32]

(PV-TEG) Hybrid System	Pmax(W)
Mono-crystalline silicon (m-si)- TEG	0.675
Poly-crystalline silicon (p-si)- TEG	0.5
Amorphous- silicon (a-si)- TEG	0.08

Table 2-2: The parameters of the (m-Si)PV/TEG hybrid system components [32]

Solar radiation	Photovoltaic cell						Thermoelectric module			
	G (W/m ²)	Voc (V)	Isc (A)	Pmax (W)	FF (%)	η (%)	T _{pv} (°C)	Voc (V)	I _{sc} (A)	Pmax (mW)
720	0.599	1.057	0.474	74.9	18.3	28.6	0.064	0.107	1.69	4
820	0.599	1.214	0.542	74.44	18.35	30	0.078	0.133	2.59	5.2
860	0.600	1.316	0.581	73.9	18.84	30.8	0.082	0.137	2.79	5.4
920	0.599	1.424	0.627	73.46	18.93	31.8	0.089	0.155	3.40	5.9
960	0.599	1.470	0.645	73.25	18.66	32.1	0.093	0.156	3.62	6.1
1000	0.599	1.533	0.671	73.11	18.65	32.8	0.095	0.159	3.77	6.2
1020	0.599	1.574	0.687	72.89	18.70	33	0.099	0.165	4.07	6.4
1080	0.599	1.646	0.716	72.62	18.41	33.2	0.101	0.167	4.19	6.8

Zhu et al. (2016) [59] presented, numerically and experimentally study for the PV-TEG hybrid system that was consisting of the mono-crystalline silicon PV cell, Bi₂Te₃ TEG and heat absorber (copper plate), figure (2-8) referred for it. The analysis result by using ANSYS and the

finite element method to solve the heat transfer governing equations that the optimum thickness of heat conductive plate (copper plate) was 4 mm. Also, at specific boundary conditions, such as a thermal flux of 800 W/m^2 on the top side of copper plate, the air convection coefficient of all the surface is set as $5 \text{ W/m}^2 \text{ K}$ and ambient temperature of 27°C . The experimental results showed that the power output of the hybrid system increased by 25 % compared to the PV cells.

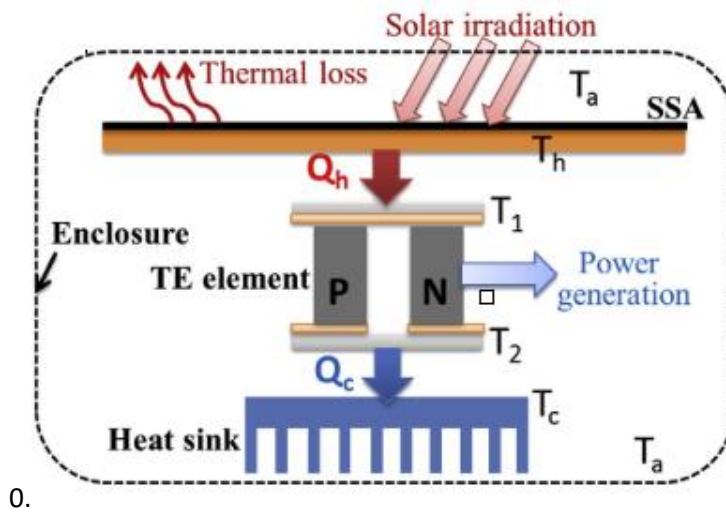


Figure 2-8: Schematic of PV-TEG hybrid system [59].

Rodriguez et al. (2017) [56] suggested a hybrid photovoltaic-thermoelectric generation system with a new empirical model, that might be operate in the role of a standard style of an integrated solar system. A model consisted of crystalline silicon (c-Si) photovoltaic panel array with area of 600 cm^2 , concentrator lens of radiation, thermoelectric generation of Bi_2Te_3 , and cooling unit by water, linked inside selfsame optic level. Performance of a model and influencing parameters were examined empirically in Mexico climatic conditions. In order to determine the optimal configuration of the heat exchanger and the air channel, several configurations were analyzed using the finite element method by software

COMSOL MULTIPHYSICS 4.4. Experimental results showed that the hybrid system generated 7.0 watts of electrical power and 30 watts of thermal energy.

Mahmoudinezhad et al. (2018) [57] performed a feasibility study of a hybrid CPV/TEG system for low solar concentrations, as shown in figure (2-9). An experimental and numerical investigation was carried out to study the performance of the hybrid system in Iran. The experiment was carried out using concentrated radiation from a solar simulator while finite volume method was used to perform the numerical simulation. The authors argued that the experimental results were in agreement with the simulation results. In the P-V curve, the maximum power of CPV in the experiments for 8 suns and 37 suns were obtained 0.283 W and 0.852 W, respectively, while these values for numerical simulation were 0.314 W and 0.902 W, respectively. On other hands, the maximum power generation by the TEG for 8 suns was obtained 2.43 mW and 2.89 mW for the experimental and numerical studies, respectively. For 37 suns these values for the experiments and numerical simulation were 24.1 mW and 25.6 mW, respectively. It was found via the experiment that the maximum and minimum efficiency of the CPV were 35.33% and 23.02%, while these values for the TEG were 1.20 % and 0.63 %, respectively. Also, it was found experimentally, that the electrical efficiency of CPV-TEG was 36.35%, whereas this value for CPV only was 35.33 % at 8 sun.

showed the highest output voltage amongst all the three TEGs under both high and low concentrated light levels.

Table 2-3: Side length and number of junctions of the thermoelectric generator (TEG) samples investigated [58].

TEG Sample	Side Length (cm)	Number of Junctions
A	3	31
B	4	127
C	6.2	49

Riahi et al. (2020) [59] designed and built a CPVT/TEG system by using a parabolic trough concentrator in outdoor environment in Tunisia. The PV (10 cm *10 cm) Mono-crystalline cells and TEG (TEC1-12706) modules were integrated with the rectangular receiver of the parabolic trough and heat exchanger with water. The findings reveal, for a sunny day characterized by solar radiation level reaching 935 W/m² and ambient temperature around 33 °C that the PV cell temperature in CPVT-TE system was higher compared with CPVT system due to the thermal resistance of thermoelectric modules. However, the created temperature gradient in TEG generated additional electrical power, thus providing higher electrical output (7.46% higher) compared with CPVT system. The comparisons of simulated and measured results showed a good accordance between experimental and simulated values of PV cell temperature and electrical efficiency. The maximum deviation between the simulated and measured data was around 5% and 1.3% for the PV temperature and the electrical efficiency respectively.

Summary of literatures review is tableted in Table (2-4).

Table 2-4: Summary of Literatures Review

Ref. No	The researcher, Site and year	Material		Efficiency		Remark
		PV	TEG	PV- TEG	PV	
Experimental investigations						
[44]	Wang et al. (2011) USA	Dye-sensitized solar cell	N/A	13.8 %	9.26 %	<ul style="list-style-type: none"> The hybrid system efficiency was higher by 49 % compared with efficiency of PV only
[45]	Daud et al. (2012) Malaysia	Poly-crystalline silicon	Bismuth telluride	9.064 %	5.97 %	<ul style="list-style-type: none"> Solar radiation of 868 W/m² and liquid cooling was used. Results also showed that at 868 W/m² solar radiations, prototype panel and TEG can improve efficiency up to 30 % compared with PV only.
[46]	Park et al. (2013) China	Crystalline silicon (c-Si)	Bismuth telluride	16.30 %	12.5 %	<ul style="list-style-type: none"> Hybrid system efficiency and power output increased by 30% compared to PV cells (12.5%, 50 mW).
[38]	Mohsenzadeh et al. (2017) Iran	Mono-Si 62.5 cm ² *8cell	TEC1-12706 No. 20	16.31 %	11.37 %	<ul style="list-style-type: none"> Under 1000 W/m² (thermal + electrical) efficiencies of the hybrid system with and without outer cover glass were 50.99% and 47.3% respectively. Daily average electrical and thermal efficiencies can reach 4.83% and 46.16%, respectively comparison with the photovoltaic- only system New structure for parabolic trough photovoltaic/thermal collector and receiver with a triangular channel.
[47]	Haiping et al. (2018) Chain	Double-glazing PV panel	TEG1-242-1.0-1.2-250	12.03 %	N/A	<ul style="list-style-type: none"> Parabolic concentrator and micro channel heat pipe were used.

						<ul style="list-style-type: none"> • Thermal efficiency– 45%. • PV efficiency = 11.8% • TEG efficiency = 0.23% • Overall efficiency = 57.03%
[48]	Liu et al. (2019) China	Mono crystalline 37.5 mm * 37.5mm	Bismuth Telluride	N/A	N/A	<ul style="list-style-type: none"> • Applying thermal interface material (thermal grease) with $4.2 \text{ Wm}^{-1} \text{ K}^{-1}$ enhances the heat transfer in PV-TE coupling device. • The power generation by PV cells increases at least 14% and the power generation by TEG increases at least 60% due to the decreasing thermal contact resistance.
[49]	Shittu et al. (2020) UK	Crystalline silicon (67.5cm*8.5 cm*0.2cm)	GM250-127-14-16	12.19 %	11.94 %	<ul style="list-style-type: none"> • The efficiencies of the photovoltaic-thermoelectric-micro channel heat pipe, with and without insulation compared with PV only after 1 h were 11.98%, 12.19% and 11.94%, respectively. • The average power output of the hybrid system increased from 1.86 W to 3.92 W when the solar radiation increased from 500 W/ m² to 1000 W/m².
[50]	Omar et al. (2020) Egypt	Mono-crystalline 540*670*25 (mm)	TEC1-12706	26.6% 27.2%	17.56% 18%	<ul style="list-style-type: none"> • The result of total power is increased by 20% in case 2 unsymmetrical distribution, due to the addition of TE elements. • the total power is increased by 16% in case 1 symmetrical distribution with using fans as cooling syste

Theoretical/ Numerical investigations

[51]	Sark et al. (2011) Spain	Polycrystalline silicon	Bi ₂ Te ₃	13.98 %	10.78 %	<ul style="list-style-type: none"> The value of TEG figure merit ZT =1.2 and air cooling system of TE was used. efficiency enhancements of up to 23% for roof integrated PV/TEG modules.
[52]	Najafi and K. A. Woodbury (2013) Alabama	Mono-crystalline silicon (1200*527*34) mm	Bi ₂ Te ₃	N/A	N/A	Adding 36 TEG modules to 2800(W/m ²) CPV system generates 28.398 W within a day.
[25]	Hashim et al. (2016) UK	Amorphous silicon	Bi ₂ Te ₃	10.2%	N/A	<ul style="list-style-type: none"> The passive cooling system was using, output power of (PV-TEG) Hybrid system increased to 163mW. Output power can be increased when PV-TEG is operated in vacuum
[53]	Yin et al. (2017) China	Mono-Si/ p-Si/a-Si/polymer cells (30mm*30mm)	Bi ₂ Te ₃	N/A	N/A	<ul style="list-style-type: none"> Three different cooling system were used, but the water cooling system is the best and affected for hybrid system. At low concentration, Mono crystalline silicon and Polycrystalline silicon are the suitable in hybrid system

[54]	Soltani et al. (2018) Iran	Mono-crystalline silicon	TEC1-12706	N/A	N/A	<ul style="list-style-type: none"> At a solar irradiance of 998 W/m², the electric power of the device is found to be 22.714 W. Maximum thermal efficiency is about 57% (240 W). Parabolic trough solar collector was used
[55]	Gu et al. (2019) China	Crystal silicon c-Si, Amorphous silicon a-Si, Copper indium gallium diselenide (CIGS), and	Bismuth telluride	N/A	N/A	<ul style="list-style-type: none"> Thermal resistance between the PV, TEG and TEG –cooling system was reduced by using thermal gel layer which improve the heat transfer. The (PV-TEG) hybrid system produced 1.24-2.85 % higher
Numerical and experimental investigations						
[32]	Cotfas et al. (2016) Romania	(CdTe) Mono-crystalline silicon (m-Si) Poly-crystalline silicon (p-Si) Amorphous silicon (a-Si)	Bismuth telluride	N/A	N/A	<ul style="list-style-type: none"> m-Si provided the best system performance compared to p-Si and a-Si. The temperature of the photovoltaic cell at 1000 (W/m²) irradiance was for m-Si 32.5° C, p-Si 33.1° C and a-Si 35.7°C. The maximum power gain for m-Si was 7% when irradiance was increased to 920 W/m². Heat sink from aluminum with cooling water was used
[43]	Zhu et al. (2016) China	Mono-crystalline silicon (m-Si)	Bismuth telluride	23 %	19 %	<ul style="list-style-type: none"> Hybrid (PV-TE) system efficiency increased by 25% compared to that of the PV only. An additional contribution of 648 J of electrical energy from TEG even when there is no sunlight. Copper plate as a thermal absorber was utilized. PV-TH hybrid system was putting in a closed system

[56]	Rodriguez et al. (2017) Mexico	Crystalline silicon PV array area 600 cm ²	TGM 127-1.4-2.5	14.2 %	10.7 %	<ul style="list-style-type: none"> • The system generates 7 W electric power and 30 W thermal power. • Fresnel Lens for concentrating the solar radiation was used.
[57]	Mahmoud inezhad et al. (2018) Iran	GaInP/GaInAs/Ge	Bismuth Telluride	36.35 %	35.33 %	<ul style="list-style-type: none"> • Max. CPV efficiency: 35.33% (8 suns) • Min. CPV efficiency: 23.02% (37 suns). • Max. TEG efficiency: 1.20% (37 suns). • Min. TEG efficiency: 0.63% (8 suns). • Xenon lamp solar simulator and cooling water system were used. • the maximum power of CPV in the experiments for 8 suns and 37 suns were obtained 0.283 W and 0.852 W respectively, while for numerical simulation were 0.314 W and 0.902 W. • the maximum power generation by the TEG for 8 suns and 37 suns were obtained 2.43 mW and 2.89 mW experimentally respectively, while for numerical simulation were 24.1 mW and 25.6mW, respectively.
[58]	Lashin et al. (2020) Saudi Arabia	GaInP/GaInAs/Ge triple-junction (1cm*1cm)	GM250-31-28-12 GM200-127-14-10 GM200-49-45-25	N/A	N/A	<ul style="list-style-type: none"> • The (CPV-TEG) Hybrid system was Compared to using only the CPV on a heat sink. • The power generated by the CPV/TEG hybrid system was increased by 7.4%, 5.8%, and 3% using the 30*30 mm²,40*40 mm²andthe 62*62 mm²TEG modules respectively. • Xenon Arc Lamp and Heat Sink/ Passive cooling was used. • The sample B (TEG with 4-cm

					side length) showed the highest output voltage at both high and low concentrated light level.
[59]	Riahi et al. (2020) Tunisia	Mono-crystalline (10 cm*10 cm)	TEC1-12706	15% N/A increased	<ul style="list-style-type: none"> • Electrical efficiency = 7.27% (7.46% higher compared with CPVT system). • Heat exchanger with water and Parabolic trough were used.
	Present Work Iraq/ Kerbala	Mono-crystalline (51 cm*68 cm)	TEC1-12715	6.2% 4.5% 5.83% 4.2%	<ul style="list-style-type: none"> • Thermal absorber (aluminum plate) was used • Thermal grease to reduce the thermal resistance between the PV,TEG and TEG –cooling system was used. • Active cooling system (Shell and Tube heat exchanger) was used. • Four solar simulators (Halogen projector) with 1000 (W/m²) solar intensity was used. • Optimum model of hybrid system was S4 model • Numerically, the electrical output power of the hybrid system was higher by 36.94% and 16.8% than that PV panel and PV/T system. • Experimentally, the electrical output power of the hybrid system was higher by 31.66% and 16.5% than that PV panel and PV/T system.

2.5 Summary

The present work deals with the following area of research which represent the gap of interest:

1. Testing the possibility of coupling the TEG modules with large dimensions photovoltaic panel as (PV-TEG) hybrid system.
2. Investigating the optimum number and distribution of thermoelectric modules (TEG) that must be integrated with the photovoltaic panel in the hybrid system to harvest the wasted heat and achieve more power output.
3. Using appropriate and affective cooling system.
4. Studying the effect of different values of solar radiation intensity from the value of 1000 (W/m²) upwards on the (PV-TEG) hybrid system performance.

2.6 Scope of the present work

1. Numerically, testing four configurations of (PV-TEG) hybrid system are called:
 - I. S1 model: hybrid system consists of integrating the photovoltaic panel with 204 items of TEG module (full covered).
 - II. S2 model: hybrid system consists of integrating the photovoltaic panel with 94 items of TEG module (partially covered in the vertical arrangement).
 - III. S3 model: hybrid system consists of integrating the photovoltaic panel with 85 items of TEG module (partially covered in the horizontally arrangement).
 - IV. S4 model: hybrid system consists of integrating the photovoltaic panel with 50 items of TEG module (partially covered in the matrix arrangement).

The reason for choosing the previous numbers and distributions to

ensure that the distance between the thermoelectric module and the last one is the same distance in each test model in line with a decrease in the number of thermoelectric modules and thus the distribution of heat transmitted from the back surface of the solar cell is equal on the hot sides of the thermoelectric modules.

2. Design and manufacturing a cooling system (heat exchanger).
3. The performance of an optimal model for hybrid system will be compared with a simple PV system alone and PV with a heat exchanger (PV/T) system numerically and experimentally, under the same environmental and boundary conditions using an efficient cooling system.

**Chapter Three: Mathematical Model, Numerical
Simulation, and Models Optimization**

Chapter Three

Mathematical Model, Numerical Simulation, and Models Optimization

3.1 Introduction

This chapter is divided into four main sections: the first section includes mathematical equations which governing the heat transfer through the photovoltaic- thermoelectric hybrid system. The second section presents numerical analysis of the conceptual design of the hybrid system photovoltaic-thermoelectric with a heat exchanger (PV-TEG). To investigate temperature distribution on different layers of the proposed system, four design models with different distribution and number of thermoelectric modules have been numerically simulated. Moreover in the third section, the details of (Data Reduction) formulas have been used for calculating electrical power and efficiencies of proposed hybrid systems based on numerical simulation results. Finally, the fourth sections discussed determining the optimum model of the hybrid system.

3.2 Mathematical model

This section shows the governing equations of the heat transfer in the PV/T and PV -TEG hybrid systems. These equations are the continuity, momentum, and energy equations. But before that, the physical model description, operation, and assumptions that need to be laid out first.

3.2.1 Physical model description and operation

In the current study, three-dimensional numerical models have been developed to investigate the thermal performance of PV, PVT, and PV-TEG systems. Figure (3-1) depicts the conceptual model of PV-TEG model. The only difference between the PV-TEG and PVT systems is the absence of the TEG module layer in the PVT system. The (PV-TEG) hybrid system consists of Mono-crystalline silicon photovoltaic (m-Si) PV cells. PV cells are attached to

the top of thermoelectric generator TEG modules (the hot side) via a conductive plate from Aluminum to transfer the heat from the PV panel to the hot side of the TEG as well as a heat exchanger (shell and tube water collector) with cooling water under the cold side of TEG to increase the temperature difference between the hot and cold sides of the TEG.

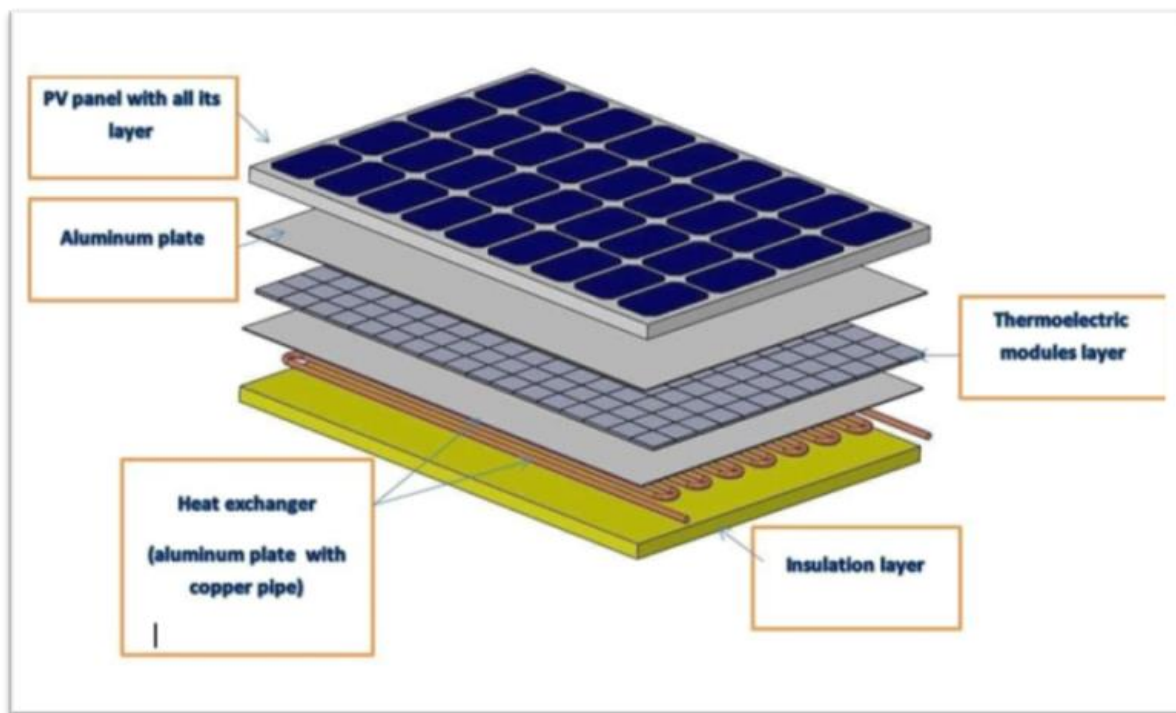


Figure 3-1: Simulated PV -TEG hybrid System

During operation, $1000 \text{ (W/m}^2\text{)}$ of solar irradiation strikes the upper surface of the photovoltaic module, so one portion of the solar energy is converted to electricity by PV; another portion is lost to the environment such as through radiation and convection from the glass layer, and the remaining heat is transferred to the TEG module via heat conduction. Finally, the Seebeck effect converts a portion of the thermal energy absorbed by the TE module to electricity. At the same time, the heat exchanger removes the majority of the heat from the working water that flows through it. Figure (3-2) illustrates the energy pathway for the simulated PV-TEG system.

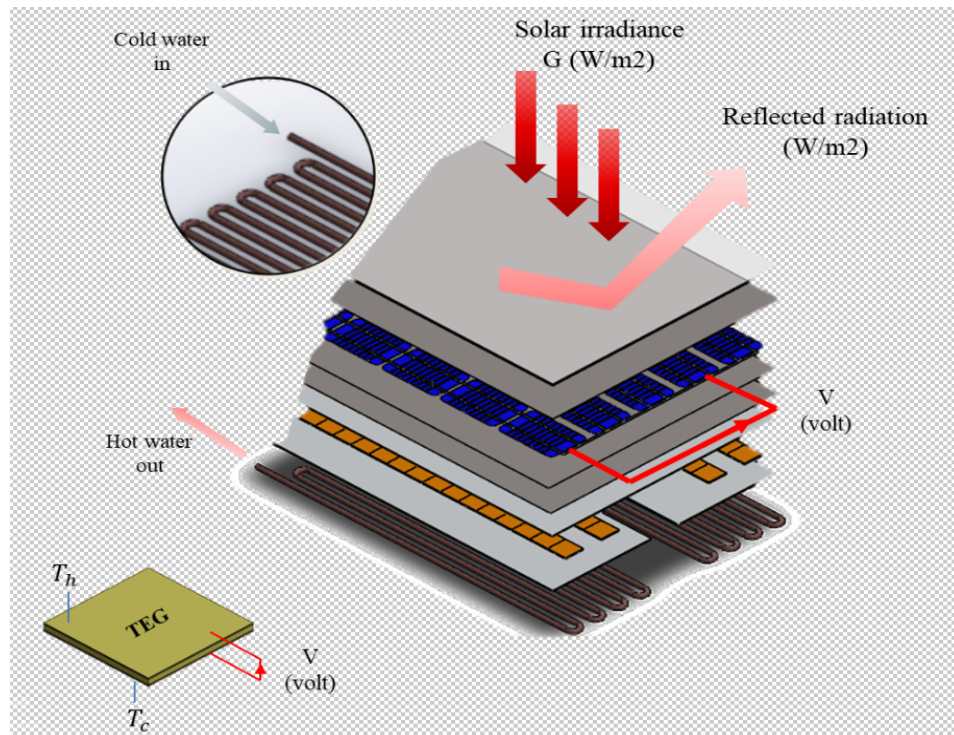


Figure 3-2: Illustrates the energy pathway for the simulated PV-TEG system.

3.2.2 Assumption

In this study, a hybrid system is more complicated than a PV-alone and PV/T system. For simplicity, the following assumptions are adopted in numerical simulation and data reduction:

1. The transmissivity of ethyl vinyl acetate (EVA) is approximately 100%.
2. No dust on surface will affect solar energy absorptivity.
3. The simulation is performed based on three dimension and steady-state heat transfer process. The heat flux and temperature values are uniform on the surface at the same height and considered only in the flow direction
4. Sides and backside heat losses are negligible, the heat is transfer only in the normal direction.
5. Properties of cooling water and solid material are constant.
6. There is no thermal gradient in the glue layers(thermal paste) because their thickness is very thin, and their thermal conductivity is high.

7. Physical parameters and properties of the materials in the TE module are taken as constant and independent of temperature.
8. The contact thermal resistance between the adjacent layers in the systems are negligible
9. The bottom side of the absorber tube is assumed to be adiabatic, so the thermal radiation loss between the heat exchanger and the ground is zero.
10. Constant fluid (water) properties, incompressible, fully developed, and turbulent flow according to the Reynolds Number as given:

$$Re = \frac{\rho V D}{\mu} \quad 3-1$$

Where ρ is the water density(kg/m³), μ is the water dynamic viscosity (N.s/m²), D (m) is diameter of pipe, and V is the water velocity(m/s). Re for pipe flow may be expressed as [60]:

$$Re = \frac{4 \cdot \dot{m}}{\pi D \mu} \quad 3-2$$

- I. At $Re < 2000$ is Laminar flow
- II. At $2000 < Re < 4000$ is Unstable flow
- III. At $Re > 4000$ is Turbulent flow.

At 5 (l/min), temperature of water 20 (°C), $\mu = 1.0016 \cdot 10^{-3}$ (N.s/m²), and $D = 1.27$ (cm), the $Re = 8345 > 4000$. So, the water flow is turbulent at selected volume flow rate value is about 7(l/min),

3.2.3 Governing equations

The respective governing equations employed for both the PVT and PV-TEG systems for turbulent flow are solved at a steady-state [61] [62] as follows:

I. Continuity equation

$$\frac{\partial}{\partial x} \rho u + \frac{\partial}{\partial y} \rho v + \frac{\partial}{\partial z} \rho w = 0 \quad 3-3$$

Where ρ is the fluid density, the velocity of the fluid at any position inside the flow of the field was described with the local velocity components (u, v, and w), generally functions for space x, y, and z, respectively.

II. Momentum equation :

From Newton's Second Law of Motion, the momentum equations have been derived, involving the balance of the sum of the forces acting on the fluid element. These forces are equal the product between the acceleration and mass of fluid element. By employing Newton's Second Law on 3-dimensional fluid elements and balancing the forces in all three directions, the following equations were obtained

X – Component

$$\rho \left(u \frac{\partial u}{\partial x} + v \frac{\partial u}{\partial y} + w \frac{\partial u}{\partial z} \right) = \rho f_x - \frac{\partial p}{\partial x} + \mu \left(\frac{\partial^2 u}{\partial x^2} + \frac{\partial^2 u}{\partial y^2} + \frac{\partial^2 u}{\partial z^2} \right) \quad 3-4$$

Y – Component

$$\rho \left(u \frac{\partial v}{\partial x} + v \frac{\partial v}{\partial y} + w \frac{\partial v}{\partial z} \right) = \rho f_y - \frac{\partial p}{\partial y} + \mu \left(\frac{\partial^2 v}{\partial x^2} + \frac{\partial^2 v}{\partial y^2} + \frac{\partial^2 v}{\partial z^2} \right) \quad 3-5$$

Z – Component

$$\rho \left(u \frac{\partial w}{\partial x} + v \frac{\partial w}{\partial y} + w \frac{\partial w}{\partial z} \right) = \rho f_z - \frac{\partial p}{\partial z} + \mu \left(\frac{\partial^2 w}{\partial x^2} + \frac{\partial^2 w}{\partial y^2} + \frac{\partial^2 w}{\partial z^2} \right) \quad 3-6$$

The previous equations show the conservation of momentum in a fluid flow and also known as equations of Navier-Stokes [63].

III. Energy equation:

The first law of thermodynamics exhibits the exchange of energy for a system which is the result of applied work and heat transfer through that region. In its most complete formulation, the energy equations are given as [64]. To calculate the energy transfer, equation (3-3) can be simplified in partial differential forms as follow: -

$$\left(\frac{\partial(\rho u_i T)}{\partial x_j} \right) = \frac{\partial}{\partial x_i} \left[(\Gamma + \Gamma_t) \frac{\partial T}{\partial x_j} \right] \quad 3-7$$

Where, Γ = molecular thermal diffusivity

Γ_t = turbulent thermal diffusivity

IV. The turbulence model

The most generally used turbulence model for engineering simulation is the standard $k-\varepsilon$ turbulence model. The $(k-\varepsilon)$ model was based on the Boussinesque approximation of the Reynolds turbulent stresses. The turbulent eddy diffusivity is expressed in turbulence parameters k and ε . Two additional scalar transport equations, one for the turbulent kinetic energy k and the other for the turbulence dissipation ε , are solved to model the turbulence effects. The eddy viscosity of this model is obtained as [65]:

$$\mu_t = \rho C_\mu \frac{k^2}{\varepsilon} \quad 3-8$$

$$\nabla \cdot \left(\rho k \mathbf{V} - \frac{\mu_t}{\partial k} \nabla K \right) = P - \rho \varepsilon \quad 3-9$$

$$\nabla \cdot \left(\rho \varepsilon \mathbf{V} - \frac{\mu_t}{\partial \varepsilon} \nabla \varepsilon \right) = C_1 P - C_2 \rho \frac{\varepsilon^2}{k} \quad 3-10$$

where P is the usual Reynolds stress turbulence production term given as:

$$P = \mu_t \left[2 \left(\left(\frac{\partial u}{\partial x} \right)^2 + \left(\frac{\partial v}{\partial y} \right)^2 + \left(\frac{\partial w}{\partial z} \right)^2 \right) + \left(\frac{\partial u}{\partial y} + \frac{\partial v}{\partial x} \right)^2 + \left(\frac{\partial u}{\partial z} + \frac{\partial w}{\partial x} \right)^2 + \left(\frac{\partial v}{\partial z} + \frac{\partial w}{\partial y} \right)^2 \right] \quad \dots \quad 3-11$$

C_μ , C_1 , and C_2 are constants. ∂k and $\partial \varepsilon$ are effective Prandtl numbers for turbulent kinetic energy and rate of dissipation, respectively [66].

3.3 Numerical simulation

This section describes numerical simulation for the following proposed systems: traditional photovoltaic, photovoltaic /thermal, and photovoltaic-thermoelectric hybrid systems. Solving the continuity, momentum, and energy equations allows one to analyze the temperature distribution of the various PV panel layers, both sides of the TEG, and the heat exchanger under the forced turbulent convection flow of water flowing inside a straight, circular tube with uniform axial velocity, temperature, and heat flux. Building the software (its

structure or sections) is also shown. The ANSYS division responsible for commercial applications of computational fluid dynamics (CFD) (version 2021 R1 of Workbench), is used to gain from the comparison [67]. This software is selected in the current work because such software gives more precise results and is nearer to the experimental results.

Firstly, The goal of isolated heat exchanger testing under varying water flow rates is to identify the flow rate at which the heat exchanger's surface temperature remains constant. Secondary, the temperature distribution is analyzed for the photovoltaic panel and (PV/T) collector system. Finally, the hybrid system is analyzed in four stages (S1, S2, S3, S4) in the following order under the same boundary conditions and tested water flow rate value.

1. Photovoltaic system (PV) only.
2. Photovoltaic-Thermal (PV/T) system.
3. Photovoltaic-Thermoelectric (PV -TEG) hybrid system:
 - **S1 model:** The hybrid system of (PV + 204 items of TEG modules Full covered the backside of the PV module
 - **S2 model:** The hybrid system of (PV + 94 items of TEG modules with Vertically arrangement covered the backside of PV module)
 - **S3 model:** The hybrid system of (PV + 85 items of TEG modules with Horizontally arrangement covered the backside of PV module)
 - **S4 model:** The hybrid system of (PV + 50 items of TEG modules with matrix arrangement covered the backside of the PV module).

The thermal modeling of photovoltaic, photovoltaic/thermal, and photovoltaic-thermoelectric hybrid systems were conducted via alternating steps. Steps can be arranged as a geometrical domain, meshing, setup and

solution methods.

3.3.1 Geometric domain

Solid work version 2021 has been utilized to modeling 3D domain of the solar PV panel, PV/T, and PV-TEG systems that are modeled with control volumes built around each grid. All the simple and complex geometric shapes are presented in this section. Firstly, the x-y plane is chosen to design the test model. After that, an extrude order is applied to obtain the three-dimensional structure of the test model, which was preprocessor for FLUENT (version 2020 R1) in the ANSYS workbench program.

The geometric dimensions of the test models are the same as the dimensions of the experimental rig as shown in the Table (3-1) [68] [57][60]. The 3D geometric models of the three systems are shown in figure(3-3), figure(3-4), and figure (3-5) (a, b, c and d).

Table 3-1: Geometrical dimensions of the PV Panel, TEG module, and the heat exchanger system [68] [57] [60]

Parameters	Dimensions (m)
PV panel	
Top Glass Layer	0.510 x 0.680 x 0.003
EVA Layer	0.510 x 0.680 x 0.0005
PV Cell Layer	0.510 x 0.680 x 0.0003
EVA Layer	0.510 x 0.680 x 0.0005
Tedlar Layer	0.510 x 0.680 x 0.0005
Thermal Concentrator(Conductive Plate)	0.500 x 0.680 x 0.002
TEG Module	
Ceramic	0.040 x 0.040 x 0.0005
Thermoelectric Element (P-N) 127 Pair	0.040 x 0.040 x 0.002
Ceramic	0.040 x 0.040 x 0.0005
Heat Exchanger (Sheet and Tube)	
Aluminum plate (absorber)	0.500 x 0.680 x 0.002
Copper pipe	
Length	9.660
Diameter	0.0127
Thickness of pipe	7.2×10^{-4}

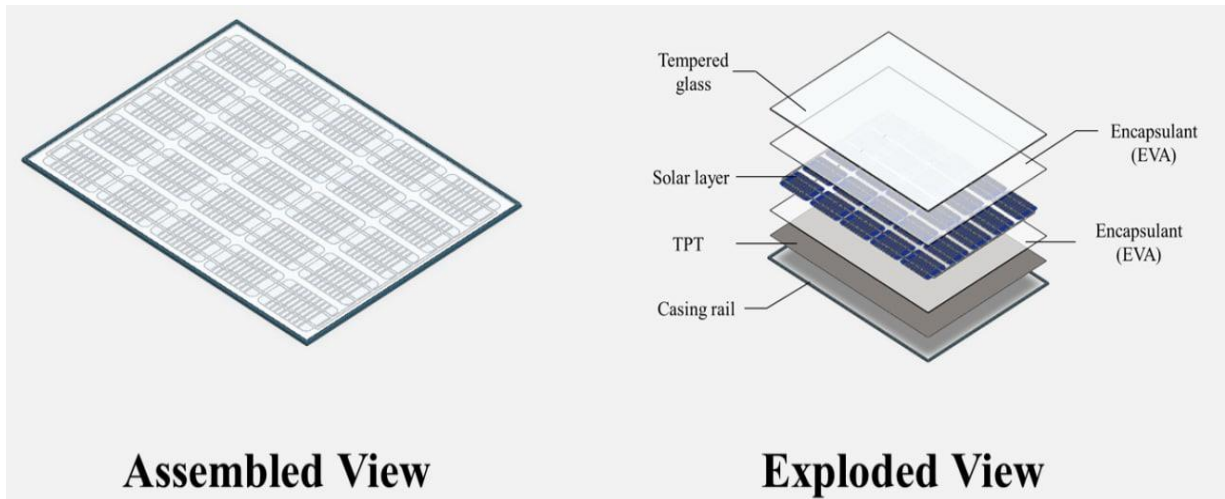


Figure 3-3: The 3D geometric model of photovoltaic system only

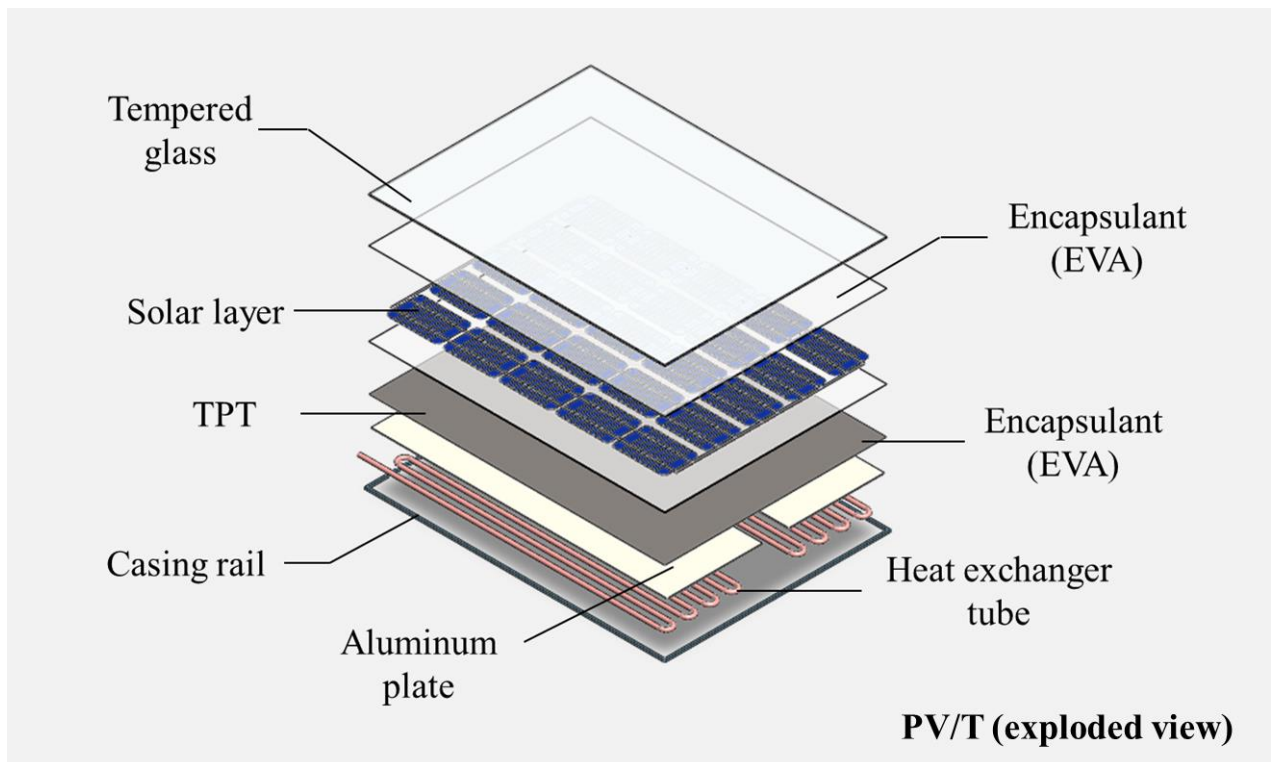
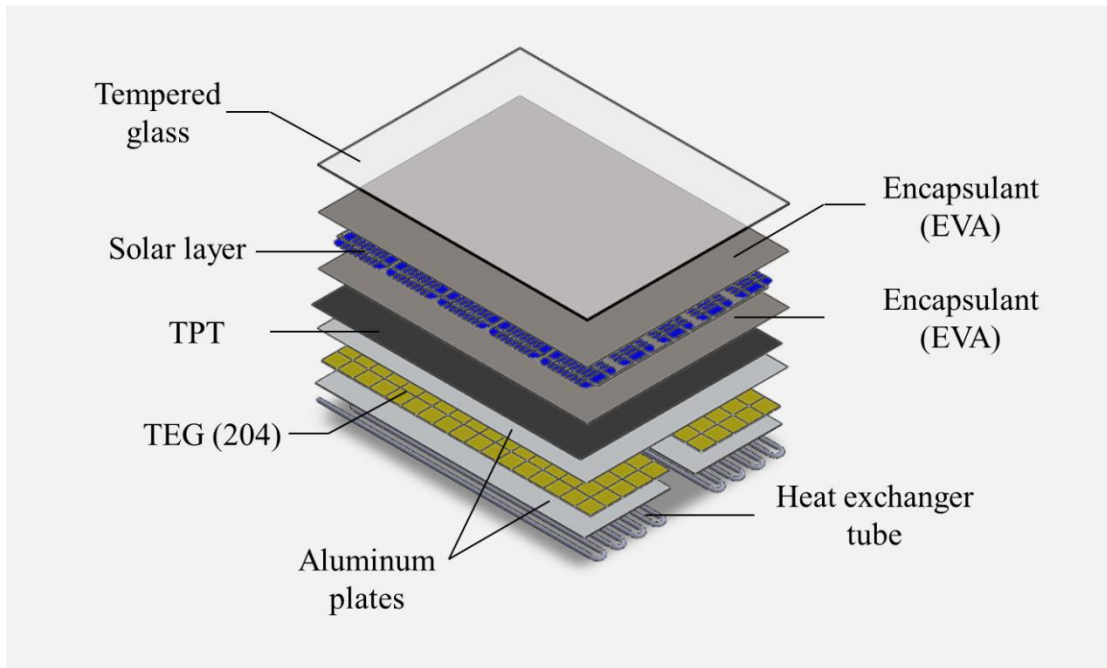
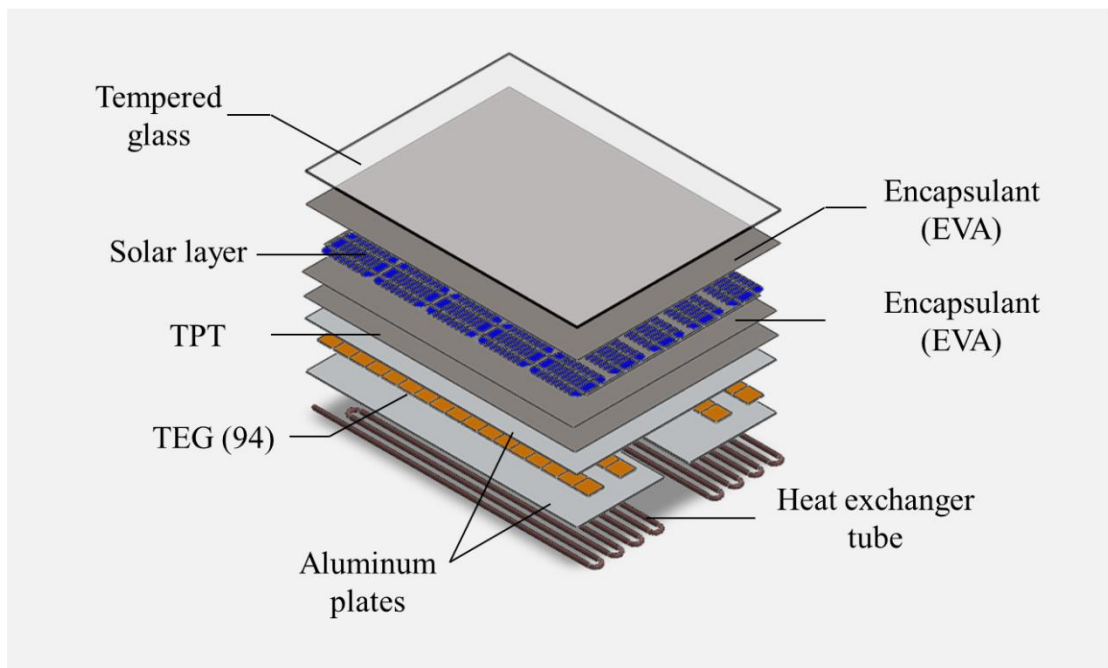


Figure 3-4: The 3D geometric model of photovoltaic/Thermal (PV/T) System

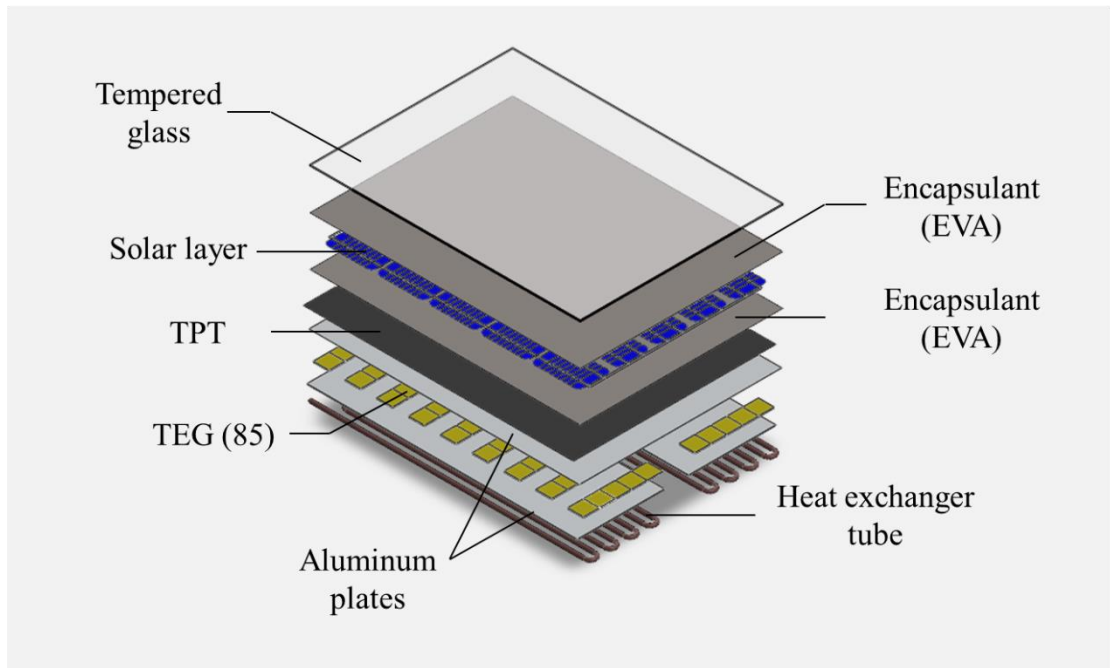


(a) The S1 model of the PV -TEG hybrid system

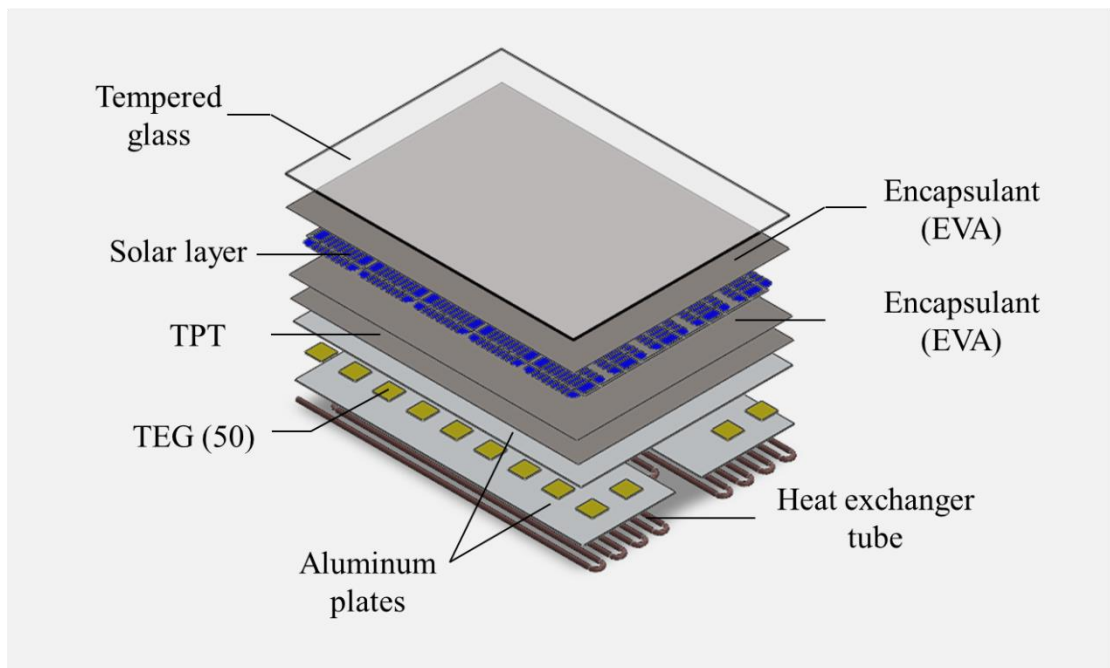


(b) The S2 model of PV -TEG hybrid system

Figure 3-5: 3D Geometric model of : (a) S1, (b) S2, (c) S3, and (d) S4 PV-TEG Hybrid System



(c)The S3 model of PV -TEG hybrid system



(d)The S4 model of the PV-TEG

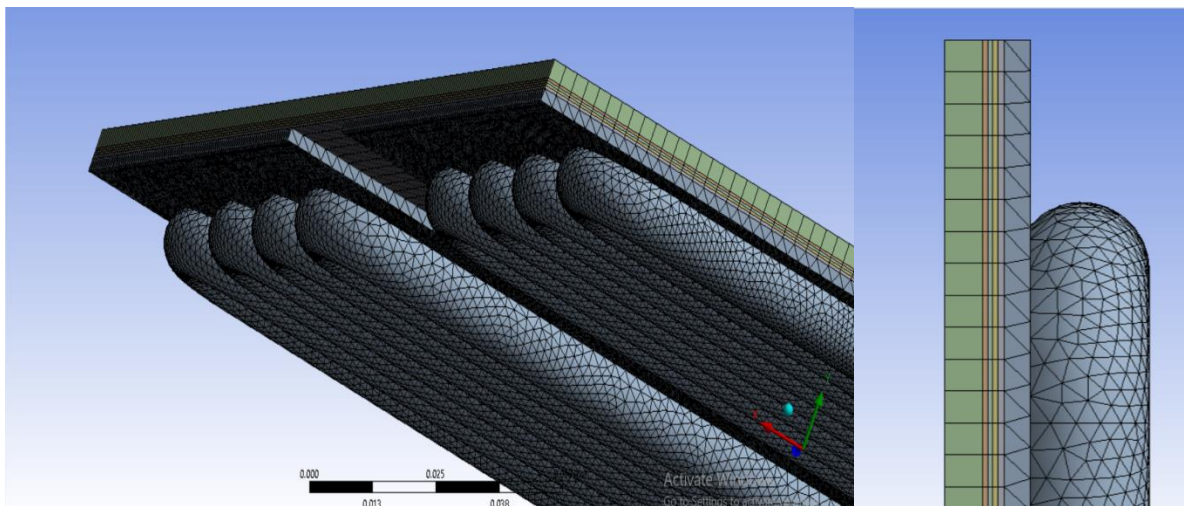
Figure 3-5: Cont.

3.3.2 Mesh generation

Meshing can be defined as a process to divide a geometry into number of elements and nodes. Therefore, when load is applied on the geometry, the load can be distributed uniformly on the geometry. As the number of elements and nodes increases (i.e., the elements become smaller), so does the time required to provide an accurate result. The hexahedral elements of fine size and patch conforming method are employed to create a good quality mesh for each PV layer, the TEG layers, and both the absorber plates between the PV panel and the TEG modules and in heat exchange. In contrast, the tetrahedral mesh is probably the most applicable material regarding the mesh quality of the copper tubes in the heat exchanger [69]. Generating the correct computational mesh for the domain under analysis was of paramount significance in fluent simulations. Therefore, the size of the mesh in the domain should be step by step increased to such level that the additional increase in the number of control volumes does not result in considerable changes in the theoretical results produce [67]. Table (3-2) lists the number of elements, and nodes which are presented in this study. The volume of mesh for the PV/T system, S1, S2, S3, and S4 hybrid systems respectively as shown in figure (3-6).

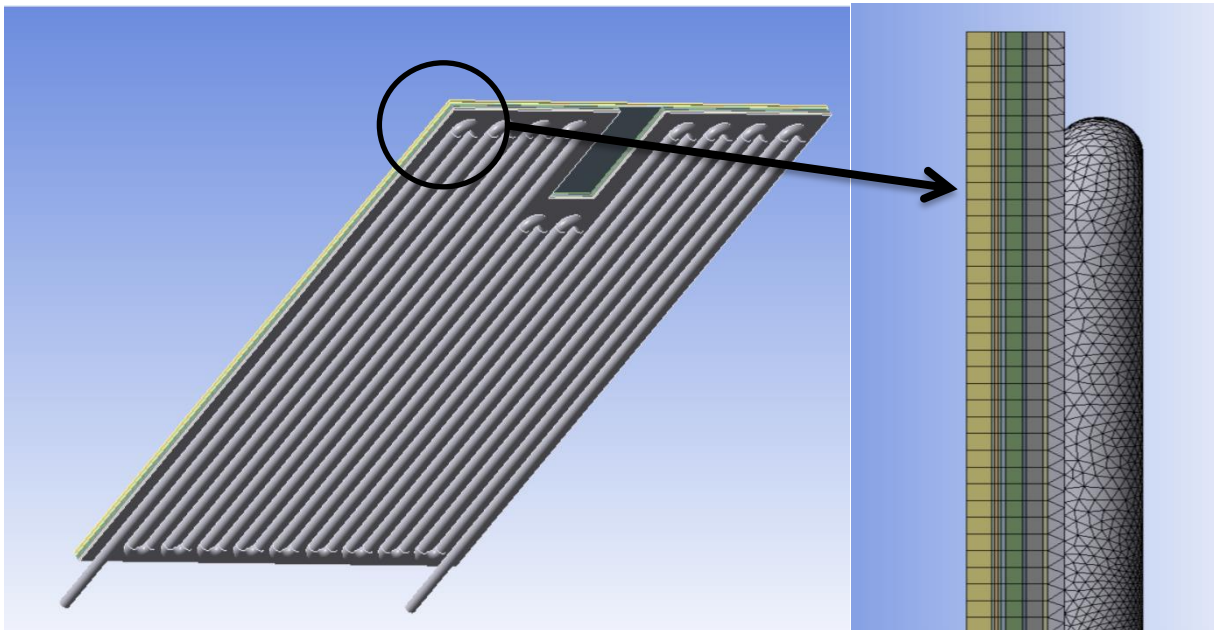
Table 3-2: Mesh settings

Setup	Specifications
Preference of Physics	CFD
Preference of Solver	Fluent
Rate of Growth	Default (1.2)
Element size	2.5mm
Maximum Size	2.5 mm
The S4 model of the hybrid system	
Element	Hexahedral & Tetrahedral
No. of Element	2855035
No. of Nods	8038811

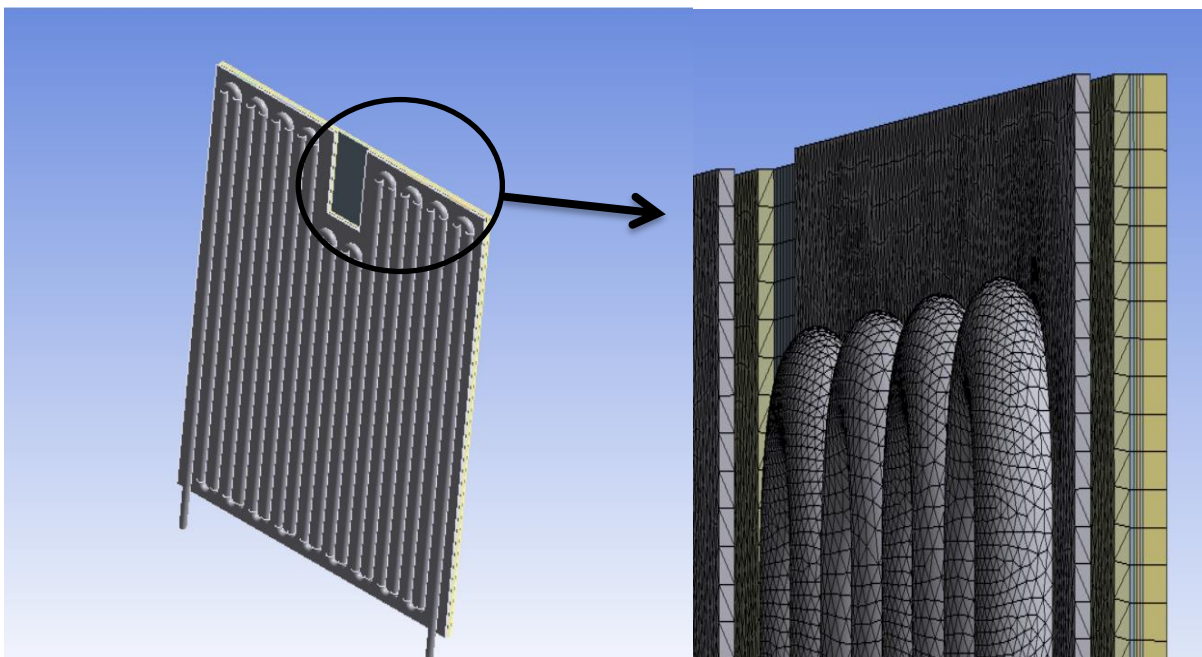


(a) 3D mesh of the PV/T System

Figure 3-6: Schematic of the generated 3D mesh of (a) PV/T system, (b) S1 model of (PV –TEG) hybrid system, (c) S2 model of (PV –TEG) hybrid system, (d) S3 model of (PV –TEG) hybrid system and (e) S4 model (PV –TEG) hybrid system

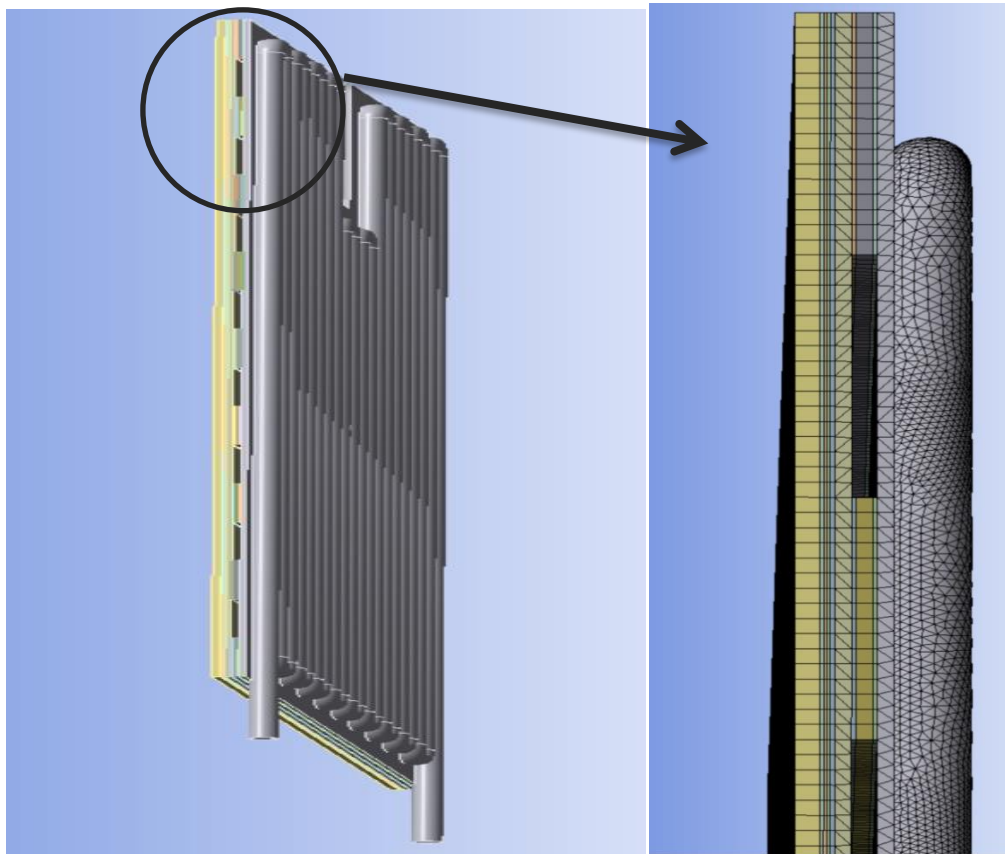


(b)3D mesh of the S1 model of PV -TEG Hybrid System

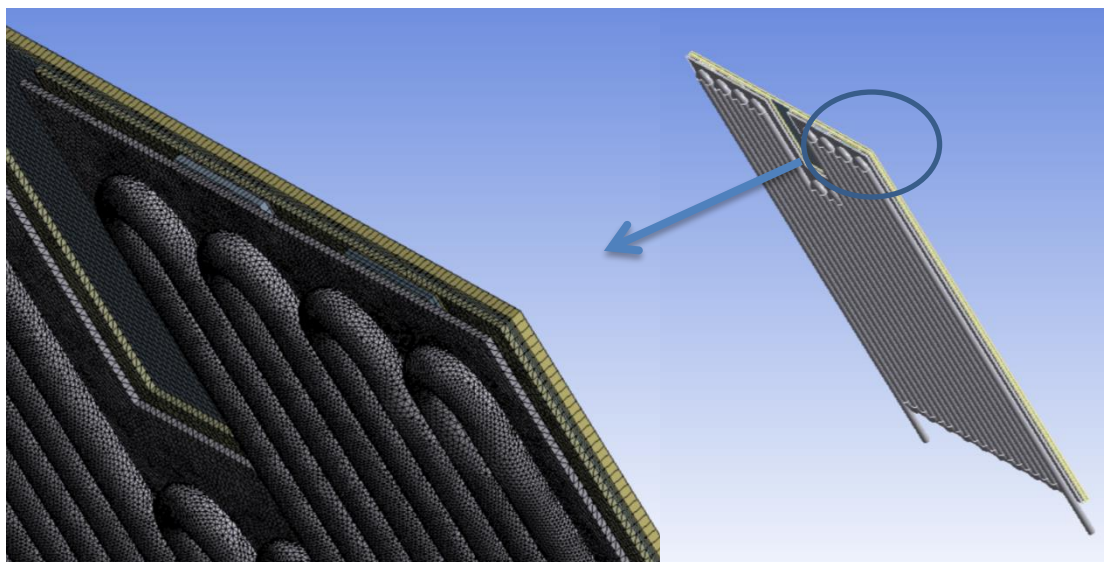


(c)3D mesh of the S2 model of PV -TEG Hybrid System

Figure 3-6: Cont.



(d) 3D mesh of the S3 model of PV -TEG Hybrid System



(e) 3D mesh of the S4 model of PV -TEG Hybrid System

Figure 3-6: Cont.

3.3.3 Setup and solution

3.3.3.1 Boundary conditions and operating parameters

The inlet boundary conditions specified as inlet volume flow rate of water, inlet water temperature, ambient temperature, and the heat flux. The outflow boundary condition is applied at the outlet. Wall boundary conditions are used to bound fluid and solid regions. The interface between the water and the copper pipes defined as the wall with a coupled condition to affect the conjugate heat transfer from the absorber pipe to the water.

The side surfaces the PV panel only, other layers and bottom surface of the hybrid systems are defined as the wall with a zero heat flux condition to affect the insulated condition. The input parameters used in the analysis are thermo physical properties of the simulated PV-TEG systems as shown in Table (3-3) and the boundary conditions detail in Table (3-4).

Table (3-3) Thermo physical properties of the simulated PV-TEG systems [9] [59].

Layer	Heat capacity, C_p [J/ (kg.K)]	Density, ρ [kg/m ³]	Thermal conductivity, k [W/ (m.K)]
Glass	500	2450	0.98
EVA	2090	960	0.23
Silicon	677	2330	148
TPT	1250	1200	0.36
Water	4180	998.2	0.61
Ceramic	880	3720	25
Bi ₂ Te ₃ (p-n)types	708.4	92.74	0.92
Aluminum	871	2719	202.4
Copper	385	8960	400

Table 3-4: Boundary conditions in detail

Boundary	Type	Boundary condition
Inlet	Inlet water temperature Volume flow rate	$T_{in \text{ water}} = 20 \text{ C}^\circ$ $=7 \text{ (l/min)}$
	Ambient Temperature	$T_{amb} = 28 \text{ C}^\circ$ Flow Direction: Normal to Boundary
Exit	Temperature-out let	$T = T_{out} = 21 \text{ C}^\circ$
Upper wall	Heat flux (G) Wind Speed(\mathbf{v}) Heat transfer coefficient of the ambient	Heat flux rang (1000 W/m^2) $\mathbf{v} = 0 \text{ (m/s)}$ $h_{amb} = 5.7 + 3.8\mathbf{v}$ if $\mathbf{v} < 5$
Other Wall	Wall	Constant heat flux: $q=0$

3.3.3.2 Solution method and checking for convergence

To solve the energy equation, the finite volume method is employed.

The following are used in the solution method [70], [71]:

- Pressure-velocity coupling: ***SIMPLE***
- Pressure interpolation scheme: ***standard***
- Up winding schemes for Momentum, Turbulence Kinetic Energy, Turbulence Dissipation Rate and Energy: ***Second-Order Upwind***.

The Monitoring of the residuals method is used for convergence of the solution. Convergence will happen when the Convergence Standard for each variable is reached. The residuals set to 10^{-4} and 10^{-7} are satisfied; the solution is said to be converging.

Figure (3-7) shows that all the scaled residuals are below 10^{-4} and 10^{-7} .

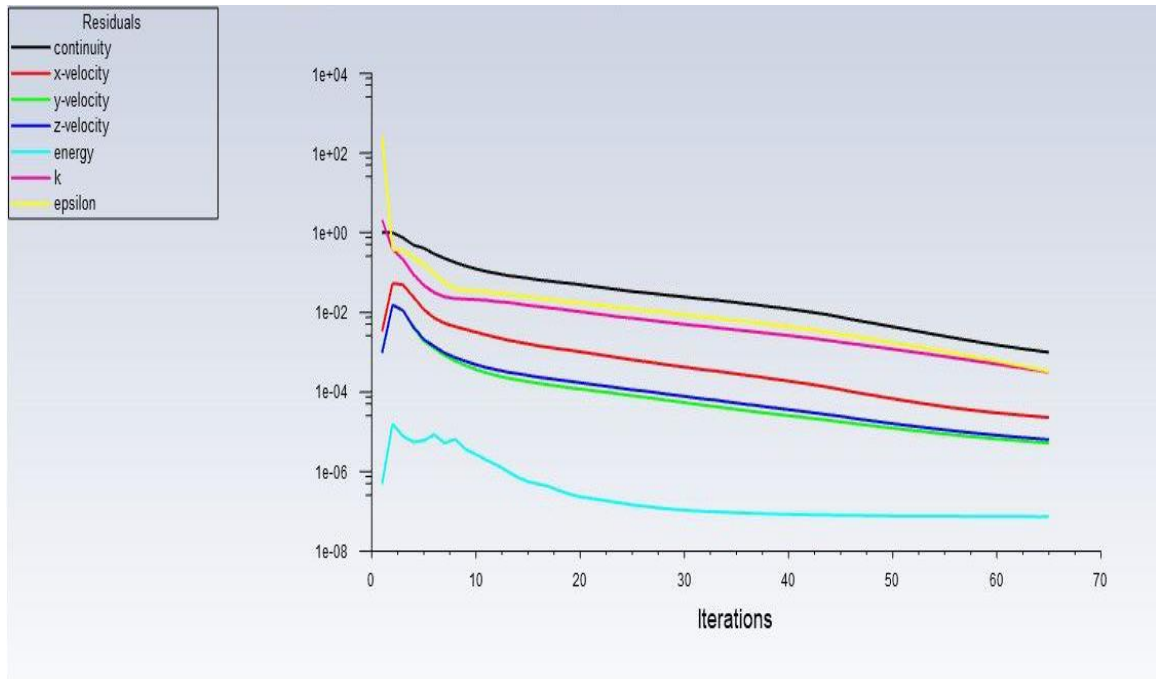


Figure 3-7: Convergence history to solve discrete conservation equations

3.3.4 Flow chart of computational model

Figure (3-8) shows a flow chart of steps of computational model construction by using the 2021 R1 version of ANSYS software to simulate the photovoltaic panel with thermoelectric generator modules as a hybrid system.

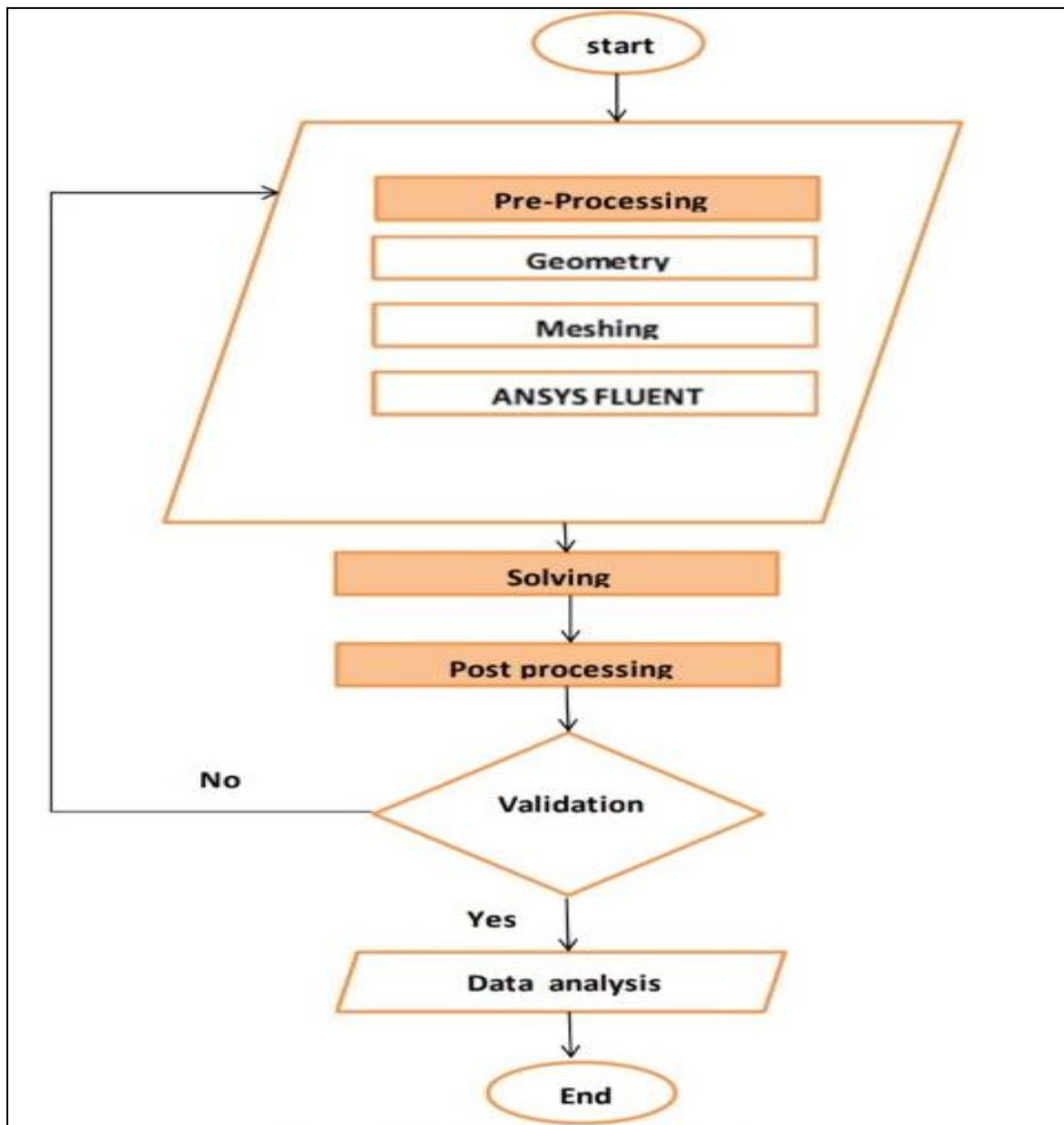


Figure 3-8: The Schematic diagram of flow chart of steps of computational model construction by using ANSYS-FLUENT software.

3.4 Data reduction

After the numerical simulation is completed, contour diagrams of temperature can be plotted. From the contour diagrams, temperature of every spot on the selected surfaces can be reviewed. Based on substituting the average temperature values of the PV surface, hot and cold TEG sides, the solar radiation level, and the specific parameters in the Table (3-5) in the following principles of data reduction, the PV efficiency and power output can be predicted in each the PV only, the PV/T system and S1, S2, S3, S4 hybrid systems.

By taking the entire PV-TEG system as a control volume, the system energy balance can be expressed as depicted in figure (3-9).

Table (3-5) Specific parameters are used in the calculations [25][57]

Parameter	Value (Unit)
τ_E	0.95
G	1000 (W/m ²)
β_0	0.0041 (K ⁻¹)
η_0	6%
α	1.85*10 ⁴ (VK ⁻¹)
ρ	1*10 ⁻⁵ (Ω .m)

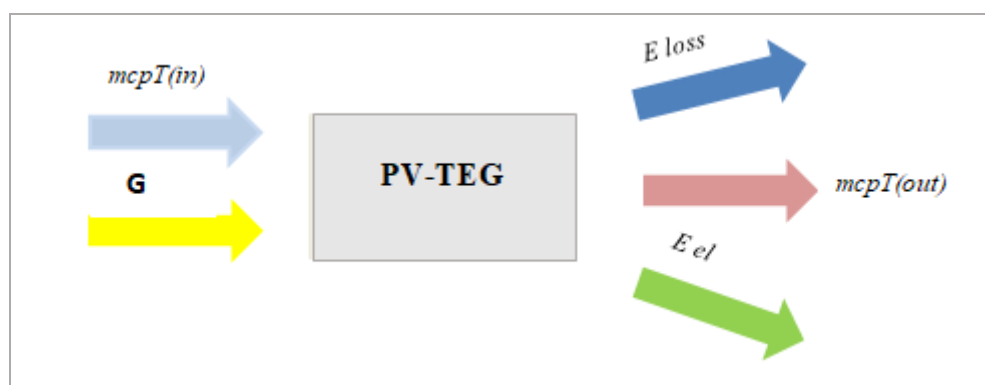


Figure 3-9: PV-TEG control volume

G, E loss and Eel denoted the rate of the input solar radiation, loss energy, and the overall generated electricity. Moreover, m.cp (in) and m.cp (out) refer to the water mass flow rate, T_{in} and T_{out} temperature of water at the inlet and

outlet of copper pipe, respectively. The input solar radiation (G) to the PVT and PV -TEG systems is $1000 \text{ (W/m}^2\text{)}$, and the solar panel output power (P_{PV}) is given [72]:

$$P_{PV} = G \cdot A_{pv} \cdot \tau_g \cdot \eta_{pv} \quad 3-12$$

Where A_{pv} and τ_g are the area of photovoltaic panel and transmittance coefficient of glass, respectively. The electrical efficiency of solar panel (η_{pv}) is given [25]:

$$\eta_{pv} = \eta_0 [1 - \beta_0 (T_{sc} - 298)] \quad 3-13$$

The TEG conversion efficiency, η_{TEG} , can be found by [62]:

$$\eta_{TEG} = \frac{T_h - T_c}{T_h} \frac{\sqrt{1 + ZTM} - 1}{\sqrt{1 + ZTM} + \frac{T_c}{T_h}} \quad 3-14$$

Where $Z = \frac{\alpha^2}{\rho \cdot K}$, TM is the mean temperature $TM = \frac{T_h + T_c}{2}$ across the TEG module [9]. After substituting the value of Z and TM in equation (3-14), The output power of the TEG is (P_{TE}) can be calculated [73]:

$$P_{TEG} = Q_k * \eta_{TEG} \quad 3-15$$

where Q_k denotes the heat transfer rate through the TE module, and is given by [9] [25]:

$$Q_k = \frac{M \cdot K \cdot A_{TE} \cdot N (T_h - T_c)}{L_{TE}} \quad 3-16$$

Where M is the number of TEG modules, the thermal conductivity of the TE is k , A_{TE} is the area of thermoelement, N is the pair number of thermoelements, and L_{TE} is the length of thermoelements.

So, the total output power of the hybrid system E_{el} , that is obtained by using [57]:

$$E_{el} = P_{PV} + P_{TEG} \quad 3-17$$

The total electrical conversion efficiency (η_{el}) of the (PV-TEG) coupled system is given [74] [36]:

$$\eta_{el} = \frac{P_{PV} + P_{TEG}}{A_{PV} * G} \quad 3-18$$

3.5 Models optimization

Based on the analysis of numerical simulation of four PV-TEG hybrid system (S1, S2, S3, and S4) models, as well as other tested models of hybrid system that will be presented in subsequent chapters, the S4 model is the optimum hybrid system. The suitable number and distribution of thermoelectric modules in the S4 model achieved the largest temperature difference between both sides of the thermoelectric modules layer compared to other tested models. Because of TEG modules electrical energy is direct proportional to the temperature difference, total generated power in the hybrid system increases. So, the optimum model (S4 model) would be investigated experimentally.

3.6 Summary

In the current study, the three-dimensional geometry of all test models was drawn using the SOLID WORK 2021 program and then exported to FLUENT code. Governing equations were solved using FLUENT R1 2021 finite volume technique. The hexahedral and tetrahedral mesh were employed for gridding the geometry and the refined region close to the wall by using a high density mesh. The mesh then smoothed utilizing smoothing algorithms obtainable in FLUENT and then selecting boundary conditions. The flow had been solved for a chosen number of iterations until taking convergence. The optimization model of tested hybrid systems was S4 Model (PV- 50 items of TEG device).

Chapter Four: Experimental Work

Chapter Four

Experimental Work

4.1 Introduction

This chapter explains the design and the construction of an experimental rig to study the performance of the optimum model of PV-TEG hybrid system. Performance of the proposed system (S4 model) has been compared with that the PV traditional system and the PV/T system. The experimental rig test stages were carried out under indoor exposure within the laboratory conditions in the Mechanical Department- College of Engineering at the Kerbala University. In order to control the intensity of the solar radiation and other influencing weather factors, the proposed systems were tested in an indoor environment. The accuracy and the calibration of the instrumentation utilized in this study are also presented. Finally, the repeatability check for some experimental results would be represented.

4.2 The experimental rig

The experimental rig consists of three main parts photovoltaic panel, thermoelectric modules and heat exchanger. The solar simulators are used to supply the solar radiation with required intensity. To measure the temperature, solar radiation intensity, output data of the photovoltaic panel, and flow rate value, thermocouples, solar meter, solar module analyzer and flow meters which are used. During the assembly of the PV-TEG hybrid configuration, a schematic diagram of the PV-TEG integrating system is shown in figure (4-1). The photograph of test rig that located in the laboratory building of Mechanical Engineering Department in Kerbala University as shown in Figure (4.2). The following section explain in detail components of the system.

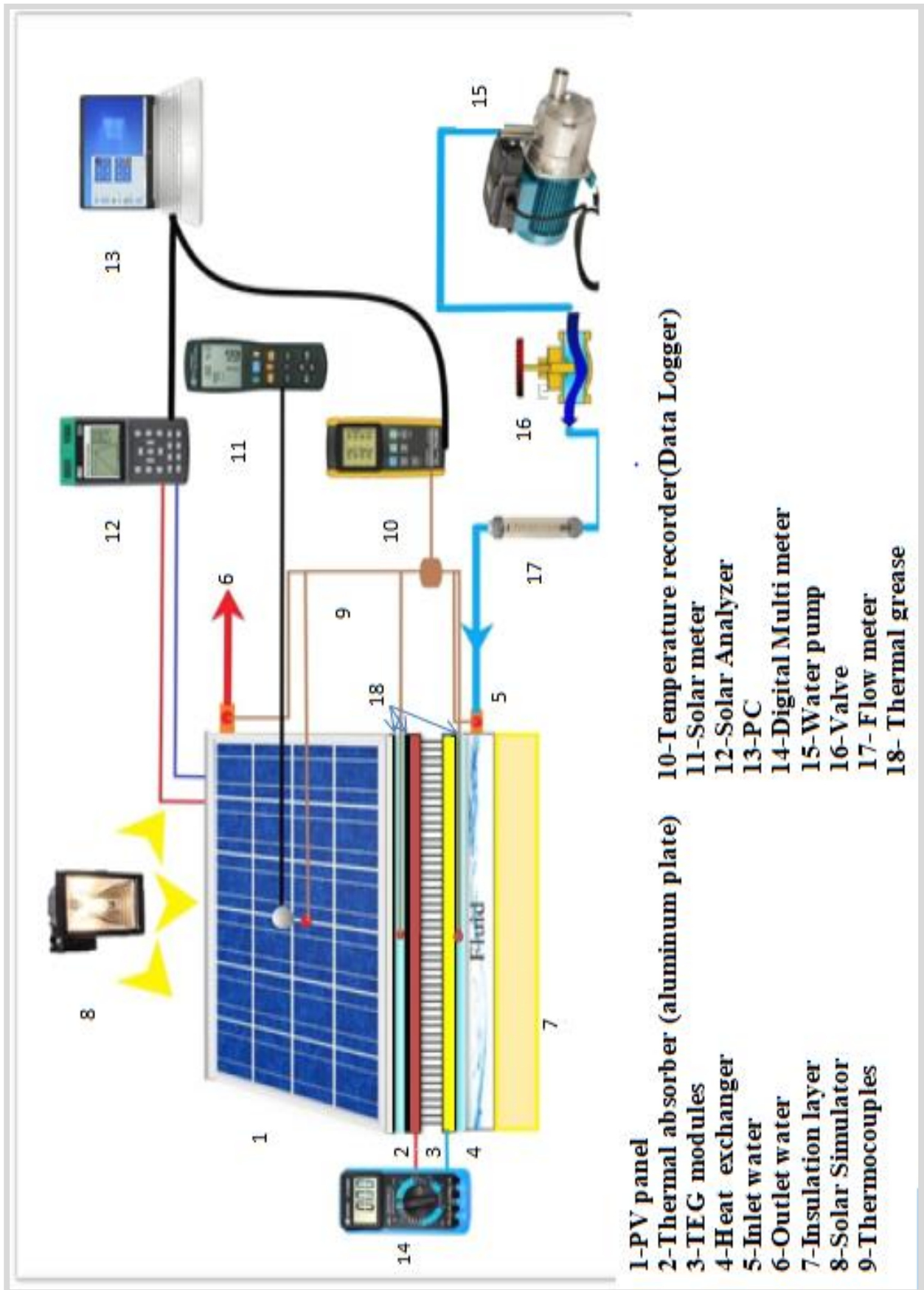
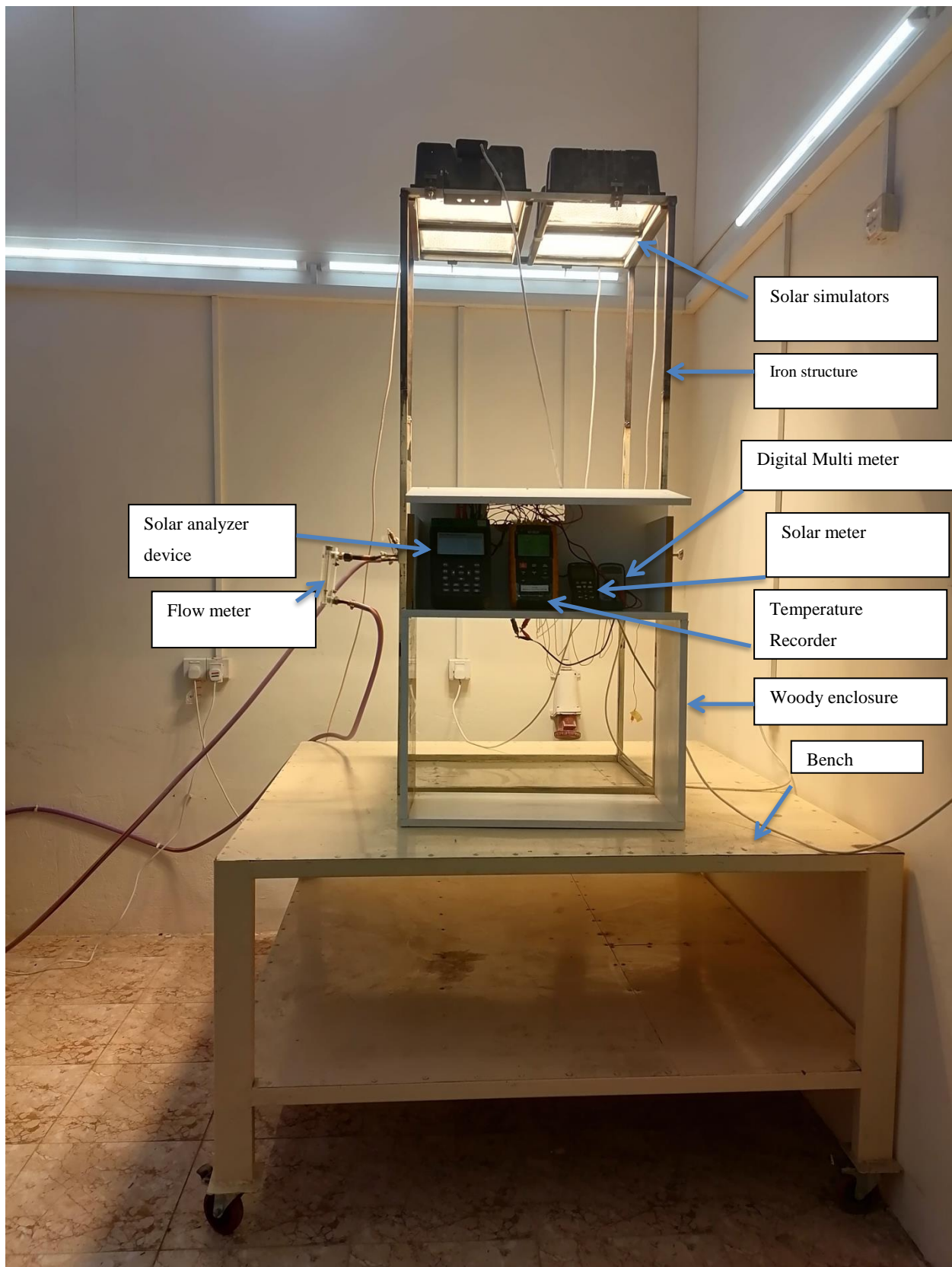
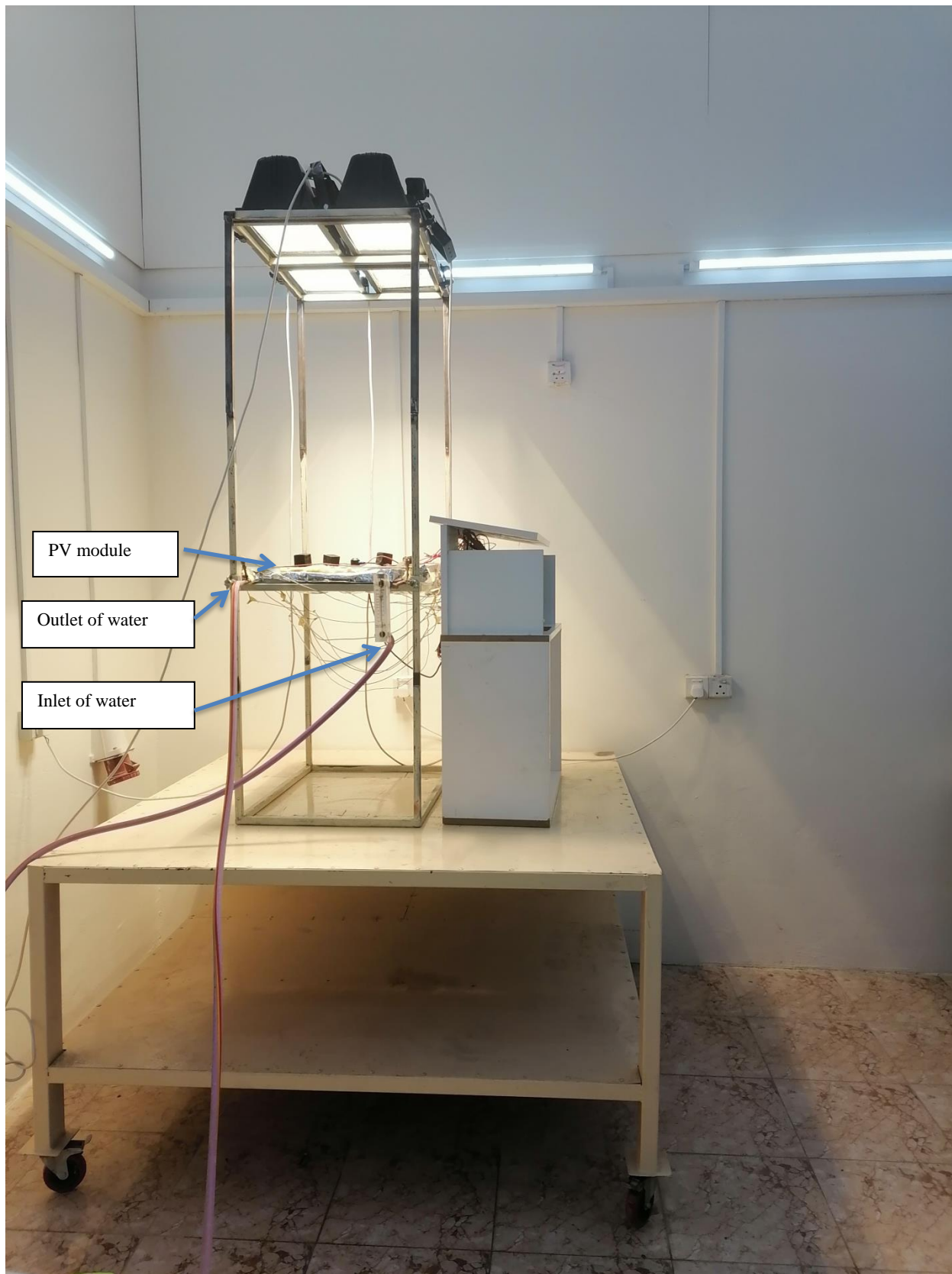


Figure 4-1: Schematic diagram of the PV -TEG integrating system.



(a) Front view of experimental rig

Figure 4-2: Photographs of experimental rig; (a)Front view and (b) Side view



(a) Side view of experimental rig

Figure 4-2: Cont.

4.2.1 The components of experimental rig:

- 1- One PV module type Mono Crystalline with dimensions (51 cm *68 cm), as shown in figure (4-3).
- 2- Thermoelectric generator modules, commercial type (TEC1-12715), as shown in figure (4-4). The 50 items of thermoelectric modules performance test were conducted inside the laboratory, during which the voltage generated at different ranges of temperature difference was calculated. The obtained results are included in the appendix (A).
- 3- Sheet of Aluminum as a flat plate of 2mm thickness and (50 cm*68 cm) dimensions as shown in figure (4-5).
- 4- A heat exchanger (Shell and Tube) typically consists of Aluminum plate with (50 cm* 68 cm* 0.2 cm thickness) dimensions, 9.96 m length, and 1.27 cm diameter of copper tube soldered on the flat plate. It is manufactured inside the laboratory according to the required measurements after preparing the raw materials and the necessary equipment. Firstly, the heat exchanger with its dimensions is sketched by SOLID WORK program. Then, the raw materials such as Aluminum sheet and copper pipes are prepared and cut according to the required dimensions. After that, the copper tubes are connected together and welded by oxy-acetylene torch welding. As well as, the welded copper pipes are welded to the Aluminum plate by lead solder wire welding. On the other hand, another Aluminum plate is placed in contact with the copper tubes and connected to the first plate by screws. In addition to fill the spaces between the two plates with insulating foam. The purpose of this step to prevent heat transfer through the sides of the heat exchanger, in addition to take advantage of the screws and the additional plate to install the glass wool insulation. The insulation plate prevents heat transfer from the heat exchanger to the surrounding from its lower side.

- The manufacturing stages of the heat exchanger are shown in the figure (4-6).
- 5- The solar simulator has four halogen lamps, each having (1000 W) and rated at 220 V with dimensions (27*24*13 height) cm. The halogen lamps are arranged in 2*2 metrics for uniform irradiance distribution, as shown in figure (4-7).
 - 6-Two iron structures are designed to support the PV-TEC hybrid system with all its parts. One of them consists of a slide part on which the PV and other components of the hybrid system are held to control the radiation intensity. Also, the solar simulators are held on the structure top. The structure is designed with 75 cm*54 cm *175 cm (L*W*H). Another structure is a bench with 1500 cm* 1500 cm* 75 cm (L*W*H) dimensions and four wheels for easy moving. This structure carries the first structure and the measurement instrumentations as shown in figures (4-8) and (4-9), respectively.
 - 7-Twelve thermocouples type k of 1m length were used
 - 8- Insulation of glass wool with 68 cm*50 cm (L*W) with 5 cm thickness [59] to prevent heat gain from the back surface of the thermal collector to the surrounding, as shown in figure (4-10).
 - 9- A thermal grease tape with 0.5 mm thickness and 1.4 (W/m.k) thermal conductivity that is used between the contact areas to reduce the thermal resistance [46], as shown in figure (4-11).
 - 10- A wooden enclosure is manufactured with dimensions 50 cm*30 cm*100 cm (L*W*H). It contains a hole (20 cm*8 cm) to pass the wires of the measuring devices. As well as, the thermocouple to be connected to the portable instrumentations measures in turn on a shelf (50 cm*30 cm) connected to the enclosure, which is designed for this purpose. In addition of a second shelf above with the same dimensions that is used

to protect the measuring devices from the effects of radiation as shown in figure (4-12).

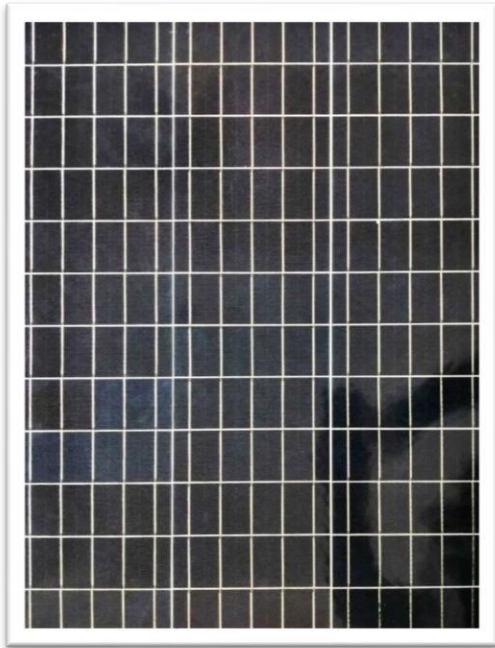


Figure 4-3: PV module



Figure 4.4: Thermoelectric module

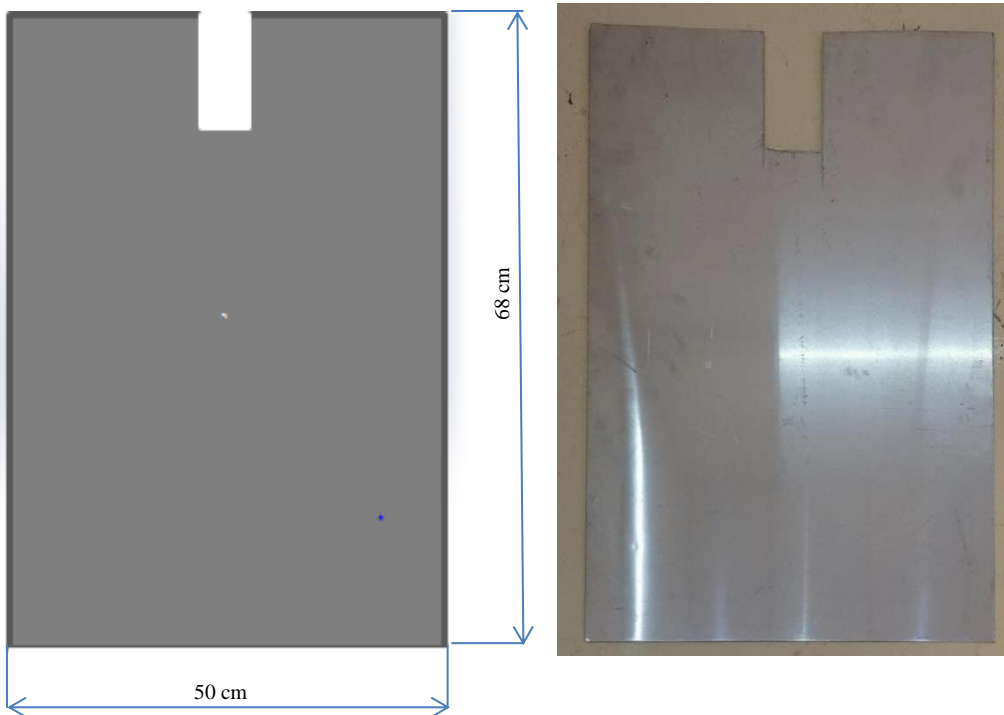
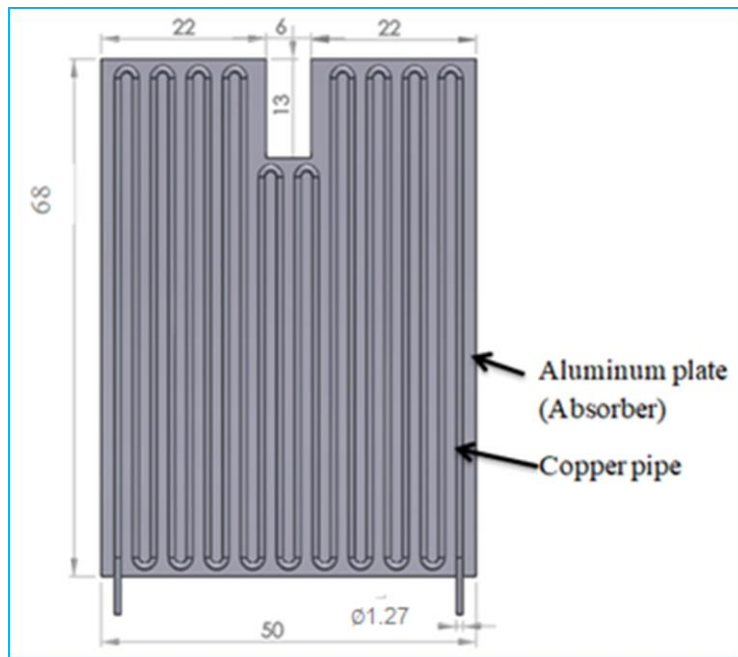


Figure 4-5: Aluminum sheet



(a) Schematic diagram of heat exchanger



(b) Aluminum Sheet



(d) Copper coil

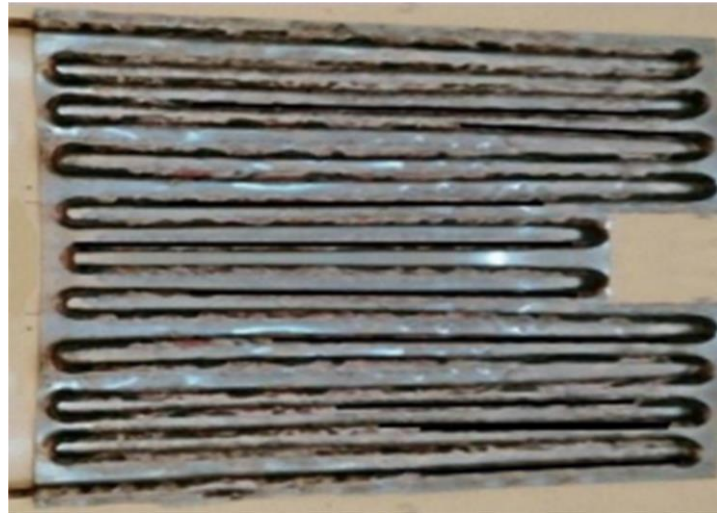


(c) Lead solder wire

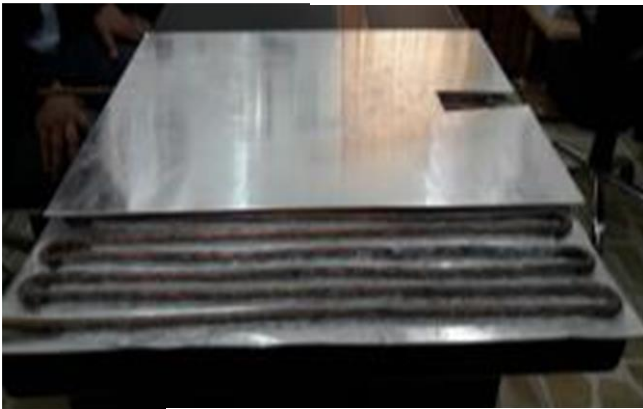


(e) Cutting and joining the copper pipe pieces

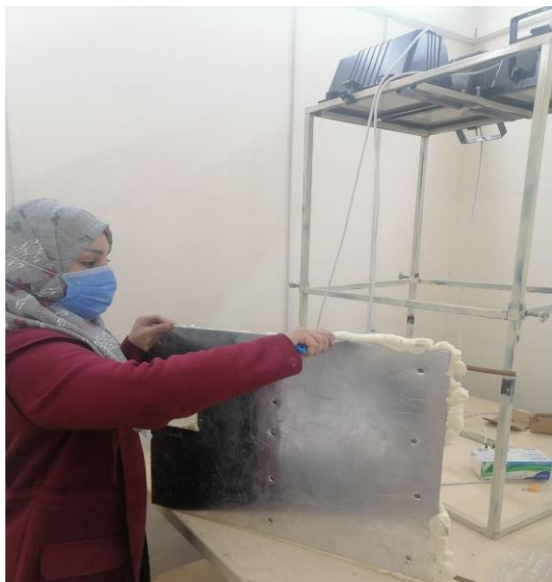
Figure 4-6: Heat exchanger manufacture stages



(f) *Welding the copper pipes on the aluminum*



(g) *Putting and linking other aluminum plate above the heat*



(h) *Filling the space between the aluminum plates with foam insulation*



(i) *Heat exchanger*

Figure 4-6: Cont..

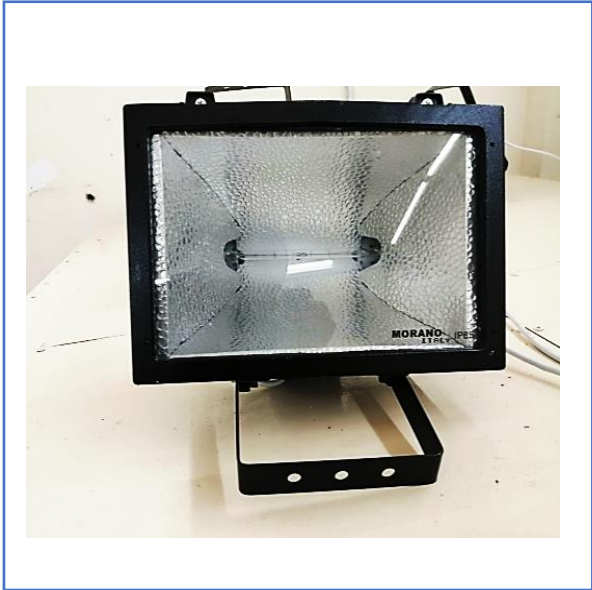


Figure 4-7: Solar Simulator



Figure 4-8: Iron structure with slider part



Figure 4-9: Bench



Figure 4-10: Glass wool



Figure 4-11: Thermal grease



Figure 4-12: Wooden enclosure

Electrical data and technical properties of components of the PV and TEG module at standard test conditions (STC) used in constructing the experimental rig are tabulated in Tables (4-1) and (4-2), respectively. While optical specifications of some used materials that had been displayed in chapter three.

Table 4-1: Electrical and technical data of PV module at STC [57][68]

Model of Module	Mono-Crystalline	Open circuit voltage	21.6 V
Peak power	50 W	The voltage at max. power	18 V
No. cell	36	Nominal temperature	45±(2) °C
Dimension of cell	125*50 mm	Relatives humidity %	Up 100
Nominal Voltage	12 V	Dimensions of Module	680*510*25 mm
Current at max. power	2.86 A	Weight	9.3 kg
Short Circuit Current	3.17 A	Power tolerance	± 3%
Temperature cell range	- 40 to +85 °C	Current coefficient	0.04 %C ⁻¹
Voltage coefficient	-0.4 %C ⁻¹	Thickness of glass cover	3 mm [57]
Thickness of back sheet	0.5mm [68]	Thickness of encapsulant	0.4 mm [68]

Table 4-2: Electrical and technical data of TEG module [9][75]

Model of Module	TEC1-12715
Material	Bismuth Telluride (Bi ₂ Te ₃)
No. of thermoelements pair	127
Dimensions of module	40*40*3 mm
Seebeck coefficient	185 μVK ⁻¹
Electrical resistivity	1*10 ⁻⁵ Ω.m
Thermoelement length	2 mm
Max. Temperature gradient	90 °C
Net weight	50

4.2.2 Measurement Instrumentations

Different types of measurement instrumentations are used in the experimental work as shown below:

I. Temperature measurement

Temperature recorder and thermocouple sensors are utilized to monitoring the temperature variation during the working of the PV-TEG system.

1. Temperature recorder

A digital Temperature recorder type Lutron BTM-4208SD, 12 channels with SD memory card is used to record the thermocouples reading as shown in figure (4-13). SD memory card could store the data along working and then transfer the data to the spreadsheet. The accuracy of a device is $\pm (0.4 \% + 0.5) ^\circ\text{C}$.

2. Thermocouples

The twin wire thermocouples type k, Nickel Chrome/ Nickel Aluminumwire and insulated with high temperature glass as shown in figure (4-14). This devices have been used to measure the temperature of specific sites in the PV, PV/T, and PV-TEG systems. The accuracy of a device $\pm 0.25 ^\circ\text{C}$.

II. The current- voltage characterization

Solar module analyzer type PROVA 200A was utilized to record the characteristics V_{oc} , I_{sc} , V_{mp} , I_{mp} and P_m , FF and the I-V test curve of module as shown in figure(4.15). Test results could be saved and downloaded to a computer for later analysis using the application software (Solar Module Analyzer 6AV131029) with an optical USB cable for interface to the computer. The accuracy of a device are $\pm (1\%) \text{ V}$ and $\pm (1\%) \text{ A}$.

III. Solar radiation measurement

Solar meter, type TES 132 was used to measure solar irradiance to range 2000 (W/m^2), as shown in figure (4-16). Tests results can be saved and downloaded to a computer for later analysis using the application software (PANEL 8.01) with a USB cable for interface to a computer. The accuracy of a device is $\pm (5\%) \text{ W}/\text{m}^2 \pm 0.38 \text{ }^\circ\text{C}$ from 25°C .

IV. Flow rate measurement

The Flow meter, type ZYIA (1-10) litter /min, was utilized to measure the water flow rate as shown in figure (4-17).

V. Digital multi meter measurement

Multi meter, type TOTAL (ONE –STEP TOOLS STATION TMT 46001) illustrates in figure (4-18). This advice has been used to measure two or more electrical values principally voltage (volts) DC and AC voltage range: 200V- 600V. DC current (amps) range: $200\mu\text{A}$ -10A and resistance (ohms)range: 200Ω - $2\text{M}\Omega$. It is a standard diagnostic tool for technicians in the electrical/electronic industries.



Figure 4-13: Temperature Recorder
Type Lutron BTM-4208SD



Figure 4-14: Thermocouple Type (k)



Figure 4-15: Solar Module Analyzer
Type PROVA 200A



Figure 4-16: Solar Meter Type TES132



Figure 4-17: Flow Meter Type ZYIA



Figure 4-18: Digital Multi meter Type
TMT 46001

4.3 Design considerations

Water flow rate used in this study was calculated by using a simulation analysis developed by ANSYS FLUENT software for heat exchanger with main boundary conditions, as shown in the Table (4-3) below:

Table 4-3: Test Conditions

Solar irradiance	1000 W/m ²
Ambient temperature	28 °C
Wind speed	0 m/s
Inlet cooling water temperature	20°C
Flow rate range	1-9 (l/min)
Coolant	Water

Figure (4-19) shows the optimum volume flow rate of cooling fluid 7 (l/min), at which the temperature of the Aluminum sheet in the heat exchanger decreased to the lowest value. Whereas, any increment in the flow rate of running water inside the heat exchanger will not effect on the temperature distribution of the heat exchanger surface. So, for practical requirements, the coolant flow rate was 7 (l/min).

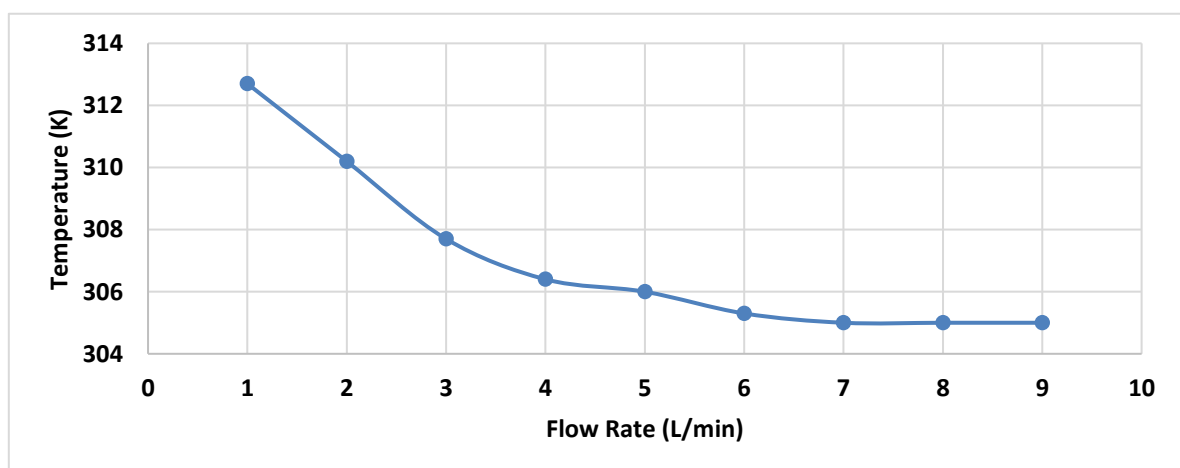


Figure 4-19: Temperature distribution average on heat exchanger surface with volume flow rate at solar radiation 1000 (W/m²).

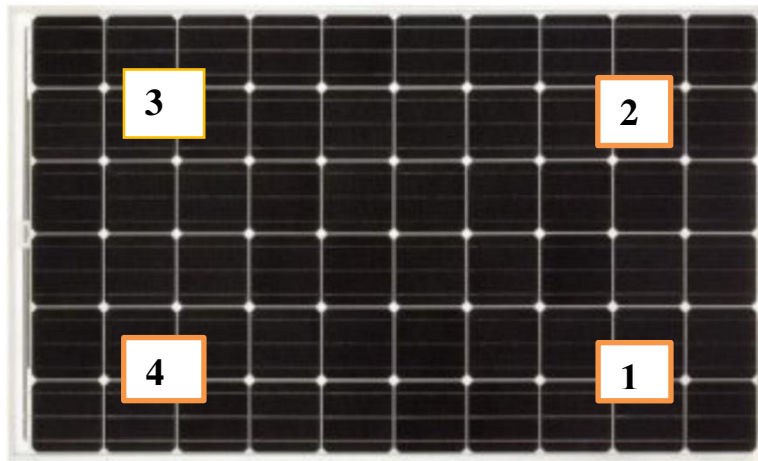
4.4 Test rig building

Generally, iron structures are constructed to support the PV module, the water PV/T system, and the PV -TEG hybrid system individually. In addition to all experimental rig components and measurement instrumentations that were previously mentioned. Moreover, the solar simulators are fixed on top of the iron structure and bonded with caution to avoid falling. the light of solar simulators is exposed normally down on the PV module that is installed and fixed on the slide part in the structure.

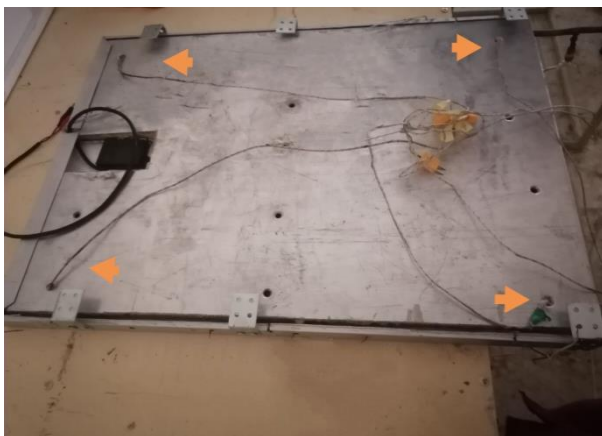
In both a PV/T system and photovoltaic- thermoelectric coupling system, the flow meter device is fixed perpendicularly to the horizontal plane to measure the flow rate of inlet cooling water. Control gate valve to supply chosen flow rate at the constant head. The four insulated and calibrated thermocouples are distributed on the PV panel front surface; a schematic diagram of the locations of thermocouples connection is shown in figure (4-20) (a). Six thermocouples are tied, two at inlet-outlet water pipe positions and four on the back surface of the heat exchanger aluminum plate, as shown in figure (4-20) (b). In addition, in the hybrid system, with two thermocouples are attached to the aluminum plate (thermal concentrator) by placing them in a made incision in the plate surface, as shown in figure (4-20) (c).

Next, all thermocouples are connected with a thermometer, and the wires of the PV module are connected to the solar analyzer. In addition, the solar meter is fixed on the photovoltaic surface to measure solar irradiance.

The PV panel is separately attached to the front side of an aluminum plate operating as the thermal concentrator to extract more heat from the backside of the PV panel. Subsequently, the 50 items of thermoelectric generator modules are sandwiched between the aluminum plate's backside and the front side of a heat exchanger. The thermic contact between contact areas is realized with the thermal grease tape. The thermocouples (T_h) are stuck in the made incision in the aluminum plate that are assumed to be the temperature of TEG hot side. Furthermore, the other thermocouples (T_c) are fixed at the backside of the heat exchanger aluminum plate that are assumed to be the temperature of thermoelectric cold side.



(a) Thermocouples location on the PV front surface



(c) Thermocouples location on the heat exchanger



(b) Thermocouples location on the Aluminum plate

Figure 4-20: Schematic diagram of locations of thermocouples connection on the: (a) PV module, (b) heat exchanger, and (c) Aluminum plate (thermal absorber)

4.5 Test procedures

The PV, PV/T, and PV-TEG experimental measurements started in November 2021 in the laboratory. The experimental indoor tests are taken in the controlled room, at constant environment temperature $T_a=28\text{ }^\circ\text{C}$ and wind speed $=0\text{ m/s}$, for three systems (PV only, PV/T system, and PV-TEG hybrid system). Firstly, for the Photovoltaic system, moving the solar panel up or down and using the solar meter to record the radiation intensity. At the same time, Four thermal isolated thermocouples have been fixed on the front surface of the PV panel and connected to Temperature Measurement Data Logger device. In addition, Solar Module Output Measurement has been linked with the PV panel to measure the PV electrical properties. The values of solar radiation ranging from 1000 to 2000 (W/m^2) by increase 250 (W/m^2) at each step had been tested.

After two hours of system operation to reach a steady state, the measured readings such as a temperature, current (I_{mp}), voltage (V_{mp}), electrical power P_m , and efficiency have been recorded at each solar radiation value. Second, the PV/T system has been tested in the same laboratory conditions that had been mentioned previously in Table (4-3) with the solar simulator and solar meter to determine the solar radiation at 1000 (W/m^2) at the volume flow rate of 7 (l/min). Following procedures are followed:

- 1- The gate valve is adjusted at the chosen value of the volume flow rate of water input to the heat exchanger.
- 2- Water is supplied to the system and connected -to the thermocouples of the PV/T system with a temperature recorder. In addition, the sensors of the solar meter is set up connect at specific place.
- 3- Waiting a five minutes until the temperature of the PV module in the system reaches stability.

- 4- Read temperatures of the front surface of PV module, PV/T system, and inlet and outlet water that get out to heat sink by calibrated thermocouples type k.
- 5- Record the temperature of ambient around the experimental rig every five minutes to make sure it stays stable.
- 6- Evaluate the electrical efficiency of the PV/T system by using the calculation equation of electrical efficiency that was hinted at formerly.
- 7- Download readings of instruments by handrecording on a computer to offer and compare it with a traditional photovoltaic system.

Finally, the PV -TEG hybrid system is tested in the same laboratory conditions. Bismuth Telluride TEG 50 pieces are set on the back surface of the aluminum plate and closely arranged in series for high voltage generation, as shown in figure (4-21). The hot sides of TEG modules is paste to the aluminum plate, whereas the TEG cold sides is touched the upper surface of the thermal exchanger. After that, all formed test steps have been repeated. Figure (4-22) shows details of the experimental rig.

The PV panel output energy and electrical efficiency have been evaluated. As well as, the electric energy of TEG modules has obtained by measuring the total open voltage of the TEG items with Digital Multi meter. It is also possible to roughly estimate the total power produced by TEG modules by using the formula [8]:

$$P_{TEG} = V_{oc} * I \quad 4-1$$

Where V_{oc} is the voltage of a thermoelectric generator and was given by:

$$V_{oc} = \alpha_{np} * \Delta T \frac{R_L}{R_{in} + R_L} \quad 4-2$$

Where R_L is the load resistance, R_{in} is the internal resistance of TEG, $\Delta T = (T_h - T_c)$ is the temperature difference across the two junctions, and α_{np} is referred to as the Seebeck coefficient. The electric current (I) flowing through the thermoelectric generator was given by:

$$I = \frac{s}{(1+s)^2} \frac{(\alpha n p \Delta T)^2}{R_{in}} \quad 4-3$$

Where $s = R_L/R_{in}$ is the ratio of the load resistance to the device's internal resistance. The power output depends on the ratio s , and the maximum power output was obtained at the matched load (i.e., when $R_L = R_{in} = 2.05\Omega$)

So total output P_{TEG} of all thermoelectric modules [43]:

$$P_{TEG} = \frac{V_{oc}^2}{4R_{in} * M} \quad 4-4$$

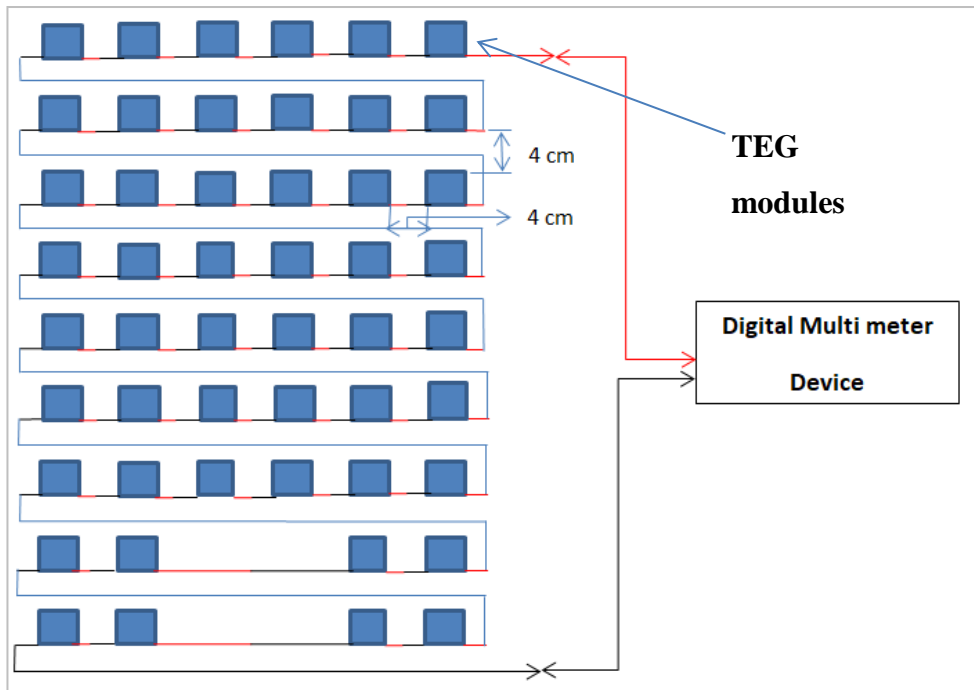
Where M is the TEG modules number. The hybrid system's total power and overall efficiency are compared with that of the PV only and PV/T system.

The improvement ratio and the deviation (difference) percentage are calculated as [76]:

$$\text{The improvement ratio} = \frac{\text{Final value} - \text{Starting value}}{\text{Starting value}} * 100\% \quad 4-5$$

The deviation (difference) percentage is calculated as :

$$\text{The deviation percentsge} = \frac{\text{Final value} - \text{Starting value}}{\text{Final value}} * 100\% \quad 4-6$$



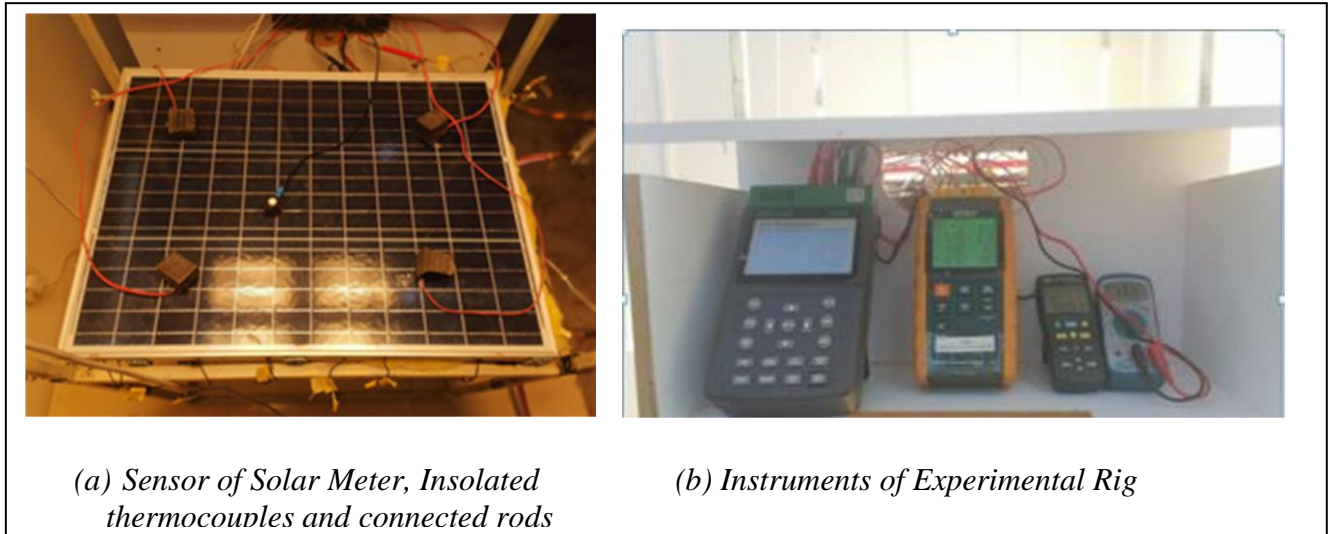
(a) Schematic diagram of TEG modules arrangement and tying

Figure 4-21: Arrangement the TEG items on the back surface of the thermal absorber



(b) Detail pictures of TEG modules arrangement and tying

Figure 4-21:Cont..



(a) Sensor of Solar Meter, Insolated thermocouples and connected rods

(b) Instruments of Experimental Rig

Figure 4-22: Details of experimental rig parts

4.7 Calibration

The measurement instrumentations were calibrated by Central Organization for Standardization and Quality Control Metrology Department- Physics Section and by the Renewable Energy Directorate in Ministry of Science and technology.

- 1- Thermometer type Lutron BTM-4208SD.
- 2- Solar meter type TES 132.
- 3- Thermocouples.

The calibration results of thermocouples and solar meter device are shown in appendix (B)

The flow meter used to measure the water flow rate that was calibrated by using a graduated flask filled with the water coming out of the experimental rig at a specific flow rate. The time for the water to reach a specific point on the flask is recorded. After that, procedure should be completed for three times, and the average values were represented in a curve with the flow meter values as shown in figure (4-23). The uncertainty calculation of the cooling water flow rate measurement will be shown in Appendix-D.

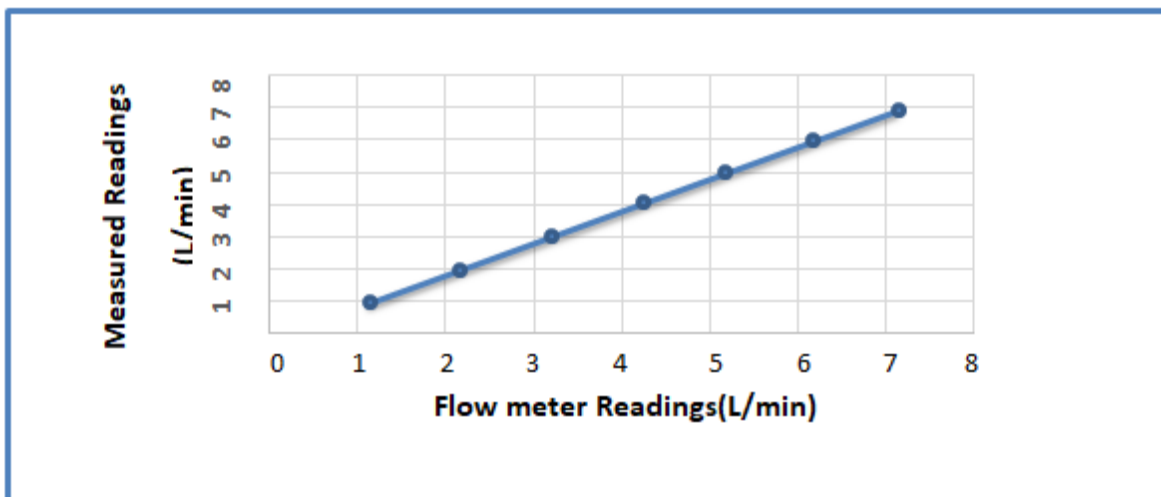


Figure 4-23: Calibration of the water flow meter

4.8 Repeatability

Repeatability is the variance induced by the instrumentation or the variation detected when the same operator measures the same part multiple times. As well as, reproducible variance occurs when different operators measure the same part using the same instrumentation.

This experiment repeated the test under the identical conditions to confirm its repeatability.. Standard deviation of Pm is calculated by using the following equation [77]:

$$\sigma = \sqrt{\frac{1}{M} \sum_{i=1}^M (x_i - \bar{x})^2} \quad 4-7$$

x_i is the element, σ is the standard deviation, M is the number of measurements, and \bar{x} is the mean. In Appendix D, Table D-1 shows the standard deviation of Pm with good repeatability of the data presented. Also, figure (D-1) shows the output power of the S4 model hybrid system as a function of light intensity over the G range: 1250(W/m²), 1500(W/m²), 1750(W/m²), 2000 (W/m²) at specific operation conditions.

Chapter Five: Results and Discussion

Chapter Five

Results and Discussion

5.1 Introduction

This chapter includes three sections: the first section presents the numerical results of the temperature distribution on different layers of the photovoltaic panel, PV/T, and four models of PV-TEG hybrid system (S1, S2, S3, and S4), as well as the electrical power and efficiency of all systems. The second section displays the experimental results of the selected thermoelectric hybrid system model (S4 model), obtained in a controlled environment in the Mechanical Department laboratory of Kerbala University college of engineering. In addition, a comparison has been performed between the numerical and experimental outcomes in the third section.

5.2 Numerical results

5.2.1 Temperature distribution contour

Figures (5-1) to (5-6) illustrate the temperature distribution contours for different layers in the PV panel only, PV/Thermal system, and tested models of hybrid system. The surface temperature of PV is to be the same average temperature of the glass layer for all of the above systems. In addition, the average temperature of both thermoelectric sides, hot and cold, and temperature difference between both sides of TEG and other surfaces are calculated for four models.

Figure (5-1) shows that the average front temperature of the PV panel (glass cover) is higher about 65 (°C). Because of the high light intensity and assumption of no cooling system, the PV temperature is high. It is also noticed that the temperature distribution of the PV module front surface is

not uniform. Because of the regions near the frame that without silicon cells, the temperatures of these regions are low compared to other regions in the PV module surface, as indicated in figure.

In contrast, Figure (5-2) shows the contour of temperature distribution of the PV module with a declining temperature gradient through the PV/T system. The average front surface temperature of the PV in the PV/T system is about 44 (°C) and less than that in the PV only. Because of high flow rate of cooling water through the pipe of the heat exchanger, more wasted heat is removed from the PV and that leads to lower of T_{sc} in PV/T system. It is also noticed that a clear gradient in temperature distribution on the PV surface due to the direction of cooling water that flows through the heat exchanger pipes.

Figures (5-3) to (5-6) show the contour of temperature distribution in the layers of the four hybrid models (S1, S2, S3, and S4). It can be seen that, the average front surface temperature of PV module increases with decrease TEG items in the models of hybrid system. Because of thermoelectric modules effect that absorbs a thermal emission from the back of the PV panel, the average temperature of PV module upper surface decreases with TEG number increases. The average front surface temperature of the PV (T_{sc}) in the S1, S2, S3, and S4 hybrid systems are about 31.2 °C, 33.18 °C, 33.76 °C, and 46 °C, respectively.

In the hybrid system models, Table (5-1) shows the average front surface temperatures of the PV in all test systems and the temperature difference (ΔT) between the two TEG sides for hybrid system models. It can be seen that the temperature difference (ΔT) decreases as the number of TEG items goes up. The TEG modules with high cooling water flow rate

absorb the heat from the PV panel's back surface, that causes a decrease of the PV panel's front surface temperature (T_{sc}) at the same boundary condition. So, the hot side temperature of TEG modules layer decreases with decreasing of T_{sc} and leads to a lower in the temperature difference (ΔT). The results show that the temperature difference (ΔT) values for the S1, S2, S3, and S4 models are about 2.25°C, 4.29°C, 5.02°C, and 11.2°C, respectively.

It also noticed that the average temperature of the PV surface and temperature difference (ΔT) of the S4 model are higher compared with that of the other models. Because of the PV panel's front surface temperature (T_{sc}) is high, the temperature of TEG hot side rises and the temperature difference (ΔT) increases.

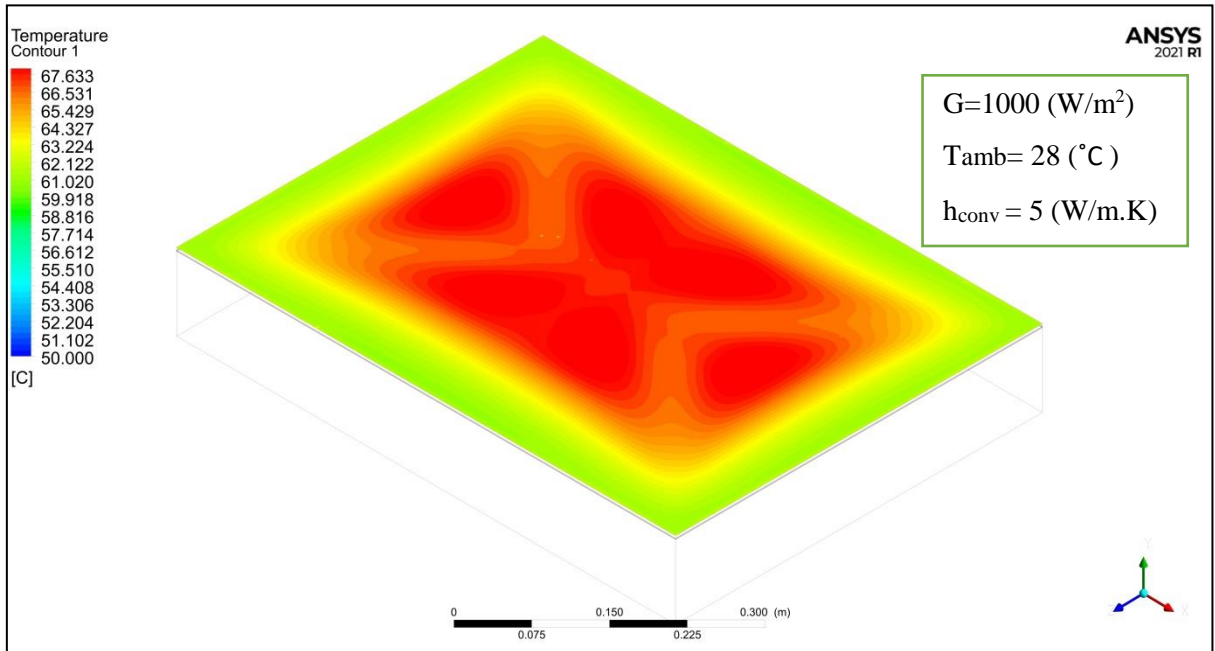
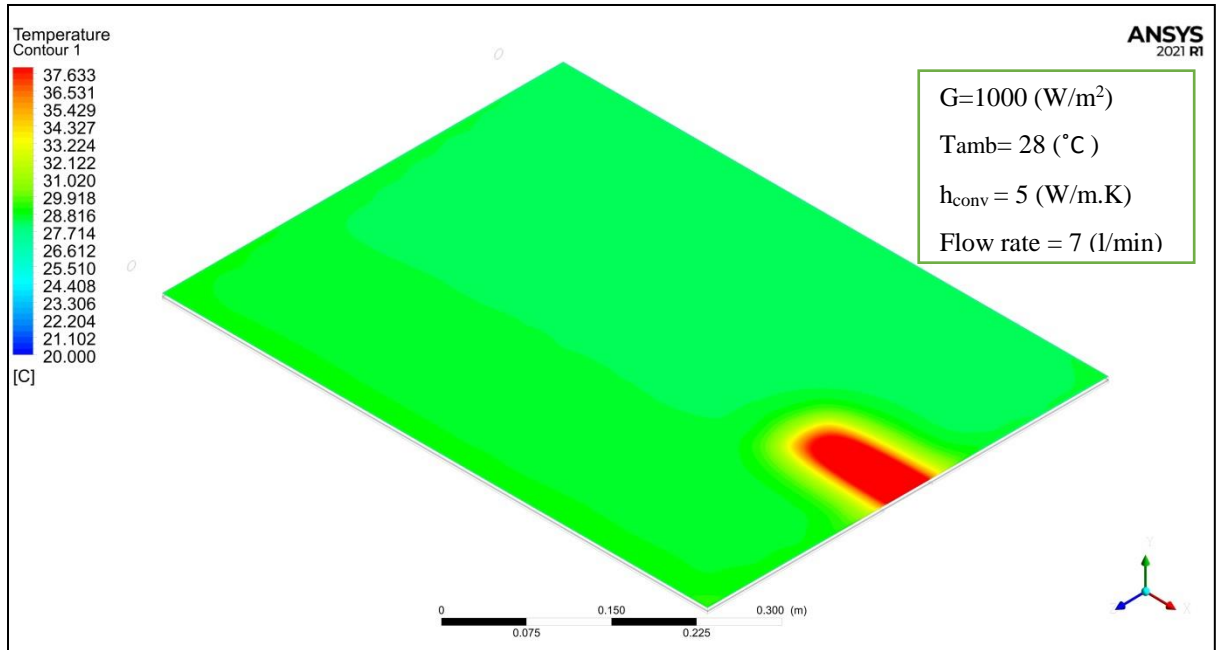
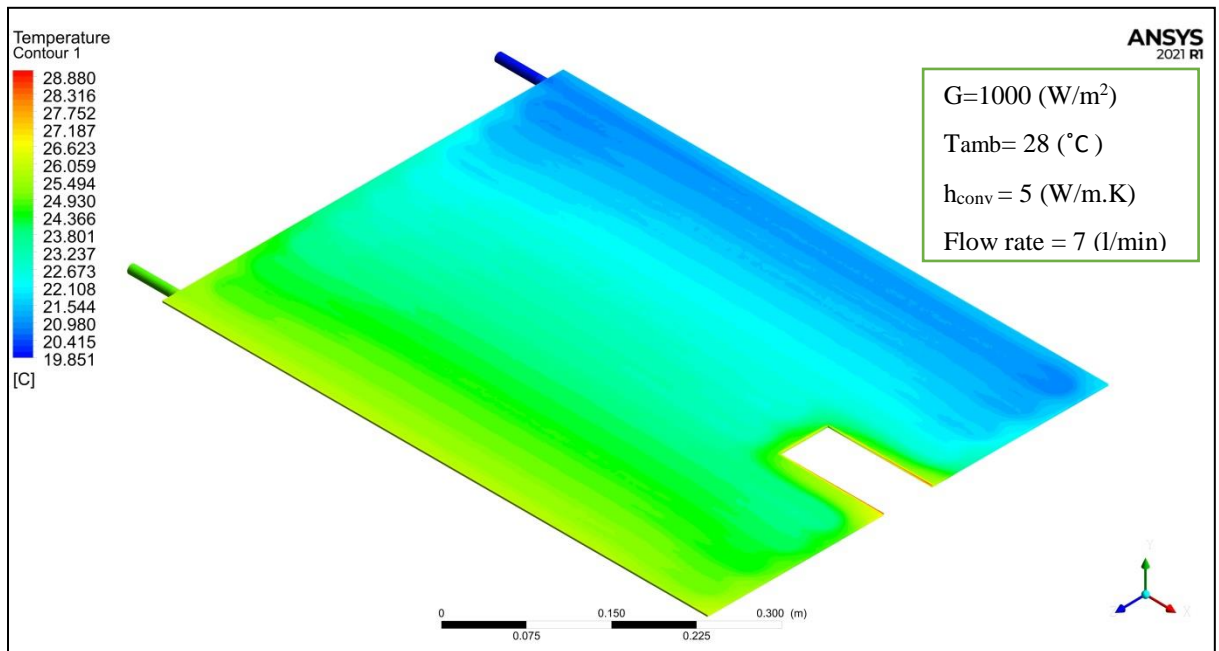


Figure 5-1: Temperature distribution of the front surface of PV cells in the PV system only.

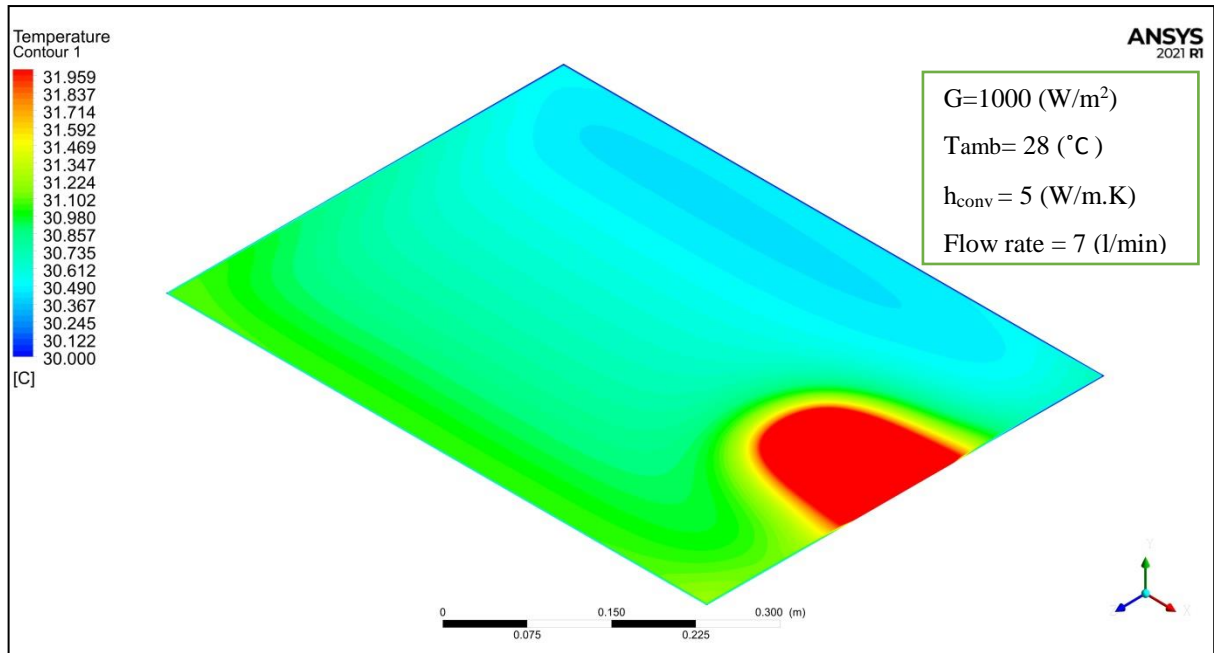


(a) Front surface of PV panel

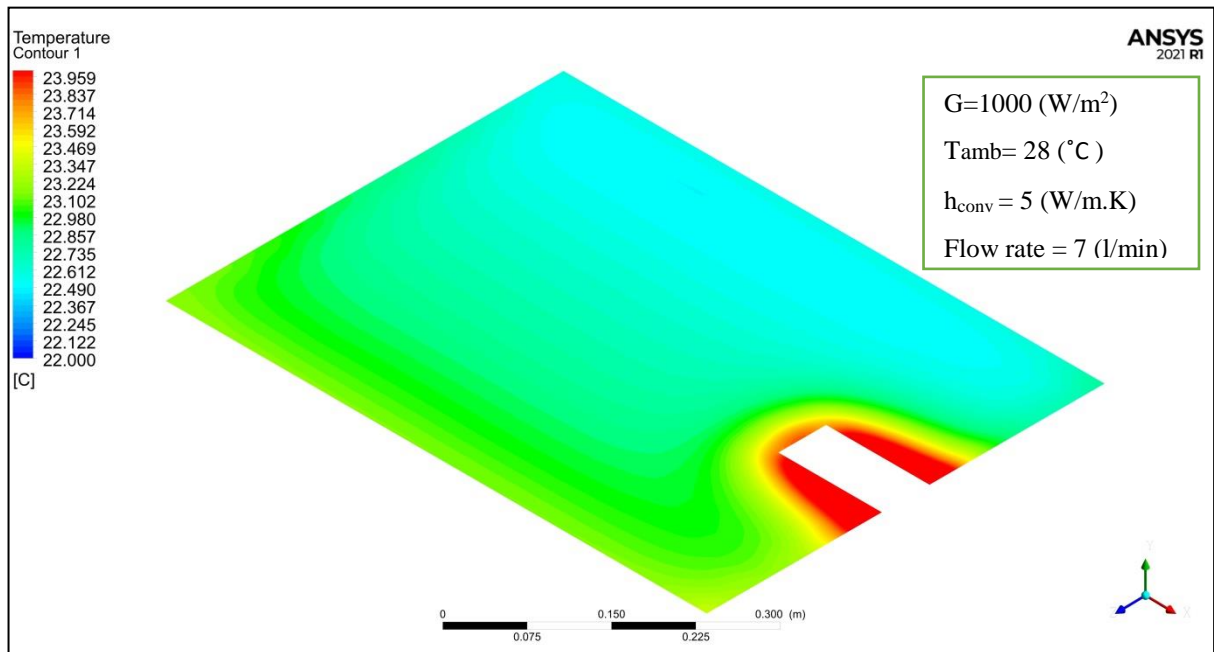


(b) The top surface of heat exchanger in the PV/T system

Figure 5-2: Temperature distribution of (a) the front surface PV panel and (b) heat exchanger in the PV/T system.

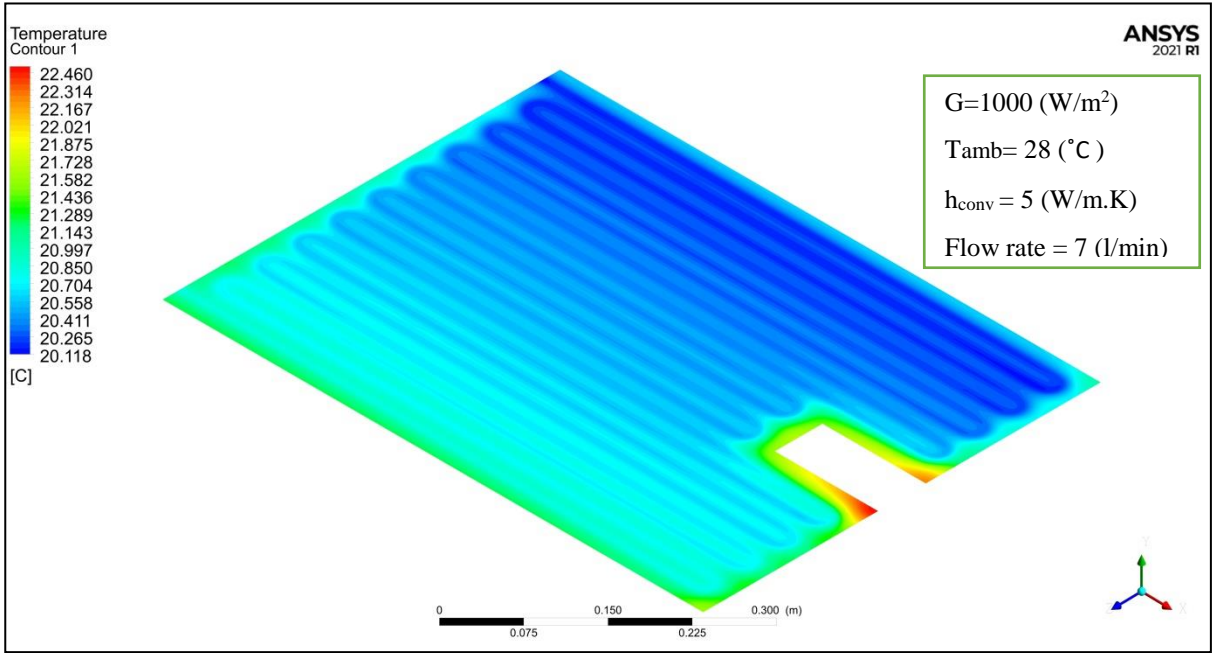


(a) Front of top surface of PV panel

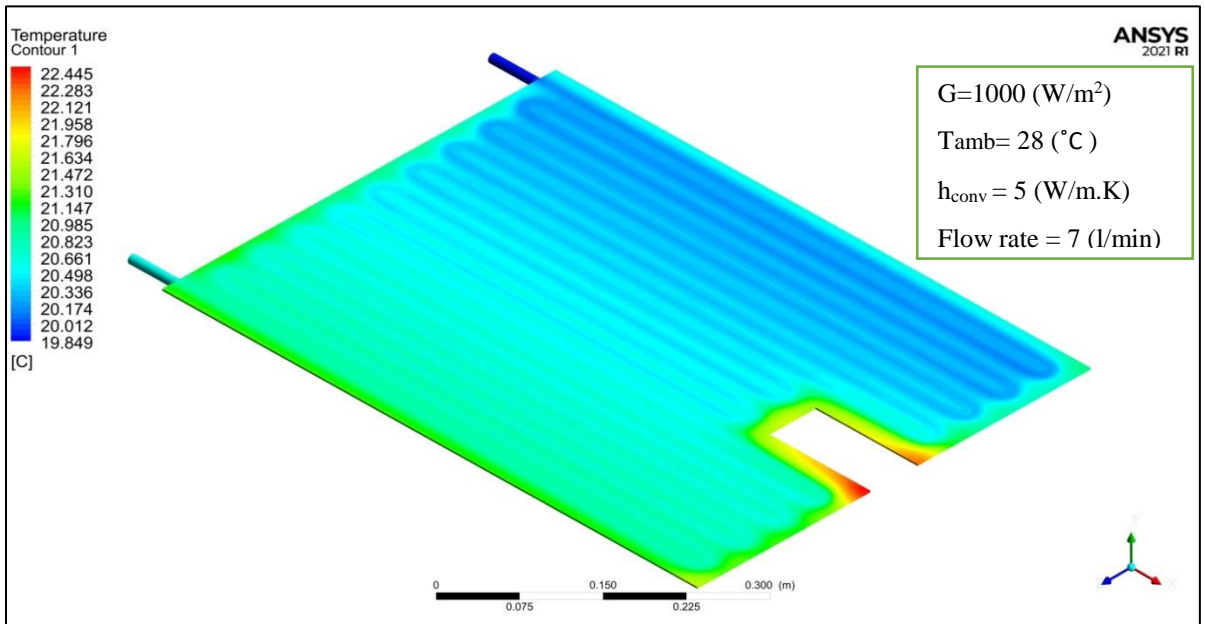


(b) The hot side of TEG modules layer

Figure 5-3: Temperature distribution (a) front surface of PV panel, (b) TEG modules hot side, (c) TEG modules cold side, and (d) top surface of heat exchanger in the (S1) model PV-TEG hybrid system.

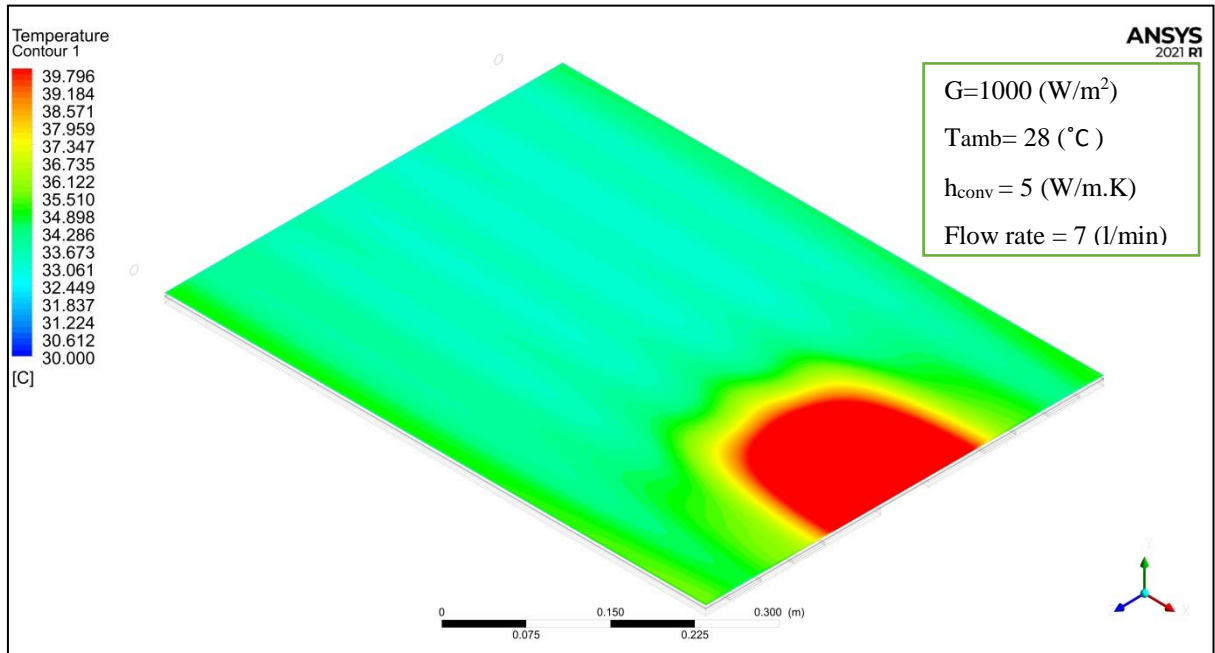


(c) The cold side of TEG modules layer

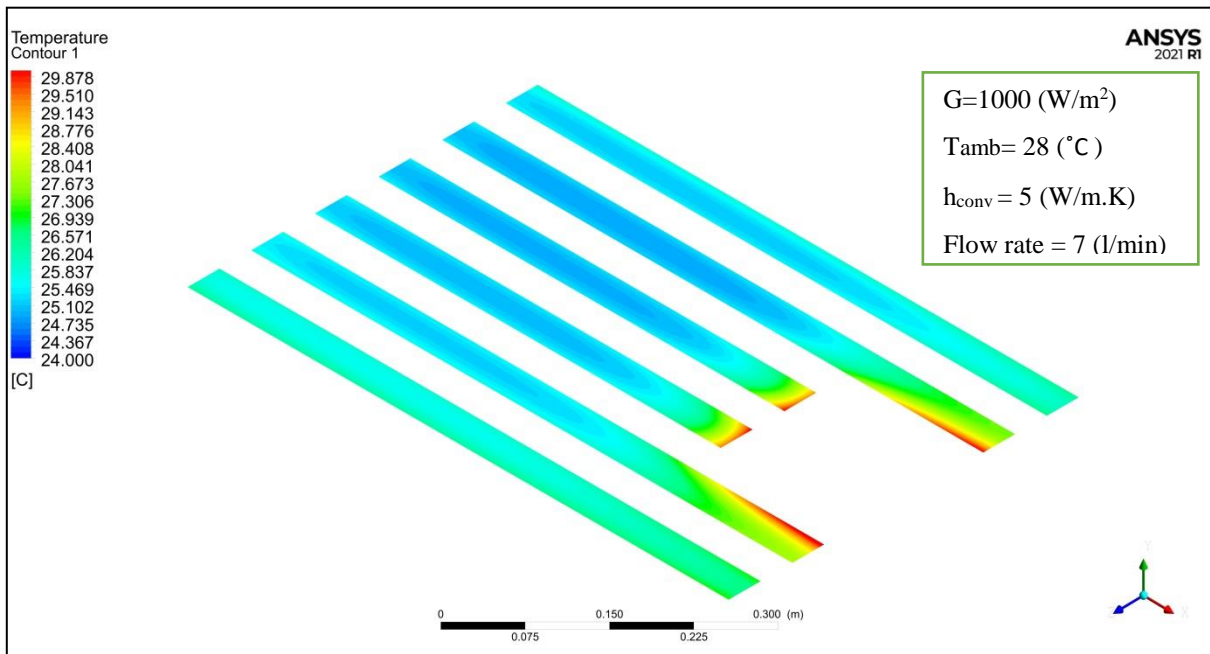


(d) The top surface of heat exchanger in the S1 model of PV-TEG hybrid system

Figure 5-3: Cont.

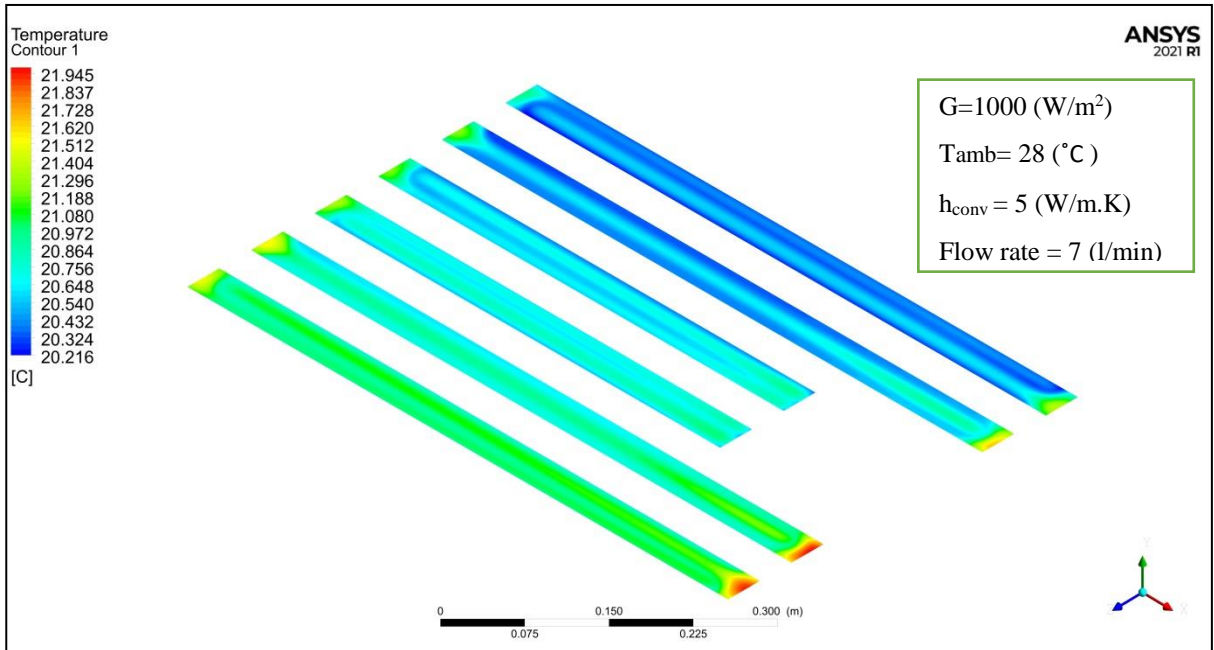


(a) Front surface of PV panel

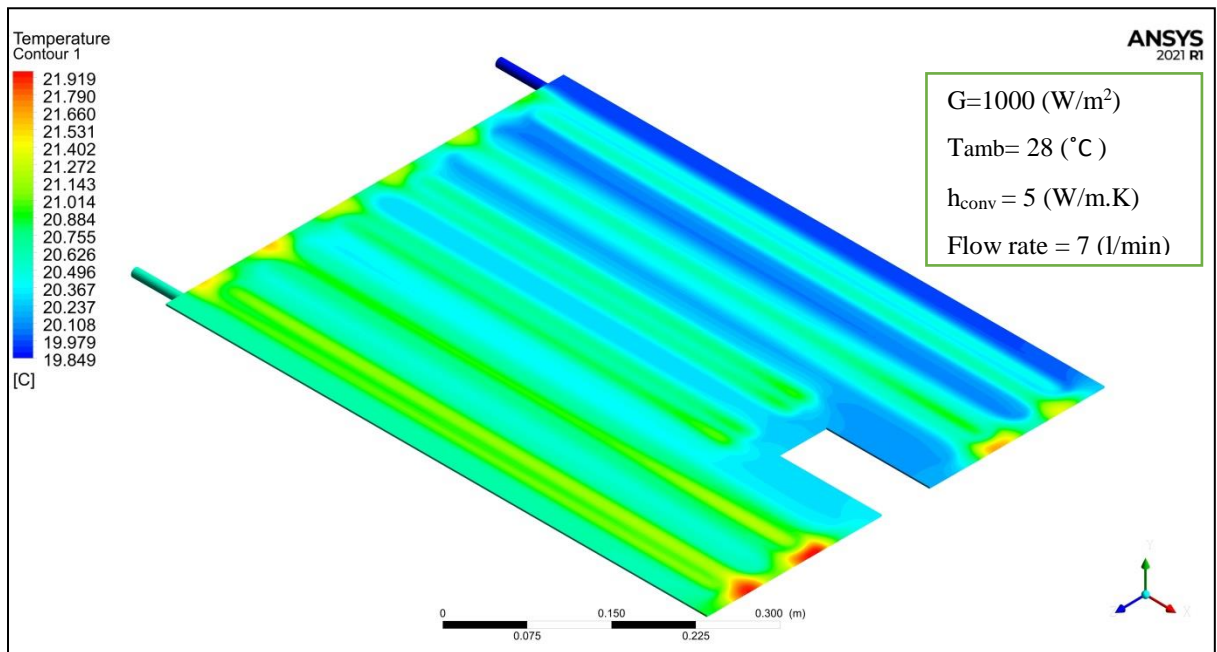


(b) The hot side of TEG modules layer

Figure 5-4: Temperature distribution of (a) top surface of PV panel, (b) TEG modules hot side, (c) TEG modules cold side, and (d) top surface of heat exchanger in the PV-TEG hybrid system (S2) model.

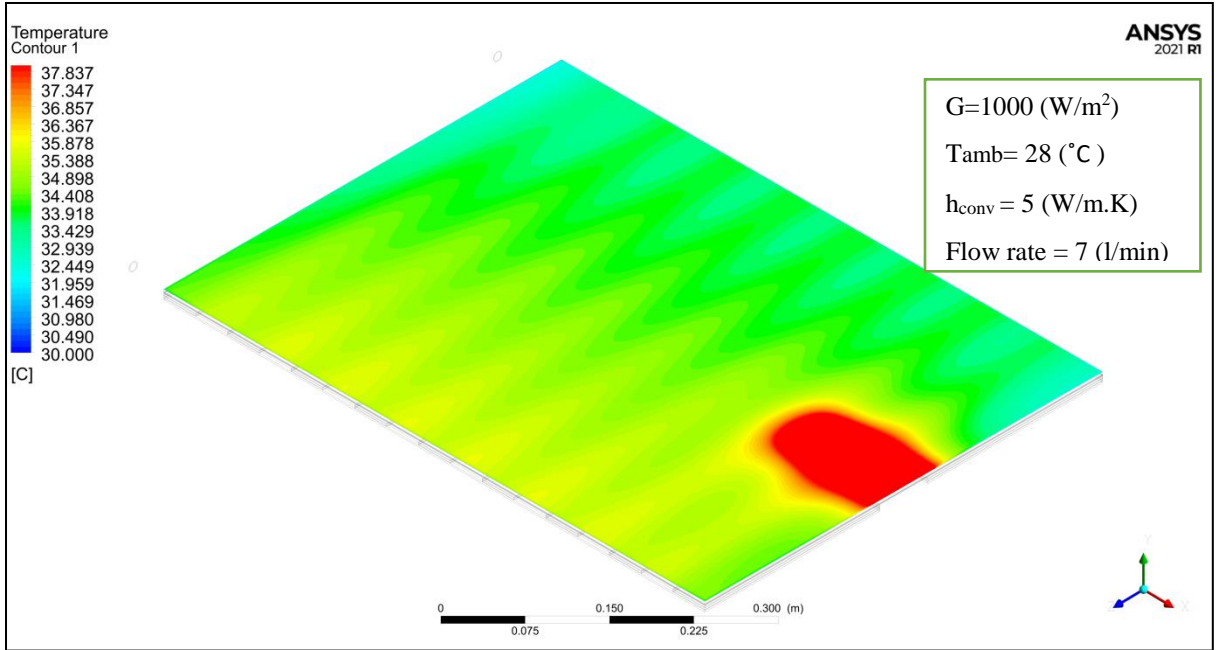


(c) The cold side of TEG modules layer in the S2 model of PV-TEG hybrid system

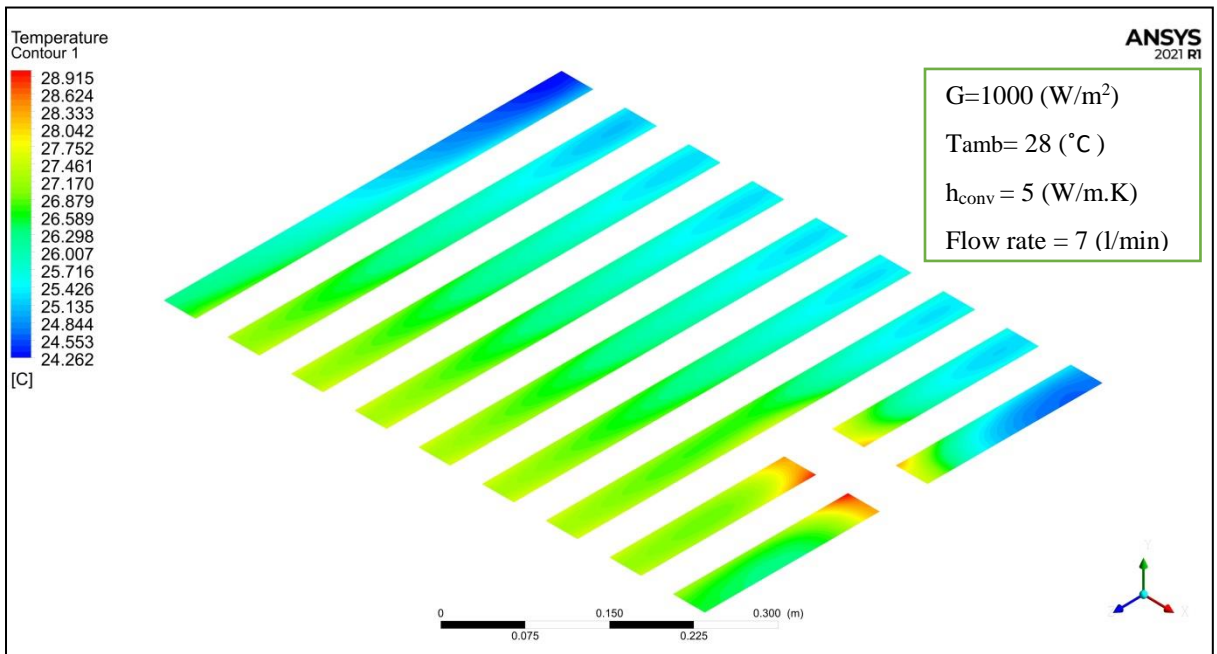


(d) The top surface of heat exchanger in the S2 model of PV-TEG hybrid system

Figure 5-4: Cont.

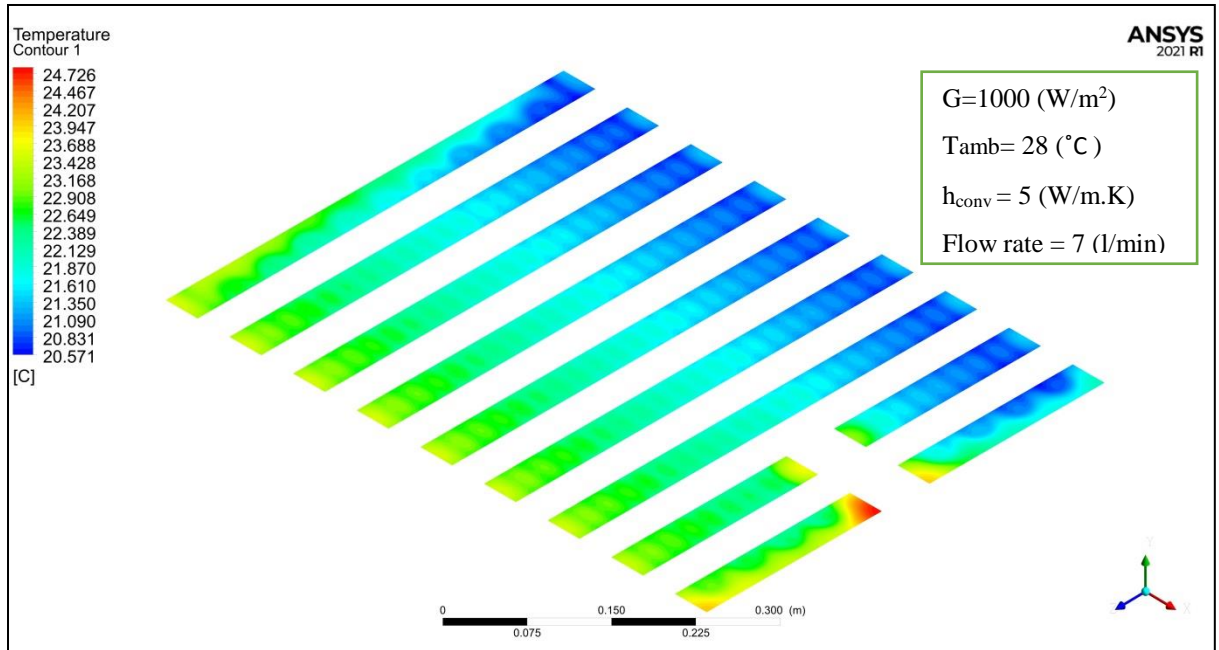


(a) The front surface of PV panel in the (S3) model

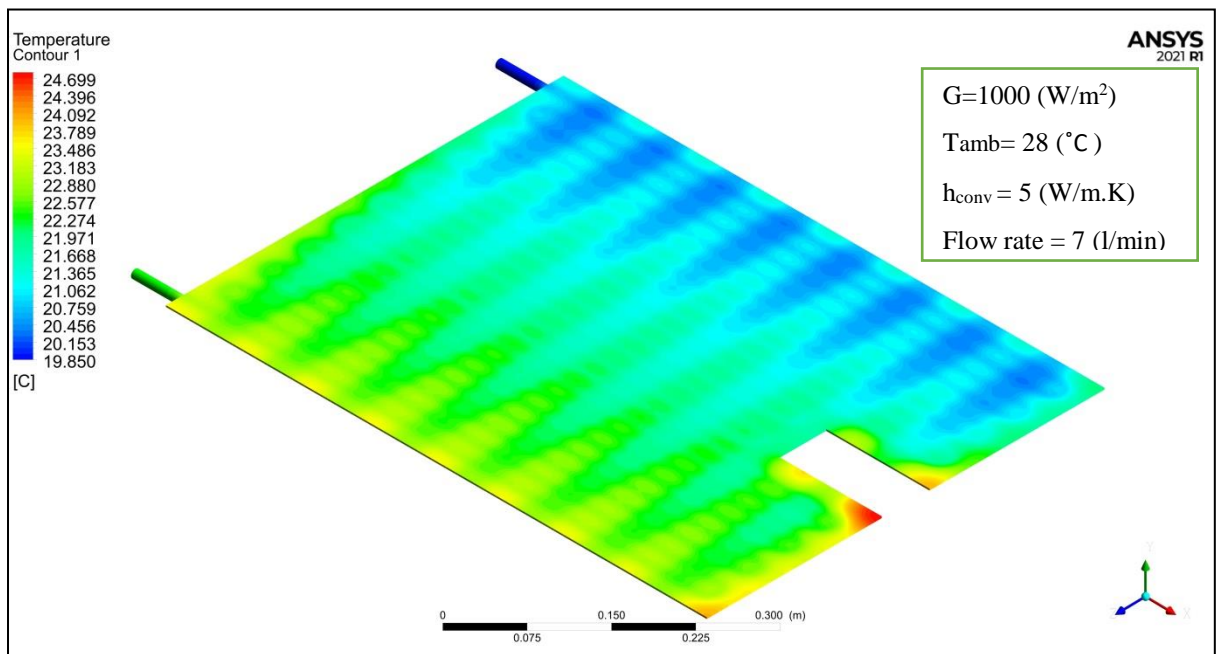


(b) The hot side of TEG modules layer in the S3 model

Figure 5-5: Temperature distribution on the (a) front surface of PV panel, (b) TEG modules hot side, (c) TEG modules cold side, and (d) top surface of heat exchanger in the PV-TEG hybrid system (S3) model.

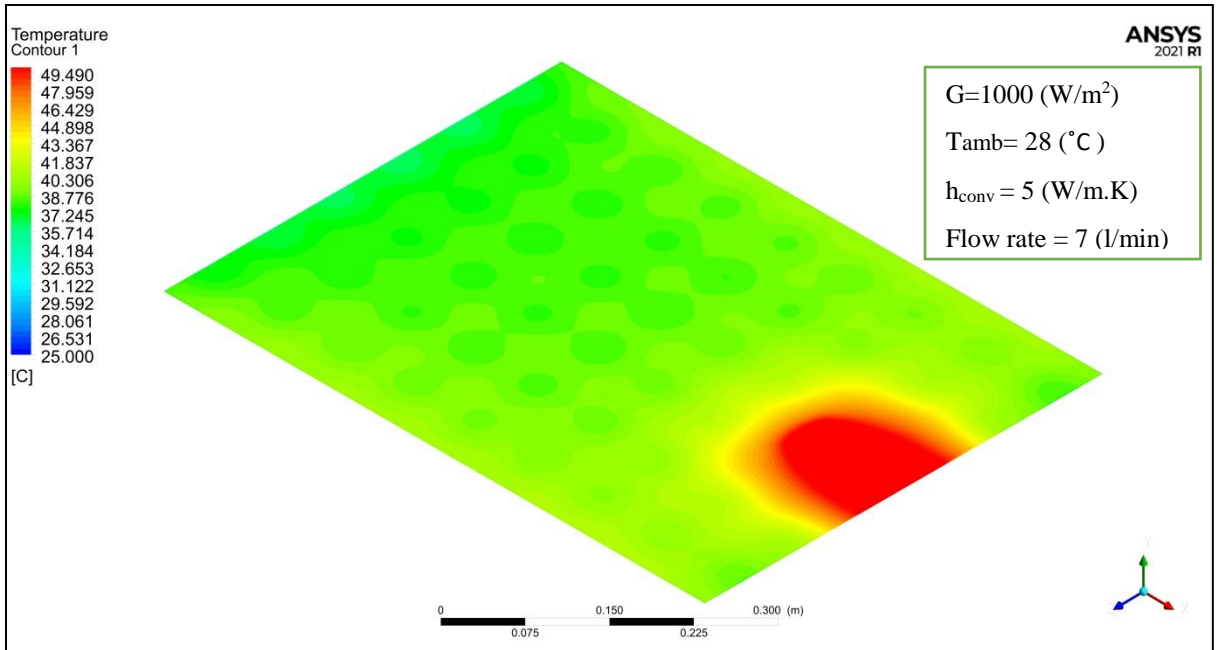


(c) The cold side of TEG modules layer in the S3 model of PV-TEG hybrid system

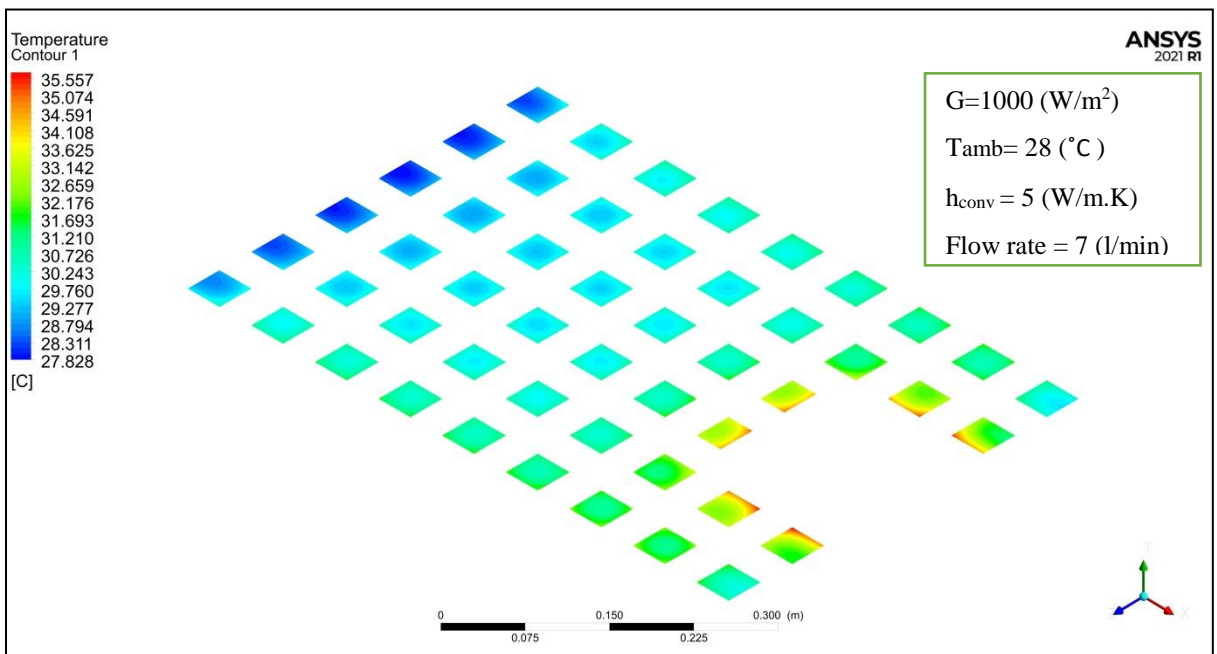


(d) The top surface of heat exchanger in the S3 model of PV-TEG hybrid system

Figure 5-5: Cont.

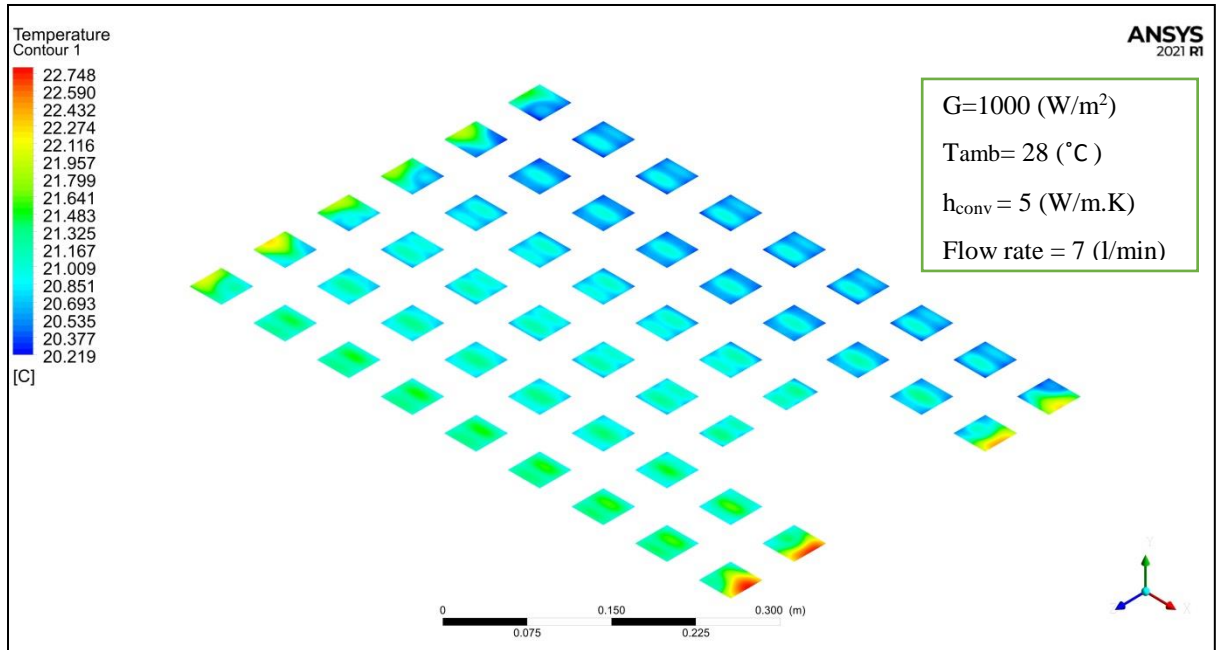


(a) The front surface of PV panel in the (S4)

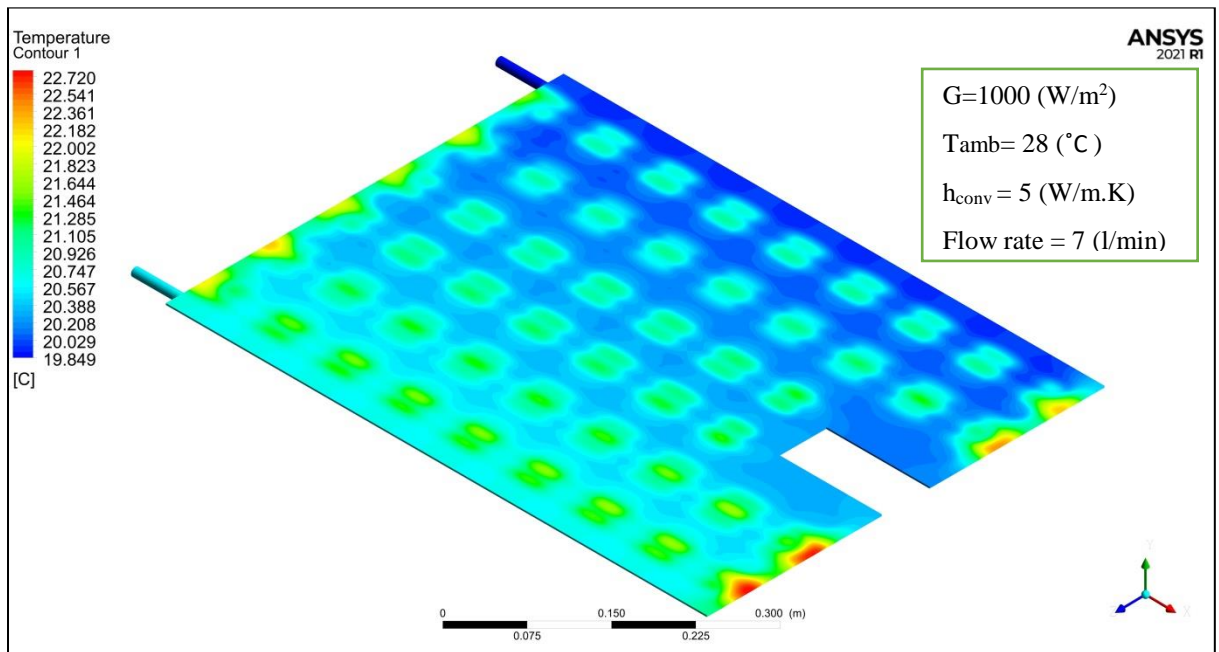


(b) The hot side of TEG modules layer in the S4 model

Figure 5-6: Temperature distribution on the (a) front surface of PV panel, (b) TEG modules hot side, (c) TEG modules cold side, and (d) top surface of heat exchanger in the PV-TEG hybrid system (S4) model.



(c) The cold side of TEG modules layer in the S4 model



(d) The top surface of heat exchanger in the S4 model

Figure 5-6: Cont.

Table 5-1: The average surface temperature of the PV module in each PV only, PV/T system and (S1, S2, S3, S4) hybrid systems

System	Tsc (°C)	Tc (°C)	Th (°C)	$\Delta T(^{\circ}C)=Th - Tc$
PV Only	65	-	-	-
PV/T	44	-	-	-
PV -TEG				
S1	31.24	20.73	22.98	2.25
S2	33.18	20.89	25.18	4.29
S3	33.76	20.86	25.88	5.02
S4	46	21.14	32.6	11.46

5.2.2. Electrical power and efficiency of tested systems

Based on the PV surface temperature profile (Tsc), the solar radiation level (G), the TEG hot side temperature, and the TEG cold side temperature, the electrical efficiency and power output of proposed systems are calculated. The outcomes are achieved by substituting the average temperature values of (Tsc, Th, and Tc) into formulas of data reduction that shown in the third chapter. As shown in Table (5-2), the PV efficiency and power output can be predicted for the PV only, the PV/T system, and the S1, S2, S3, and S4 hybrid systems. As well as, other models of the hybrid system, which consist of coupling the PV panel with different number of TEG modules as (24, 26, 36, 40, 60, 70, and 80 TEG items), are tested and displayed in the appendix (C).

It can be noticed that the output power and efficiency of the hybrid

system (S4 model) is higher compared to other hybrid system models because the high difference temperature between both TEG sides which means more powerful thermoelectric modules than in other models. So, all of the results show that the test model (S4) is the best way to turn the wasted heat from the photovoltaic panel in the chosen size (51 cm x 68 cm) into more electricity power by combining 50 items of TEG modules with solar cells and using a suitable cooling system. The generated electrical power of PV panel in the PV-TEG is about 18.5 (W) and generated power by TEG modules is 3 (W), So the total electrical power of hybrid system (E_{el}) is 21.5(W).

Figure (5-7) shows that under the same operating conditions and according to the (4-5) equation in four chapter, the generated electrical power of PV-TEG (S4) model is higher by 36.94 % and 16.8% than that the traditional photovoltaic system and the PV/T system, respectively.

Table 5-2: The output power and the overall electrical efficiency in the PV, PV/T and (S1, S2,S3, S4) hybrid system models

System	P_{PV} (W)	$\eta_{PV}\%$	P_{TEG} (W)	$\eta_{TEG}\%$	E_{el} (W)	$\eta_{el}\%$
PV Only	15.7	4.5	-	-	15.7	4.5
PV/T	18.4	5.58	-	-	18.4	5.3
PV-TEG						
S1	19.27	5.85	0.23	0.097	19.5	5.95
S2	19.07	5.75	0.35	0.186	19.47	5.966
S3	18.95	5.78	0.52	0.217	19.42	5.967
S4	18.5	5.5	3	0.409	21.5	6.2

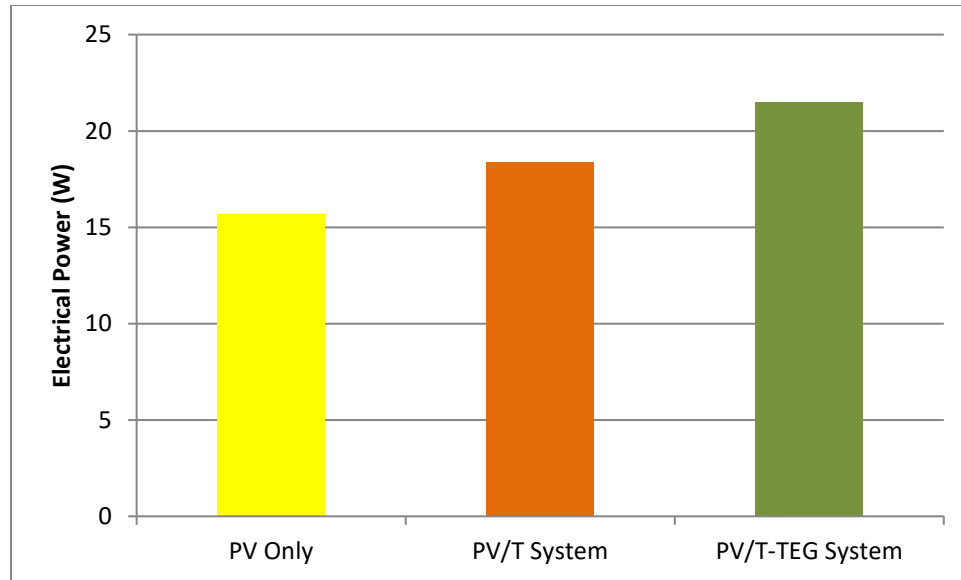


Figure 5-7: The electrical power of each PV, PV/T, and PV -TEG (S4) model hybrid system in a numerical test.

5.2.3 Validation of Numerical Results with Another work

The numerical results of this thesis are compared to the results of a previous study done in the same field and under almost the same conditions. This is done to make sure that the software used in this work is built correctly and that the numerical results are accurate and true. The results of a 3D model of a PV/T system with a heat exchanger type sheet and a serpentine tube are checked with the data from the previous study [69], which used the same input data, such as 1000 W/m^2 of solar radiation and flow rates from 1 to 7 (l/min). Figure (5-8) shows the maximum difference that does not be more than 4 % and the smallest difference is 0.4 % between the results of the current work simulation and that of the previous work simulation. So, the numerical results are pretty much the same as the results of the previous study, with an average difference of 1.3 %.

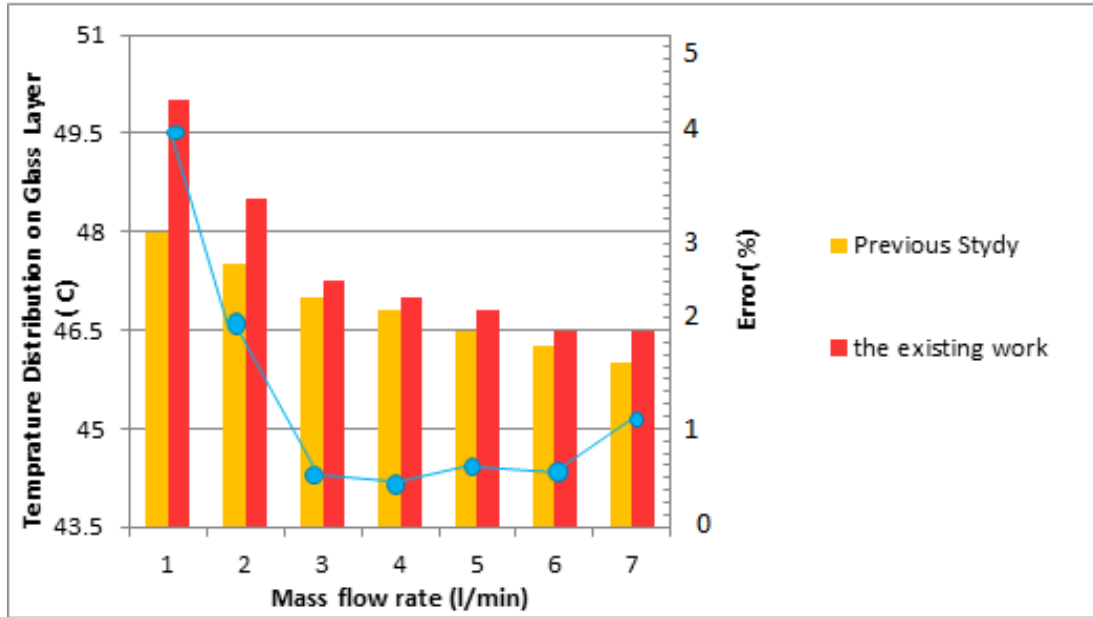


Figure 5-8: Comparison between the numerical results of the present study with the previous study [69].

5.3 Experimental Results

The outcomes of the experiments included temperature measurements, electrical measurements, and calculations of performance based on the measurements, as shown below:

5.3.1 Temperature Measurements

The temperature measurements include the ambient temperature, front surface temperatures of PV cells, and inlet and outlet cooling water temperatures. As well as, the Aluminum plate temperature that is closed to the TEG hot side temperature (T_h) and the upper surface temperature of the heat exchanger that is assumed equal to the TEG cold side temperature (T_c) in the test systems as shown in Table (5-3).

The average temperature of the PV surface is compared for the solar panel only, PV/T system, and S4 hybrid system. The results show that the average temperature of the PV module's front surface, is about 64 °C for the

PV panel, 42 °C for the PV/T hybrid, and 44.4 °C for the PV-TEG hybrid. It also can be seen that (T_{sc}) in the PV-TEG systems is higher by 5.7 % and lower by 30 % compared with PV/T and PV, respectively, due to the heat generated from absorbed solar energy and the lack of a cooling device. Furthermore, the T_{sc} is higher in PV-TEG hybrid system compared to PV/T system because the presence of a layer of thermoelectric modules between the back surface of the PV module and the heat exchanger, that acts as a resistance and raises the temperature of the photovoltaic panels.

Table 5-3: The experimental results of temperatures for PV panel, PV/T and PV-TEG systems at solar radiation 1000 (W/m²), cooling water volume flow rate 7(l/min) and $T_{amb}=28(^{\circ}\text{C})$

System	PV Temperature $T_{sc}(^{\circ}\text{C})$	Hot TEG Temperature $T_h(^{\circ}\text{C})$	Cold TEG Temperature $T_c(^{\circ}\text{C})$	$\Delta T (^{\circ}\text{C})=(T_h - T_c)$
PV panel	64	-	-	-
PV/T	42	-	-	-
PV -TEG (S4) model	44.4	35.5	23	12.5

5.3.2 Electrical measurements

By connecting the PV module wires to the PROVA 200A Solar Analyzer, the electrical measurements are recorded, which include the maximum power point (MPP) features electrical power (P_m), voltages (V_{mp}), and currents (I_{mp}), as well as I-V test curves of the PV panel in the tested systems. Digital Multi meter Type TMT 4600 was also used to record

the total open voltage (V_{oc}) of the thermoelectric modules. The calculated results are shown in Table (5-4).

Table 5-4: The experimental results of electrical characteristics for PV, PV/T and, (S4) model hybrid system at solar radiation $1000 (W/m^2)$, cooling water volume flow rate $7 (l/min)$, and $T_{amb} = 28 (^\circ C)$

System	TEG Voltage $V_{oc}(V)$	Electrical Power of TEG modules $P_{TEG\ max} (W)$	PV Current $I_{mp} (A)$	PV Voltage $V_{mp}(V)$	Electrical Power of PV $P_m (W)$	PV $\eta (%)$	(PV-TEG) $E_{el} (W)$	(PV-TEG) $\eta_{el} (%)$
PV panel	-		1.15	13.64	15.35	4.2		
PV/T	-		0.964	17.87	17.24	4.9		
PV-TEG S4model	31.4	2.4	1.035	17.21	17.81	5.15	20.21	5.83

The PV module's generated voltage (V_{mp}) at maximum power point (MPP) by the PV module, PV/T collector, and PV -TEG at steady state are displayed in Table (5-4). It is noticed that all the proposed systems have the same behavior for the voltage of the PV module, which is inversely proportional to the temperature of the photovoltaic cells. As temperature increases the open voltage of PV module drops by (2–2.3) mV with a one $^\circ C$ rise. For a given level of solar irradiance, the increase of the PV temperature leads to excite charge carriers for participating in conduct current and increase the PV current. Because of inverse relation between the current and voltage, the voltage drops.

Because of the cooling effect on the surface temperature profile of PV in the PV/T system, the (T_{sc}) is lower than that PV panel. As well as, existing of TEG modules layer and cooling effect in the PV-TEG hybrid system, the (T_{sc}) of PV-TEG is higher than that of PV/T system and lower than that PV panel. So, the V_{mp} of the PV-TEG hybrid system is higher than that of the PV module and slightly lower than the V_{mp} of the PV/T collector . The results show that the maximum power point of the PV module in the PV-TEG hybrid system is 17.21 V, whereas that of the PV panel only and PV/T systems are 13.64 V and 17.87 V, respectively.

Also, it can be seen that Table (5-4) displays the PV module current (I_{mp}) generated by the PV module, the PV/T system, and the PV-TEG at the maximum power point (MPP) in a steady-state. It is clear that the cell's produced current (I_{mp}) of the PV module is direct proportional to the temperature of the solar panels. The short circuit current increase (0.06–0.1%) with a one °C rise. Under a 1000 (W/m^2) light intensity, the current through the PV module is slightly higher compared with that of PV/T and PV- TEG systems due to the high surface temperature of PV cells and absence of cooling system. The maximum I_{mp} values are about (1.15 A, 1.035 A, and 0.964 A) for the PV panel, PV-TEG hybrid system, and PV/T system, respectively.

Because of the heat removing from the PV panel that moving to the cold side of the TEG by effect both of the TEG modules layer and the cooling action of the collector and the hybrid system. The PV panel ran hotter than both the PV/T and PV-TEG systems. So, the I_{mp} of the PV only is higher by 11 % and 19.3 % than that of the PV/T collector and slightly higher than the I_{mp} of the PV in the PV-TEG hybrid system.

5.3.2.1 Electrical power and efficiency calculation

The maximum power (P_m) of the solar panel, the PV/T system, the PV-TEG hybrid system, the thermoelectric modules, and the overall power of the PV-TEG integrating system are displayed in Figure (5-9). The maximum electrical output of PV cells products of the current multiplied by the voltage at maximum power point which declines with rising temperature by (0.4–0.5) %. It can be seen that instantaneous maximum power (P_m) of the solar PV/T system is more than the power of the PV module under 1000 (W/m^2) the solar irradiance, due to the cooling the PV module keeps voltage of PV module from decrement. Therefore, this effect would raise the electrical power.

On the other hand, the PV-TEG, outperformed all other test systems because of the extra power produced by the thermoelectric during the conversion of wasted heat into electricity. In a fixed-light scenario, the improvement ratio of output power of PV-TEG (S4) model is 31.66 % and 16.5% higher than that of the traditional photovoltaic alone and the PV/T system, respectively.

Electrical efficiency of the PV alone solar panel, the PV/T collector, and the PV-TEG hybrid system are displayed in Figure (5-10). This figure shows that the overall efficiency of the PV-TEG hybrid system (η_{el}) is greater about (37.78 % and 16.98 %) than those of the photovoltaic panel and PV/T systems. Because of the PV-TEG hybrid system's overall efficiency being a total power dependency according to equation (3-18). the overall efficiency improves as more power generates.

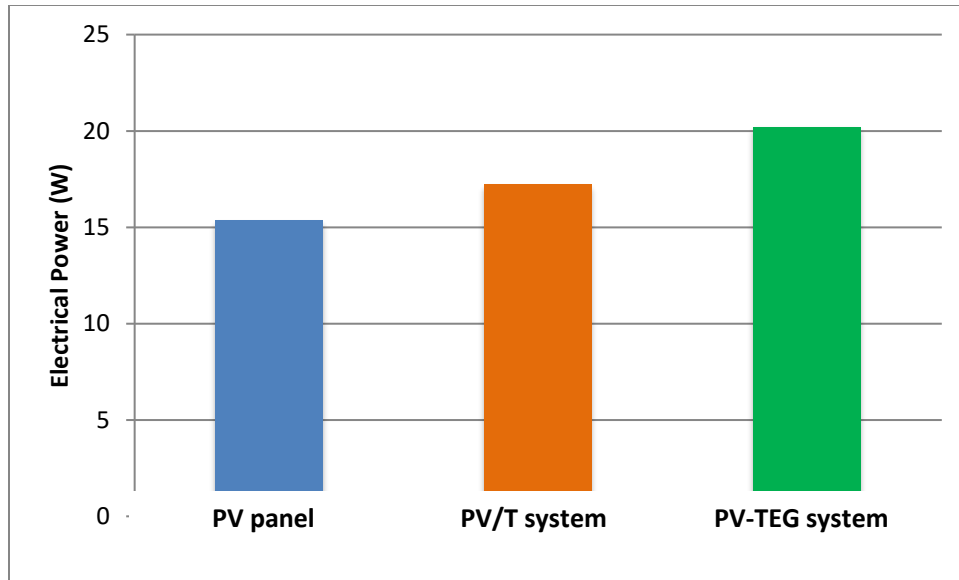


Figure 5-9: Comparison of the electrical output power between three systems (PV only, PVT, and PV -TEG) in an experimental test.

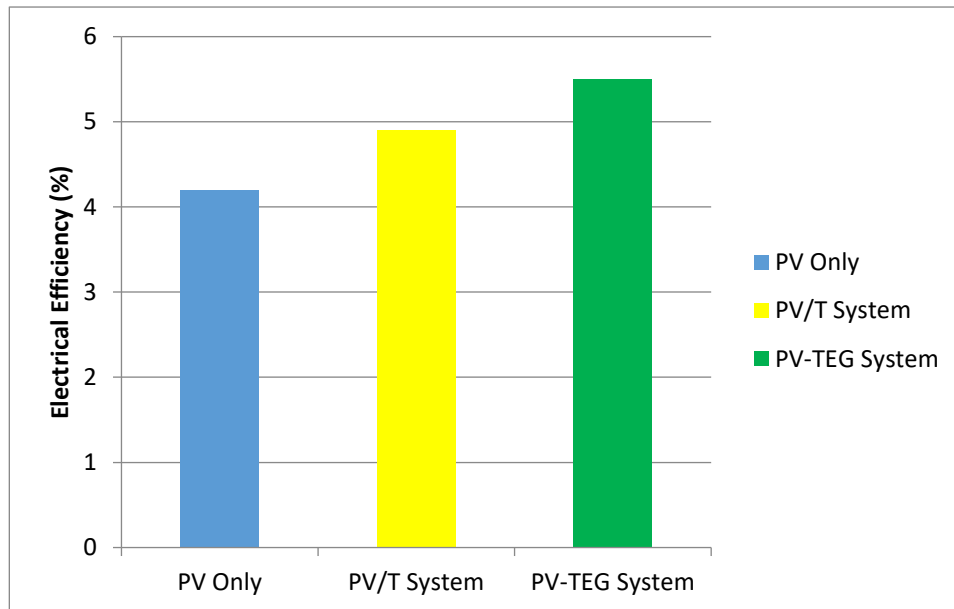


Figure 5-10: Comparison of the electrical efficiency between three systems (PV only, PVT, and PV -TEG) in an experimental test

5.4 Comparison of the results

Numerical results, such as (T_{sc} , E_{el} and η_{el}) are validated by comparing them with experimental data by calculating the deviation (difference) percentage between both results according to (4-6) equation that was mentioned in four chapter.

5.4.1 The temperature of photovoltaic module

The average front surface temperature of the PV (T_{sc}) in the PV panel, PV/T system, and PV-TEG hybrid system show a good agreement between numerical and experimental data, as shown in Figure (5-11). The difference percentage in the (T_{sc}) between numerical and experimental results are (2.9 %, 4.5 %, and 3.5 %) for the (PV panel, PV/T system, and PV -TEG hybrid system), respectively. By comparing the outcomes, it can be seen that the current work is carried out as intended and in a way that ensured errors are minimized.

5.4.2 Electrical output power and efficiency

Figures (5-12) and (5-13) present a good agreement between numerical and experimental findings of the electrical power and efficiency of the PV panel, PV /T system, and PV - TEG hybrid system. The results show that the difference percentage of the electrical output power between numerical and experimental results are (2.2 %, 6.3 %, and 6 %). As well as, the electrical efficiency η_{el} are (7.3 %, 7.5 %, and 5.96 %) for (the PV panel, PV/T system, and PV-TEG hybrid system), respectively. By comparing the outcomes, it is clear that the current work is carried out as intended and in a way that ensured errors are minimized.

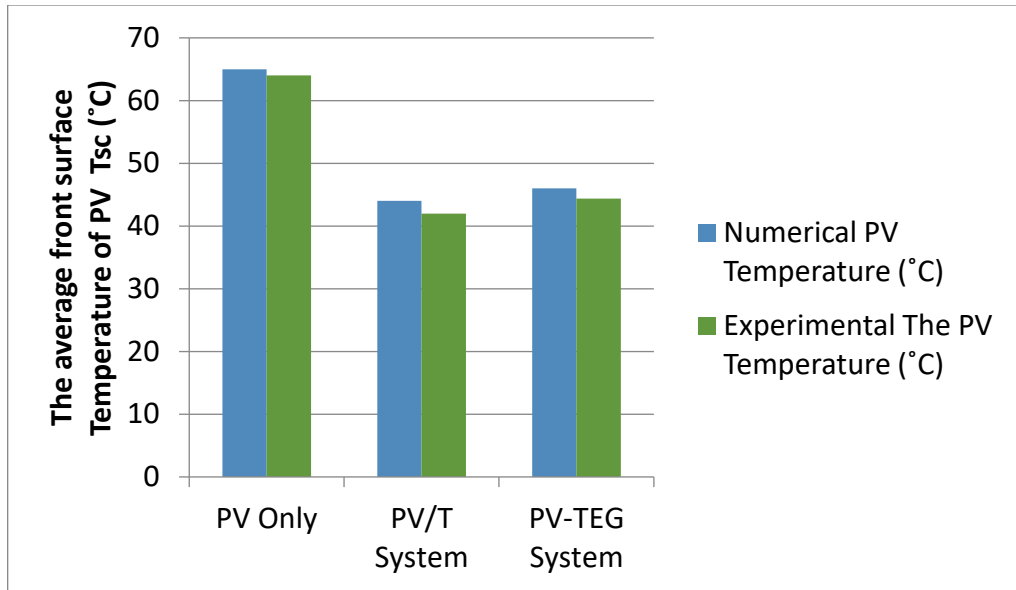


Figure 5-11: Numerical and experimental results of average front surface temperature of PV in the PV panel, PV/T system, and PV -TEG hybrid system

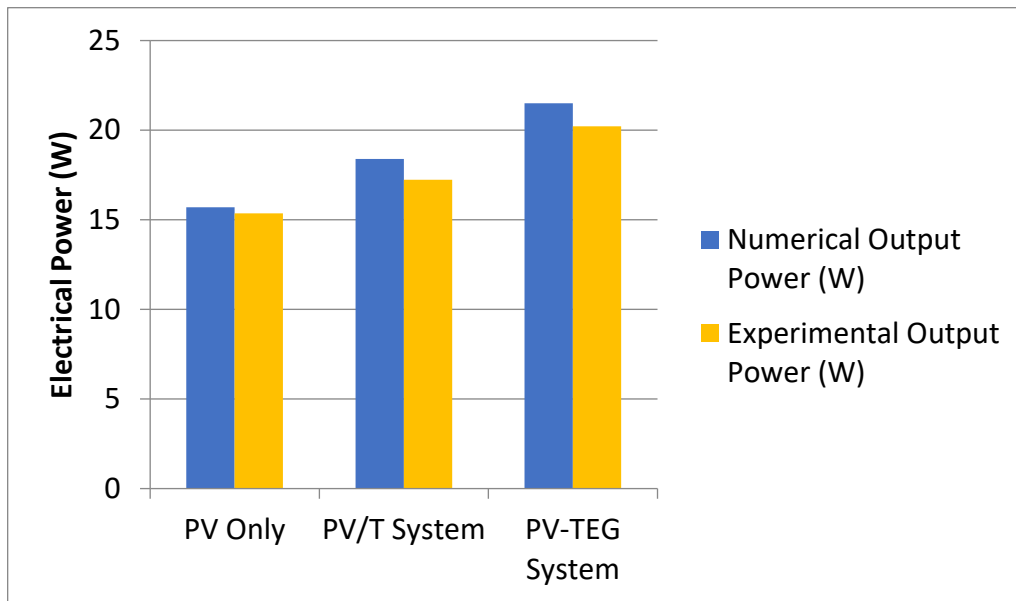


Figure 5-12: Numerical and experimental results of electrical output power of the PV panel, PV/T system, and PV -TEG hybrid system

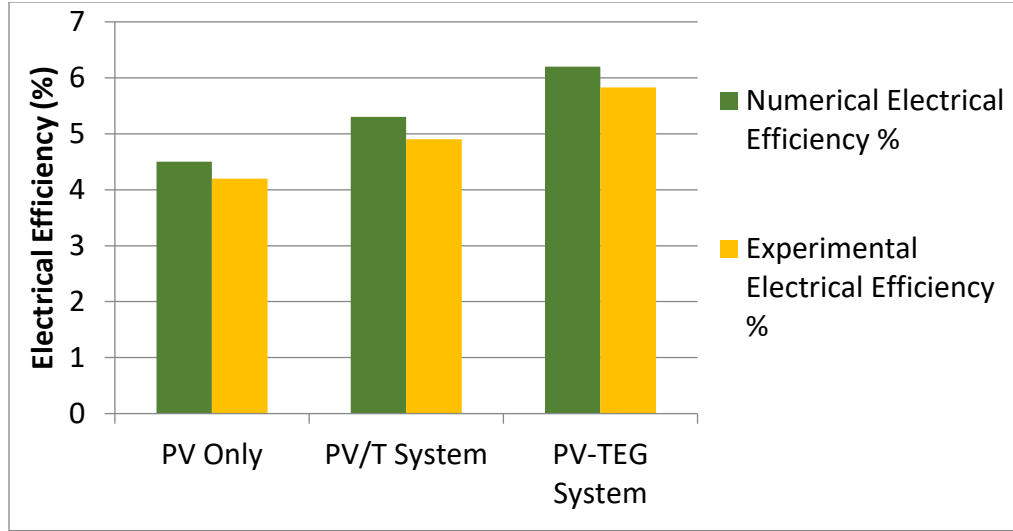


Figure 5-13: Numerical and experimental results of electrical efficiency of the PV panel, PV/T system, and PV-TEG hybrid system

5.4.3 The influence of solar radiation (G)

Figures (5-14) and (5-15) show the relationship between solar radiation and the average front surface temperature of PV (T_{sc}) in the PV panel, PV/T system, and (S4) optimum model of hybrid system. In addition the significant temperature difference between the hot side and the cold side of the TEG modules layer at a constant ambient temperature and volume flow rate numerically and experimentally, respectively. It can be seen that the relationship between the light intensity and the photovoltaic panel temperature is a direct proportional. The (T_{sc}) rises gradually in three system as G increases continuously from 1250 to 2000 (W/m^2) because of the effect of waste heat that increased in the PV panel.

It can be seen that the average front surface temperature of the PV (T_{sc}) in PV module is higher than that of other tested systems. The results show that T_{sc} increases from 71°C to 94 °C numerically and 70°C to 90°C experimentally by increasing the G value from 1250 to 2000 (W/m^2).

Because of increase G and lack of a cooling system, waste heat increases and leads to increase of T_{sc} .

In PV/T, the temperature of the PV cell only increases from 46°C to 60°C numerically and 45°C to 59°C experimentally as the light intensity is varying from 1250 to 2000 (W/m^2). Because of cooling water flow with 7 (l/min) in the heat exchanger, a wasted heat transfers from the PV back surface to the coolant directly and leads to decrease of T_{sc} in the PV/T system.

Furthermore, as increasing of G from 1250 to 2000 (W/m^2), the T_{sc} of the S4 hybrid system increases from (47°C to 67°C) and (46°C to 66°C) numerically and experimentally, respectively. In addition to a significant increase of temperature difference ΔT between the hot side and cold side of the TEG modules layer from (14°C to 21°C) and (12.5°C to 20°C) numerically and experimentally, respectively. It is also noticed that the T_{sc} in the PV-TEG hybrid system is higher than that of the PV/T system. Because of the inserting of TEG modules layer between the PV cell and the cold side of the heat exchanger and which works as a thermal resistance between two surface, the PV panel temperature increases.

Figures (5-16) and (5-17) show the output power disparities among PV panels, PV/T, and PV-TEG with varying solar radiation (G) numerically and experimentally, respectively. Because of the G is increases, the temperature difference of both TEG sides increases and leads to more output power generate via the TEG. So, the total output power of PV-TEG increases gradually according to the equations in the third chapter (3-14), (3-15), and (3-16). Furthermore, the open voltage of the TEG module increases and leads to an increasing of the TEG output power according to (4-4) equation in the four chapter.

So it can be seen that the PV-TEG generates more electricity than PV/T and the PV system, whereas PV/T produces slightly more power than the PV panel. At 2000 W/m^2 , the hybrid system generates the highest output energy. In each value of light intensity, the total electrical efficiency of the PV-TEG hybrid system is higher than that of the PV panel and PV/T systems due to the increased output power of the TEG.

All the previous results are displayed in Table (C-2) in the appendix (C).

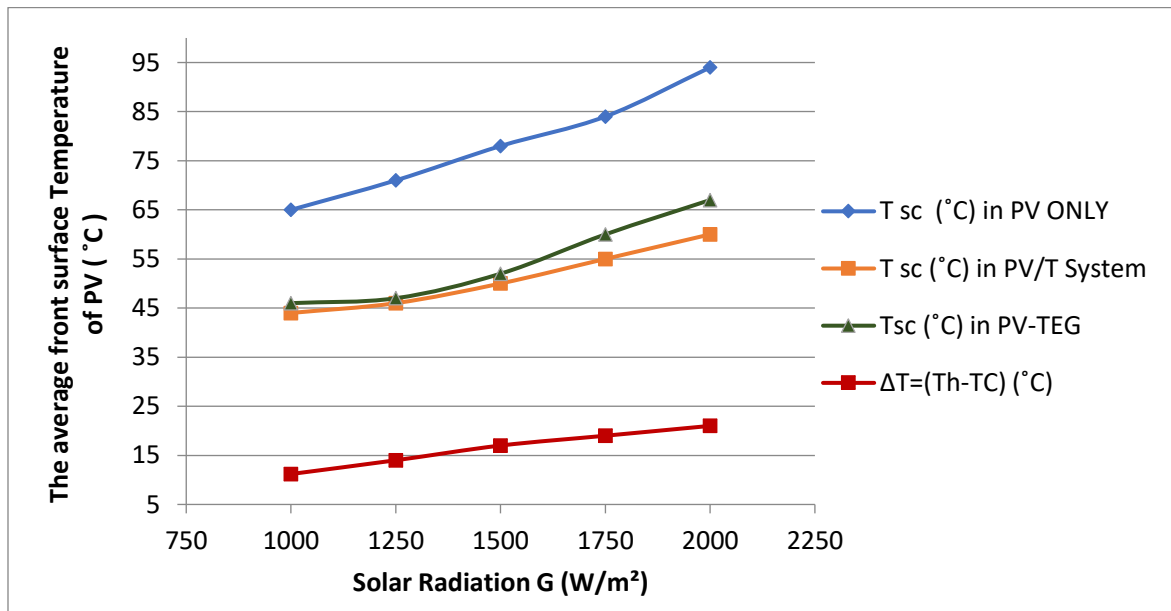


Figure 5-14: Influence of solar radiation G , numerically on the PV cell temperature in the PV only system, PV/T and PV -TEG and temperature difference between both sides of TEG

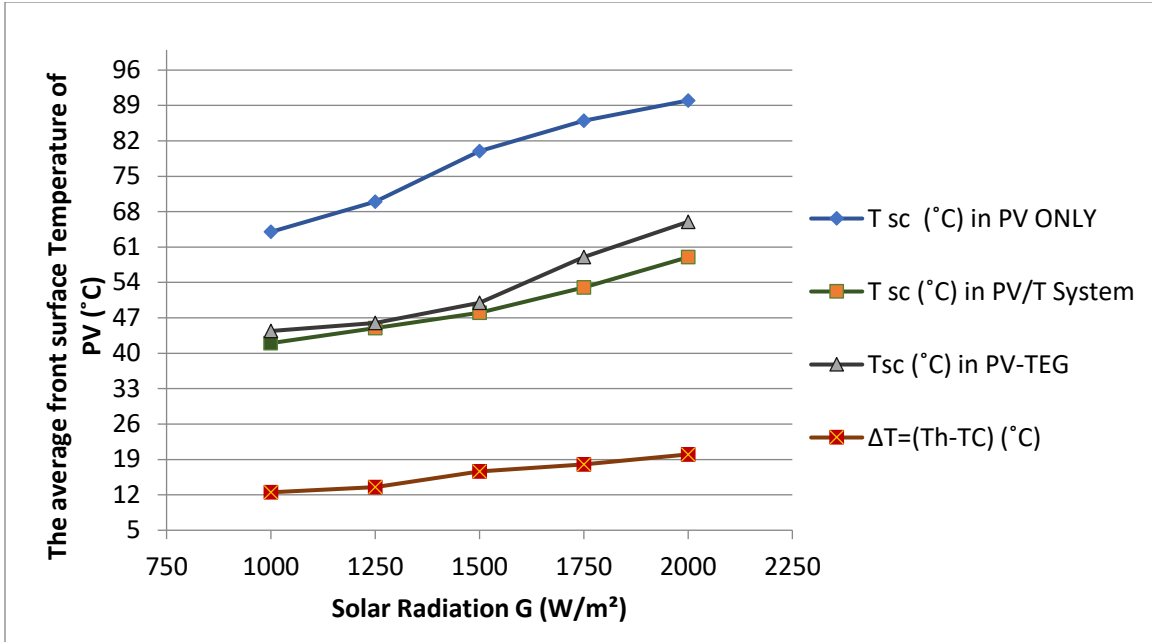


Figure 5-15: Influence of solar radiation G , experimentally on the PV cell temperature in the PV only system, PV/T and PV -TEG and temperature difference between both sides of TEG

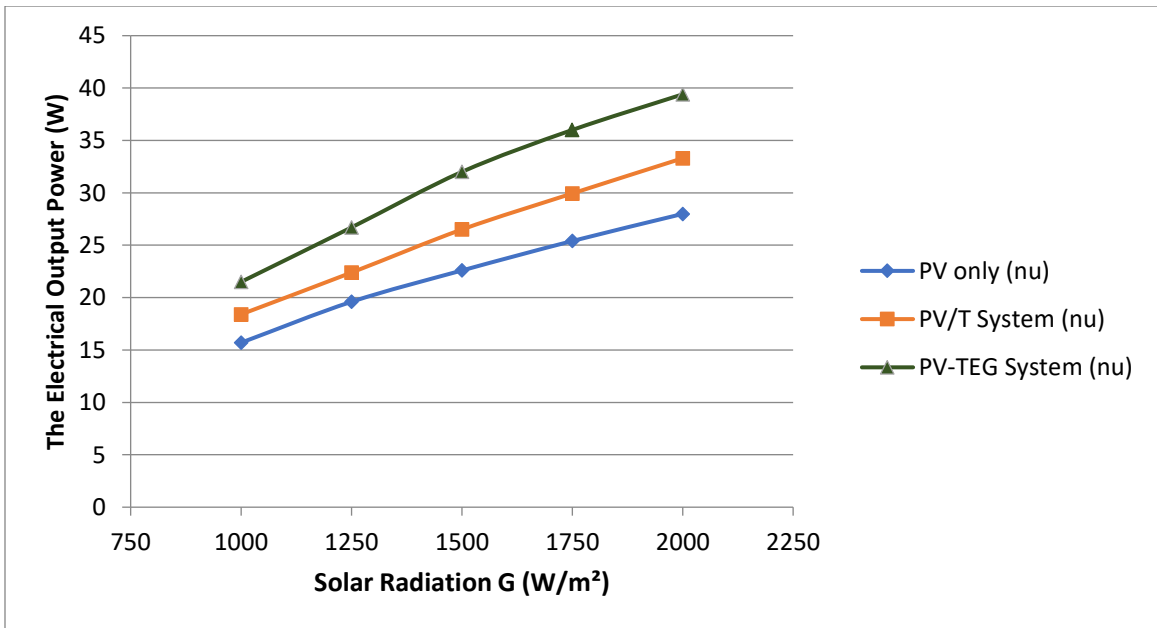


Figure 5-16: Influence of solar radiation G on the output power in the PV only, PV/T and PV -TEG numerically.

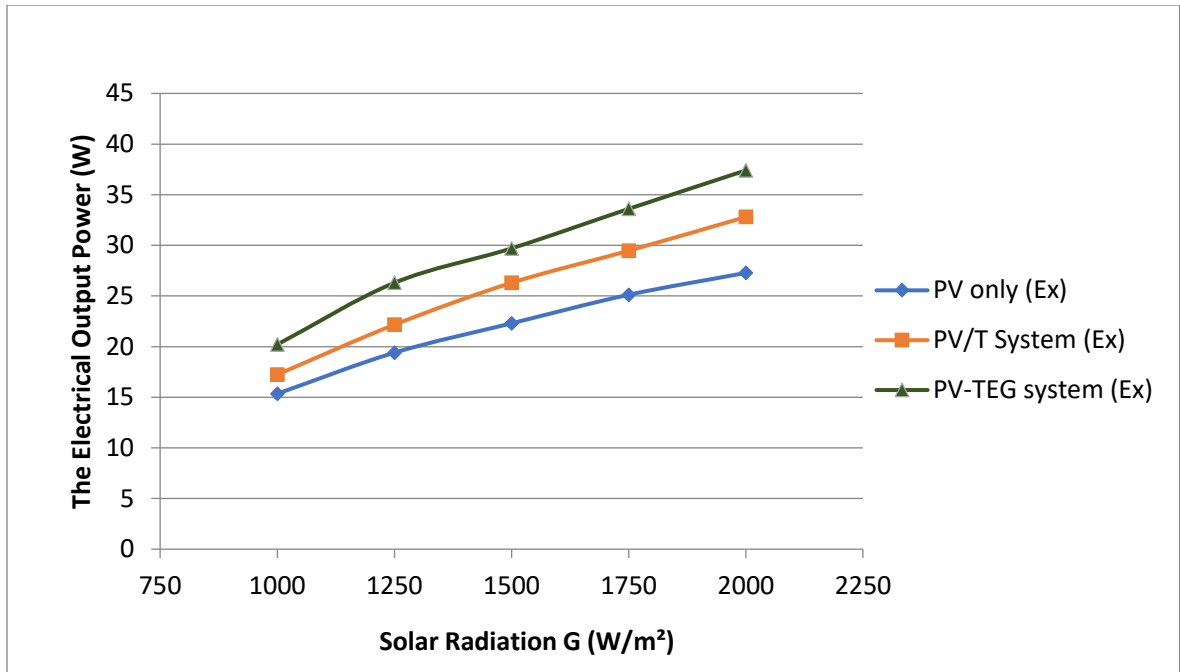


Figure 5-17: Influence of solar radiation G on the output power in the PV only, PV/T and PV-TEG, experimentally.

Chapter Six: Conclusions and Recommendations

Chapter Six

Conclusions and Recommendations

6.1 Conclusion

This study can be drawn through the following points:

- 1- Generally, the Photovoltaic – thermoelectric hybrid system is one of the successful and promising methods for harvesting the waste heat in the solar cells, converting it into additional electrical energy, and reducing the solar cells' operating temperature of the solar cells, thus improving their efficiency and maintaining their life time.
- 2- The performance of TEG modules in hybrid system depends significantly on the PV temperature and the cooling system.
- 3- The numerical simulation results referred to the S4 model are the optimal design of a hybrid system that consists of integrated the PV panel, with (51cm *68 cm) mentioned dimensions and 50 items of TEG modules.
- 4- The average front surface temperatures of the PV module (T_{sc}), are (65) °C, (44) °C, and (46) °C numerically , and (64) °C, (42) °C, and (44.4) °C experimentally in the PV panel, PV/T system, and PV -TEG hybrid system, respectively.
- 5- The average front surface temperature of PV module in the PV-TEG (S4) hybrid system is higher by 4.5 % and 5.7 % than that the PV/T system and lower by 29 % and 30 % than that photovoltaic panel, numerically and experimentally, respectively.
- 6- The electrical output power (E_{el}) and electrical efficiency (η_{el}) of the PV-TEG hybrid system are higher than that of the PV module and PV/T system in all tests. The E_{el} is about (21.5 and 20.21) W and η_{el} is about (6.2 and 5.83) % in numerical and experimental tests, respectively.

- 7- The generated electrical power of PV panel in the PV-TEG is about 18.5 (W) and generated power by TEG modules is 3 (W), So the total electrical power of hybrid system (E_{el}) is 21.5(W).
- 8- The enhancement ratio of the electrical output power E_{el} of the (S4) model hybrid system numerically is higher by 36.94 % and 16.8 %. Experimentally, it is higher by 31.66 % and 16.5 % compared with the photovoltaic panel and the PV/T system, respectively.
- 9- The difference percentage between numerical and experimental results of average temperature of the PV module top surface (T_{sc}) are (2.9 %, 4.5 %, and 3.5 %) for the PV panel, PV/T system, and PV -TEG hybrid system, respectively. In addition, the difference percentage of the electrical output power (E_{el}) and the electrical efficiency (η_{el}) between numerical and experimental results are (2.2 %, 6.3 %, and 6 %) and (7.3 %, 7.5 %, and 5.96 %) for the PV panel, PV/T system, and PV -TEG hybrid system, respectively.
- 10-The Numerical results for all studied parameters show a good level of agreement with experimental results.

6.2 Recommendations for future research

The following suggestions are made as further topics of research.

- 1- Numerically investigating the performance of the PV -TEG hybrid system compared with the PV module and PV/T system at unsteady state.
- 2- Studying the effect of cooling on the PV-TEG hybrid system performance with using different types of cooling system (passive and active).
- 3- Studying the effect of integrating thermoelectric module with solar system performance in the outdoor environment.
- 4- Using other types of non-commercial thermoelectric module with high efficiency in converting a low temperature difference between its both sides into electrical energy.
- 5- Studying cost effective of integrating PV with thermoelectric modules systems.

References

- [1] S. O. Shittu, “Investigation of a Novel Hybrid Photovoltaic-Thermoelectric Generator System,” Ph.D. Thesis, Hull University, UK 2020.
- [2] M. Thirugnanasambandam, S. Iniyar, and R. Goic, “A review of solar thermal technologies,” *Renew. Sustain. Energy Rev.*, vol. 14, no. 1, pp. 312–322, 2010, doi: 10.1016/j.rser.2009.07.014.
- [3] G. W. Crabtree and N. S. Lewis, “Solar energy conversion,” *Phys. Today*, vol. 60, no. 3, pp. 37–42, doi: 10.1063/1.2718755, 2007.
- [4] T. M. Sathe and A. S. Dhoble, “A review on recent advancements in photovoltaic thermal techniques,” *Renew. Sustain. Energy Rev.*, vol. 76, no. February, pp. 645–672, 2017, doi: 10.1016/j.rser.2017.03.075.
- [5] [https:// www. ise.fraunhofer.de](https://www.ise.fraunhofer.de), ‘Photovoltaics report’, 2017.
- [6] T. Brahim and A. Jemni, “Economical assessment and applications of photovoltaic/thermal hybrid solar technology: A review,” *Sol. Energy*, vol. 153, pp. 540–561, 2017, doi: 10.1016/j.solener.2017.05.081.
- [7] E. Radziemska and E. Klugmann, “Thermally affected parameters of the current-voltage characteristics of silicon photocell,” *Energy Convers. Manag.*, vol. 43, no. 14, pp. 1889–1900, doi: 10.1016/S0196-8904(01)00132-7, 2002.
- [8] H. T. Hashim, “Full-Spectrum Solar Energy Harvesting Using Nanotechnology-Enabled Photovoltaic/Thermoelectric Hybrid System,” Ph.D. Thesis, Cardiff University, no. September, 2015.
- [9] J. Darkwa, J. Calautit, D. Du, and G. Kokogianakis, “A numerical and experimental analysis of an integrated TEG-PCM power enhancement system for photovoltaic cells,” *Appl. Energy*, vol. 248, pp. 688–701, Aug. 2019, doi: 10.1016/j.apenergy.2019.04.147.
- [10] J. Babu, J. Darkwa, J. Calautit, D. Du, G. Kokogianakis, and P. Ponnambalam, “The role of thermoelectric generators in the hybrid PV/T systems: A review,” *Energy Convers. Manag.*, vol. 151, no. June, pp. 368–385, 2017, doi: 10.1016/j.enconman.2017.08.060.
- [11] <https://www.amazon.com/Greek-Latin-Roots-English/dp/1442233273>.
- [12] S. Sargunanathan, A. Elango, and S. T. Mohideen, “Performance

enhancement of solar photovoltaic cells using effective cooling methods: A review,” *Renew. Sustain. Energy Rev.*, vol. 64, pp. 382–393, 2016, doi: 10.1016/j.rser.2016.06.024.

- [13] K. Ranabhat, L. Patrikeev, A. A. evna Revina, K. Andrianov, V. Lapshinsky, and E. Sofronova, “An introduction to solar cell technology,” *J. Appl. Eng. Sci.*, vol. 14, no. 4, pp. 481–491, doi: 10.5937/jaes14-10879, 2016.
- [14] E. Radziemska, “The effect of temperature on the power drop in crystalline silicon solar cells,” *Renew. Energy* 28, pp. 1–12, 2003.
- [15] X. Zhang, X. Zhao, S. Smith, J. Xu, and X. Yu, “Review of R&D progress and practical application of the solar photovoltaic/thermal (PV/T) technologies,” *Renew. Sustain. Energy Rev.*, vol. 16, no. 1, pp. 599–617, 2012, doi: 10.1016/j.rser.2011.08.026.
- [16] L. Basha, “Analysis and Evaluation Tools Development of Photovoltaic Modules and System Performance,” pp. 1–134, 2012.
- [17] H. Najafi and K. A. Woodbury, “Optimization of a cooling system based on Peltier effect for photovoltaic cells,” *Sol. Energy*, vol. 91, pp. 152–160, 2013, doi: 10.1016/j.solener.2013.01.026.
- [18] D. M. Rowe, “Thermoelectrics, an environmentally-friendly source of electrical power,” *Renew. Energy*, vol. 16, no. 1–4, pp. 1251–1256, doi: 10.1016/s0960-1481(98)00512-6, 1999.
- [19] J. O’Callaghan, “Thermoelectric energy harvesting,” *Sensors (Peterborough, NH)*, vol. 28, no. 6, doi: 10.5772/intechopen.85670, 2011.
- [20] D. M. C. Rowe, *Handbook of Thermoelectric*. 1995.
- [21] T. M. Tritt and M. A. Subramanian, “Thermoelectric Materials , Phenomena , and Applications : A Bird ’ s Eye View,” vol. 31, no. March 2006, 2018.
- [22] G. Chen, “Direct Solar/Thermal to Electr. Energy Convers. Technol,” <http://web.mit.edu/nanoengineering> (accessed 3.28.20). 2009.
- [23] A. J. Minnich, M. S. Dresselhaus, Z. F. Ren, and G. Chen, “Bulk nanostructured thermoelectric materials: Current research and future prospects,” *Energy Environ. Sci.*, vol. 2, no. 5, pp. 466–479, doi: 10.1039/b822664b, 2009.

- [24] S. Twaha, J. Zhu, Y. Yan, and B. Li, “A comprehensive review of thermoelectric technology: Materials, applications, modelling and performance improvement,” *Renew. Sustain. Energy Rev.*, vol. 65, pp. 698–726, doi: 10.1016/j.rser.2016.07.034, 2016.
- [25] H. Hashim, J. J. Bomphrey, and G. Min, “Model for geometry optimisation of thermoelectric devices in a hybrid PV/TE system,” *Renew. Energy*, vol. 87, pp. 458–463, Mar. 2016, doi: 10.1016/j.renene.2015.10.029.
- [26] Y. Y. Hsiao, W. C. Chang, and S. L. Chen, “A mathematic model of thermoelectric module with applications on waste heat recovery from automobile engine,” *Energy*, vol. 35, no. 3, pp. 1447–1454, 2010, doi: 10.1016/j.energy.2009.11.030.
- [27] S. J. Kim, J. H. We, and B. J. Cho, “A wearable thermoelectric generator fabricated on a glass fabric,” *Energy Environ. Sci.*, vol. 7, no. 6, pp. 1959–1965, doi: 10.1039/c4ee00242c, 2014.
- [28] R. Amatya and R. J. Ram, “Solar thermoelectric generator for micropower applications,” *J. Electron. Mater.*, vol. 39, no. 9, pp. 1735–1740, doi: 10.1007/s11664-010-1190-8, 2010.
- [29] D. Madan, Z. Wang, P. K. Wright, and J. W. Evans, “Printed flexible thermoelectric generators for use on low levels of waste heat,” *Appl. Energy*, vol. 156, pp. 587–592, 2015, doi: 10.1016/j.apenergy.2015.07.066.
- [30] J. L. Gao, Q. G. Du, X. D. Zhang, and X. Q. Jiang, “Thermal stress analysis and structure parameter selection for a Bi₂Te₃-based thermoelectric module,” *J. Electron. Mater.*, vol. 40, no. 5, pp. 884–888, doi: 10.1007/s11664-011-1611-3, 2011.
- [31] P. V. Y. V. V. F. J. Willars-Rodríguez¹, E. A. Chávez-Urbiola, “Investigation of solar hybrid system with concentrating Fresnel lens, photovoltaic and thermoelectric generators,” *Arch. Thermodyn.*, vol. 33, no. 4, pp. 23–40, doi: 10.1002/er, 2012.
- [32] D. T. Cotfas, P. A. Cotfas, O. M. Machidon, and D. Ciobanu, “Investigation of the photovoltaic cell/ thermoelectric element hybrid system performance,” *IOP Conf. Ser. Mater. Sci. Eng.*, vol. 133, no. 1, doi: 10.1088/1757-899X/133/1/012037, 2016.
- [33] P. Fern, “Thermal management of thermoelectric generators for waste

energy recovery,” vol. 196, 2021, doi:
10.1016/j.applthermaleng.2021.117291.

- [34] Y. Zhou, S. Paul, and S. Bhunia, "Harvesting wasted heat in a microprocessor using thermoelectric generators: modeling, analysis and measurement," In 2008 Design, Automation and Test in Europe (pp. 98-103). IEEE, doi: 10.1109/DATE.2008.4484669, (2008, March).
- [35] B. I. Ismail, and W. H. Ahmed, "Thermoelectric power generation using waste-heat energy as an alternative green technology," *Recent Patents on Electrical & Electronic Engineering (Formerly Recent Patents on Electrical Engineering)*, 2(1), 27-39, 2009.
- [36] C. Babu and P. Ponnambalam, "The theoretical performance evaluation of hybrid PV-TEG system," *Energy Convers. Manag.*, vol. 173, pp. 450–460, Oct. 2018, doi: 10.1016/j.enconman.2018.07.104.
- [37] S. Y. Wu, Y. C. Zhang, L. Xiao, and Z. G. Shen, "Performance comparison investigation on solar photovoltaic-thermoelectric generation and solar photovoltaic-thermoelectric cooling hybrid systems under different conditions," *Int. J. Sustain. Energy*, vol. 37, no. 6, pp. 533–548, doi: 10.1080/14786451.2017.1345906, Jul. 2018.
- [38] M. Mohsenzadeh, M. B. Shafii, and H. Jafari mosleh, "A novel concentrating photovoltaic/thermal solar system combined with thermoelectric module in an integrated design," *Renew. Energy*, vol. 113, pp. 822–834, 2017, doi: 10.1016/j.renene.2017.06.047.
- [39] W. Xie, X. Tang, Y. Yan, Q. Zhang, and T. M. Tritt, "Unique nanostructures and enhanced thermoelectric performance of melt-spun BiSbTe alloys," *Appl. Phys. Lett.*, vol. 94, no. 10, pp. 1–4, doi: 10.1063/1.3097026, 2009.
- [40] D. Kraemer, L. Hu, A. Muto, X. Chen, G. Chen, and M. Chiesa, "Photovoltaic-thermoelectric hybrid systems: A general optimization methodology," *Appl. Phys. Lett.*, vol. 92, no. 24, doi: 10.1063/1.2947591, 2008.
- [41] X. Ju, Z. Wang, G. Flamant, P. Li, and W. Zhao, "Numerical analysis and optimization of a spectrum splitting concentration photovoltaic-thermoelectric hybrid system," *Sol. Energy*, vol. 86, no. 6, pp. 1941–1954, 2012, doi: 10.1016/j.solener.2012.02.024.
- [42] G. Li, S. Shittu, T. M. O. Diallo, M. Yu, X. Zhao, and J. Ji, "A review

- of solar photovoltaic-thermoelectric hybrid system for electricity generation,” *Energy*, vol. 158. Elsevier Ltd, pp. 41–58, Sep. 01, 2018, doi: 10.1016/j.energy.2018.06.021.
- [43] W. Zhu, Y. Deng, Y. Wang, S. Shen, and R. Gulfam, “High-performance photovoltaic-thermoelectric hybrid power generation system with optimized thermal management,” *Energy*, vol. 100, pp. 91–101, Apr. 2016, doi: 10.1016/j.energy.2016.01.055.
- [44] N. Wang, L. Han, H. He, N. H. Park, and K. Koumoto, “A novel high-performance photovoltaic-thermoelectric hybrid device,” *Energy Environ. Sci.*, vol. 4, no. 9, pp. 3676–3679, doi: 10.1039/c1ee01646f, 2011.
- [45] M. M. M. Daud, N. B. M. Nor, and T. Ibrahim, “Novel hybrid photovoltaic and thermoelectric panel,” *2012 IEEE Int. Power Eng. Optim. Conf. PEOCO 2012 - Conf. Proc.*, no. June, pp. 269–274, 2012, doi: 10.1109/PEOCO.2012.6230873.
- [46] K. T. Park, S. M. Shin, A. S. Tazebay, H. D. Um, J. Y. Jung, S. W. Jee, “Lossless hybridization between photovoltaic and thermoelectric devices,” *Sci. Rep.*, vol. 3, pp. 1–6, doi: 10.1038/srep02123, 2013.
- [47] C. Haiping, H. Jiguang, Z. Heng, L. Kai, L. Haowen, and L. Shuangyin, “Experimental investigation of a novel low concentrating photovoltaic/thermal–thermoelectric generator hybrid system,” *Energy*, 2018, doi: 10.1016/j.energy.2018.10.046.
- [48] J. Liu, H. Tang, D. Zhang, S. Jiao, “Performance evaluation of the hybrid photovoltaic-thermoelectric system with light and heat management,” *Energy*, vol. 211, p. 118618, 2020, doi: 10.1016/j.energy.2020.118618.
- [49] S. Shittu, G. Li, X. Zhao, J. Zhou, X. Ma, and Y. G. Akhlaghi, “Experimental study and exergy analysis of photovoltaic-thermoelectric with flat plate micro-channel heat pipe,” *Energy Convers. Manag.*, vol. 207, no. October 2019, p. 112515, 2020, doi: 10.1016/j.enconman.2020.112515.
- [50] A. Omar, M. Ali, and M. Halawa, “Experimental Investigation of Solar-Thermoelectric Power Generator Amira Omar, Mostafa Ali and M. Halawa Mech. Department, Faculty of Engineering, Al Azhar University, Cairo, Egypt,” pp. 12–19, doi:

10.7537/marsjas160720.03.Keywords.

- [51] N. H. Sark, N. Wang, L. Han, H. He, K. Koumoto, “Feasibility of photovoltaic - Thermoelectric hybrid modules,” *Appl. Energy*, vol. 88, no. 8, pp. 2785–2790, 2011, doi: 10.1016/j.apenergy.2011.02.008.
- [52] H. Najafi and K. A. Woodbury, “Modeling and analysis of a combined photovoltaic-thermoelectric power generation system,” *J. Sol. Energy Eng. Trans. ASME*, vol. 135, no. 3, doi: 10.1115/1.4023594, 2013.
- [53] E. Yin, Q. Li, and Y. Xuan, “Thermal resistance analysis and optimization of photovoltaic-thermoelectric hybrid system,” *Energy Convers. Manag.*, vol. 143, pp. 188–202, 2017, doi: 10.1016/j.enconman.2017.04.004.
- [54] S. Soltani, A. Kasaeian, T. Sokhansefat, and M. B. Shafii, “Performance investigation of a hybrid photovoltaic/thermoelectric system integrated with parabolic trough collector,” *Energy Convers. Manag.*, vol. 159, no. December 2017, pp. 371–380, 2018, doi: 10.1016/j.enconman.2017.12.091.
- [55] W. Gu, T. Ma, A. Song, M. Li, and L. Shen, “Mathematical modelling and performance evaluation of a hybrid photovoltaic-thermoelectric system,” *Energy Convers. Manag.*, vol. 198, no. March, p. 111800, 2019, doi: 10.1016/j.enconman.2019.111800.
- [56] P. M. Rodriguz, A. Valera, E. F. Fernández, and F. M. Almonacid, “Performance and economic limits of passively cooled hybrid thermoelectric generator-concentrator photovoltaic modules,” *Appl. Energy*, vol. 238, no. January, pp. 1150–1162, 2019, doi: 10.1016/j.apenergy.2019.01.132.
- [57] S. Mahmoudinezhad, A. Rezania, D. T. Cotfas, P. A. Cotfas, and L. A. Rosendahl, “Experimental and numerical investigation of hybrid concentrated photovoltaic – Thermoelectric module under low solar concentration,” *Energy*, vol. 159, pp. 1123–1131, Sep. 2018, doi: 10.1016/j.energy.2018.06.181.
- [58] A. Lashin, M. Al Turkestani, and M. Sabry, “Performance of a thermoelectric generator partially illuminated with highly concentrated light,” *Energies*, vol. 13, doi: 10.3390/en13143627, no. 14. 2020.
- [59] A. Riahi, A. Ben Haj Ali, A. Fadhel, A. Guizani, and M. Balghouthi, “Performance investigation of a concentrating photovoltaic thermal

hybrid solar system combined with thermoelectric generators,” *Energy Convers. Manag.*, vol. 205, no. December 2019, 2020, doi: 10.1016/j.enconman.2019.112377.

- [60] A. L. Abdullah, S. Misha, N. Tamaldin, M. A. M. Rosli, and F. A. Sachit, “Theoretical study and indoor experimental validation of performance of the new photovoltaic thermal solar collector (PVT) based water system,” *Case Stud. Therm. Eng.*, vol. 18, no. November 2019, p. 100595, 2020, doi: 10.1016/j.csite.2020.100595.
- [61] M. M. Sardouei and H. Morteza pour, “Temperature distribution and efficiency assessment of different PVT water collector designs,” *Sādhanā*, vol. 0123456789, doi: 10.1007/s12046-018-0826-x, 2018.
- [62] A. Salari, A. Parcheforosh, A. Hakkaki-Fard, and A. Amadeh, “A numerical study on a photovoltaic thermal system integrated with a thermoelectric generator module,” *Renew. Energy*, vol. 153, pp. 1261–1271, Jun. 2020, doi: 10.1016/j.renene.2020.02.018.
- [63] J. and J. D. Anderson, “Computational-Fluid-Dynamics-the-Basics-With-Applications-Anderson-J-D.pdf.” (Vol. 206, p. 332). New York: McGraw-Hill, 1995.
- [64] M. Okiishi and H. Rothmayer, *Fundamentals of Fluid Mechanics*. .
- [65] P. K. Namburu, D. K. Das, K. M. Tanguturi, and R. S. Vajjha, “Numerical study of turbulent flow and heat transfer characteristics of nanofluids considering variable properties,” *Int. J. Therm. Sci.*, vol. 48, no. 2, pp. 290–302, 2009, doi: 10.1016/j.ijthermalsci.2008.01.001.
- [66] S. Eiamsa-ard and P. Promvonge, “Numerical study on heat transfer of turbulent channel flow over periodic grooves ☆,” vol. 35, pp. 844–852, 2008, doi: 10.1016/j.icheatmasstransfer.2008.03.008.
- [67] M. Afzanizam, M. Rosli, Y. J. Ping, S. Misha, and M. Z. Akop, “Akademia Baru Simulation Study of Computational Fluid Dynamics on Photovoltaic Thermal Water Collector with Different Designs of Absorber Tube Akademia Baru,” vol. 1, no. 1, pp. 12–22, 2018.
- [68] B. S. Dallan, J. Schumann, and F. J. Lesage, “Performance evaluation of a photoelectric-thermoelectric cogeneration hybrid system,” *Sol. Energy*, vol. 118, pp. 276–285, Aug. 2015, doi: 10.1016/j.solener.2015.05.034.

- [69] J. Zhou, H. Ke, and X. Deng, “Experimental and CFD investigation on temperature distribution of a serpentine tube type photovoltaic/thermal collector,” *Sol. Energy*, vol. 174, pp. 735–742, Nov. 2018, doi: 10.1016/j.solener.2018.09.063.
- [70] S. V Patankar, *Numerical heat transfer and fluid flow*. CRC press, 2018.
- [71] A. Kazemian, A. Salari, A. Hakkaki-fard, and T. Ma, “Numerical investigation and parametric analysis of a photovoltaic thermal system integrated with phase change material,” *Appl. Energy*, vol. 238, no. January, pp. 734–746, 2019, doi: 10.1016/j.apenergy.2019.01.103.
- [72] A. Nahar, M. Hasanuzzaman, and N. A. Rahim, “A Three-Dimensional Comprehensive Numerical Investigation of Different Operating Parameters on the Performance of a Photovoltaic Thermal System with Pancake Collector,” *J. Sol. Energy Eng. Trans. ASME*, vol. 139, no. 3, doi: 10.1115/1.4035818, Jun. 2017.
- [73] G. A. O. Min, “Thermoelectric Module Design Under a Given Thermal Input : Theory and Example,” vol. 42, no. 7, pp. 2239–2242, doi: 10.1007/s11664-013-2591-2, 2013.
- [74] U. A. Saleh, M. A. Johar, S. A. Jumaat, M. N. Rejab, and W. A. W. Jamaludin, “Evaluation of a pv-teg hybrid system configuration for an improved energy output: A review,” *Int. J. Renew. Energy Dev.*, vol. 10, no. 2, pp. 385–400, 2021, doi: 10.14710/ijred.2021.33917.
- [75] F. Rajaei, M. Amin, V. Rad, A. Kasaeian, and O. Mahian, “Experimental analysis of a photovoltaic / thermoelectric generator using cobalt oxide nano fluid and phase change material heat sink,” *Energy Convers. Manag.*, vol. 212, no. March, p. 112780, 2020, doi: 10.1016/j.enconman.2020.112780.
- [76] [https:// www. calculator. academy](https://www.calculator.academy), ‘improvement-percentage-calculator’, 2022.
- [77] M. F. Al-saleh and A. E. Yousif, “Properties of the Standard Deviation that are Rarely Mentioned in Classrooms 1 Introduction 2 Some Basic Properties of the Standard Deviation,” vol. 38, no. 3, pp. 193–202, doi: <https://doi.org/10.17713/ajs.v38i3.272>, 2009.

Appendices

Appendix-A
Thermoelectric Modules (TEG) Performance Test Results

TEG 1		TEG 2		TEG 3	
ΔT (°c)	Voltage(v)	ΔT (°c)	Voltage(v)	ΔT (°c)	Voltage(v)
45	0.248	45	0.560	45	0.255
40	0.234	40	0.501	40	0.225
35	0.214	35	0.441	35	0.211
30	0.180	30	0.374	30	0.185
25	0.159	25	0.310	25	0.156
20	0.147	20	0.257	20	0.145
15	0.138	15	0.198	15	0.136
10	0.129	10	0.134	10	0.127

TEG 4		TEG 5		TEG 6	
ΔT (°c)	Voltage(v)	ΔT (°c)	Voltage (v)	ΔT (°c)	Voltage(v)
45	0.624	45	0.528	45	0.268
40	0.582	40	0.486	40	0.235
35	0.501	35	0.410	35	0.213
30	0.440	30	0.335	30	0.188
25	0.243	25	0.311	25	0.167
20	0.225	20	0.255	20	0.146
15	0.183	15	0.202	15	0.132
10	0.128	10	0.150	10	0.117

TEG 7		TEG 8		TEG 9	
ΔT (°c)	Voltage(v)	ΔT (°c)	Voltage(v)	ΔT (°c)	Voltage(v)
45	0.620	45	0.258	45	0.410
40	0.576	40	0.231	40	0.365
35	0.501	35	0.192	35	0.305
30	0.453	30	0.162	30	0.254
25	0.396	25	0.142	25	0.211
20	0.299	20	0.120	20	0.186
15	0.213	15	0.101	15	0.131
10	0.157	10	0.086	10	0.102

TEG 10		TEG 11		TEG 12	
ΔT (°c)	Voltage(v)	ΔT (°c)	Voltage(v)	ΔT (°c)	Voltage(v)
45	0.784	45	0.389	45	0.537
40	0.678	40	0.286	40	0.490
35	0.566	35	0.247	35	0.417
30	0.499	30	0.208	30	0.349
25	0.411	25	0.164	25	0.295
20	0.318	20	0.137	20	0.234
15	0.244	15	0.109	15	0.189
10	0.167	10	0.071	10	0.117

TEG 13		TEG 14		TEG 15	
ΔT (°c)	Voltage(v)	ΔT (°c)	Voltage(v)	ΔT (°c)	Voltage(v)
45	0.397	45	0.416	45	0.406
40	0.317	40	0.324	40	0.381
35	0.282	35	0.256	35	0.336
30	0.230	30	0.233	30	0.316
25	0.202	25	0.191	25	0.303
20	0.187	20	0.150	20	0.280
15	0.156	15	0.112	15	0.237
10	0.130	10	0.085	10	0.191

TEG 16		TEG 17		TEG 18	
ΔT (°c)	Voltage(v)	ΔT (°c)	Voltage(v)	ΔT (°c)	Voltage(v)
45	0.489	45	0.500	45	0.473
40	0.438	40	0.444	40	0.404
35	0.381	35	0.393	35	0.368
30	0.350	30	0.375	30	0.356
25	0.321	25	0.334	25	0.331
20	0.292	20	0.312	20	0.296
15	0.281	15	0.298	15	0.256
10	0.257	10	0.265	10	0.241

TEG 19		TEG 20		TEG 21	
ΔT (°c)	Voltage(v)	ΔT (°c)	Voltage(v)	ΔT (°c)	Voltage(v)
45	0.420	45	0.412	45	0.390
40	0.387	40	0.367	40	0.347
35	0.328	35	0.331	35	0.301
30	0.293	30	0.303	30	0.274
25	0.253	25	0.281	25	0.250
20	0.230	20	0.252	20	0.199
15	0.207	15	0.211	15	0.171
10	0.179	10	0.174	10	0.134

TEG 22		TEG 23		TEG 24	
ΔT (°c)	Voltage(v)	ΔT (°c)	Voltage(v)	ΔT (°c)	Voltage(v)
45	0.325	45	0.411	45	0.398
40	0.291	40	0.362	40	0.357
35	0.260	35	0.328	35	0.320
30	0.231	30	0.298	30	0.288
25	0.208	25	0.256	25	0.228
20	0.187	20	0.213	20	0.189
15	0.162	15	0.198	15	0.157
10	0.134	10	0.150	10	0.123

Appendix-B

Calibration of Instruments

جمهورية العراق



وزارة التخطيط
الجهاز المركزي للقياس والميطرة النوعية

العدد : ٨٤٨١
التاريخ م : ٢٠٢١ / ٤ / ٤
هـ : / /

الدائرة : التقييس
القسم : المقاييس

إلى /جامعة كربلاء - كلية الهندسة - الموارد البشرية

م / معايرة اجهزة

بهدي الجهاز اطلب تحياته
اشارة إلى كتابكم ذي العدد د/٣/٢٠٢٤ في ٢٠٢١/٨/١ نود اعلامكم الاتي :

١- تمت معايرة الجهاز العائد لكم وكانت النتائج كما مبينة في شهادة المعايرة و ينبغي الاخذ بنظر الاعتبار النتائج و التصحيحات عند القياس علما ان المعايرة نافذة لمدة سنة .

٢- نعتز عن معايرة الاجهزة الواردة في الفقرات (٣ ، ٤ ، ٥) لعدم وجود الامكانية في الوقت الحاضر .

٣- تم تمديد اجور المعايرة البالغة (٧٧٠٠٠) سبعة وسبعون الف دينار فقط بموجب وصل القبض المرقم (٣٥٠٨٣) في ٢٠٢١/٨/٣ .

الاجهزة :
Data Logger مع مزدوج حراري نوع (K) عدد ٧/
مع التقدير

المرافقات /
شهادة معايرة عدد (١) فقط .


المهندسة
خلود خالد شكري
ع/ مدير عام دائرة التقييس
٢٠٢١/١٠/٤



نسخة منه إلى /
- مكتب المدير العام للتفضل بالاطلاع مع التقدير
- شعبة القياسات الفيزيائية لطفا .

هنا محمد قادر

العراق - بغداد - الجادرية - ص . ب (١٢٠٢٢) - البريد الالكتروني : www.cosqc.gov.iq
هاتف ٨٤ / ٨٢ / ٨٢ / ٨١ / ٧٧٦١٩٨١ تليفاكس : cosac@cosac.gov.iq



Calibration Certificate
Central Organization for Standardization and Quality Control (COSQC)
Metrology Department - Physics Section (FOR-TC-012)

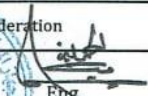
P.O. Box13032 Aljadriya street, Baghdad , Tel:7785180 - E-Mail : cosqc@cosqc.gov.iq

Certificate No.: PHT 677 / 2021

Date of issue : 12/08/2021

Customer		
Name:	جامعة كربلاء / كلية الهندسة	
Address:	العراق - كربلاء المقدسة	
Item under calibration		
Description:	Temperature Recorder 12 CH With TC (K)	Res. : 0.1 ° C
Manufacturer:	LUTRON	
Model:	BTM - 4208SD	
Serial number:	L144597	
Other identification:	(-200 ----- 1370) °C	
Date of reception:	Order no. : (260) , Date of Reception : 3/08/2021	
Condition of reception:	As Found	
Standard(s) used in the calibration		
Description:	Digital Nano volt / Micro Ohm meter	PT100
Manufacturer:	Agilent	---
Model:	34420A	---
Serial number:	MY42000734	(1 , 3)
Other identification:	ID : PHT-01- 17	ID : PHT-01-84 , 86
Calibration information		
Date of calibration:	10/08/2021 , Due to: 10/08/2022	
Place of calibration:	PH LAB. 1	
Method(s) of calibration:	Calibration method using - PROC-TC-012 (C)	
Calibrated quantity:	Temperature ° C	
Results of calibration:	Attached a complete result in Annex 1 of this certificate	
Measurement uncertainty:	The reported expanded uncertainty is based on UKAS M3003 Standard and the standard Uncertainty multiplied by coverage factor k=2 to give confidence level of 95%	
Metrological traceability:	The traceability of measurement results to the SI units is assured by the National standard maintained at Central Organization for standardization and Quality Control through calibration at : UME /CER. NO (G1KS-0127)	
Environmental conditions of calibration:	Temp. 37.51° C	RH. 23.5%
Observations, opinions or recommendations:	The results in Annex 1 should be taken into consideration	

Approved by:


 Eng.
Moyasser Ali Taher
 Head Of Physics Section
 12/08/2021

1 of 2

This certificate is issued in accordance with the laboratory accreditation requirements. It provides traceability of measurement to recognized national standards and to the units of measurement realized at the COSQC or other recognized national standards laboratories. This certificate may not be reproduced other than in full by photographic process. This certificate refers only to the particular item submitted for calibration.

Ref. Proc.Tc-012



Calibration Certificate
Central Organization for Standardization and Quality Control
Metrology Department - Physics Section (FOR-TC-012)
 P.O. Box13032 Aljadriya street, Baghdad , Tel:7785180 - - E-Mail : cosqc@cosqc.gov.iq

Certificate No.: PHT 677 / 2021
 Date of issue : 12/08/2021

Annex 1

Results

The results of the measurements are given on table below.

TC No.	Set. Value C°	Ref. (R) C°	UUC (M) C°	Error (M)-(R) C°	Uncertainty ± C°
TC 1	25	25.01	25.9	0.85	1.04
TC 2	35	34.98	35.7	0.74	0.95
TC 3	45	45.04	45.8	0.76	0.88
TC 4	55	55.01	55.80	0.79	0.92
TC 5	65	65.02	65.70	0.68	0.79
TC 6	75	23.02	23.40	0.38	0.45
TC 7	95	94.19	95.00	0.81	0.94

Calibrated by :
 Khalid Naser
 12/08/2021



Revised by:
 Hanaa Mohammed
 12/08/2021

Approved by:
 Moyasser Ali Taher
 12/08/2021

2 of 2

This certificate is issued in accordance with the laboratory accreditation requirements. It provides traceability of measurement to recognized national standards, and to the units of measurement realized at the COSQC or other recognized national standards laboratories. This certificate may not be reproduced other than in full by photographic process. This certificate refers only to the particular item submitted for calibration




REPUBLIC OF IRAQ MINISTRY OF SCIENCE & TECHNOLOGY RENEWABLE ENERGY DIRECTORATE	 <p>وزارة العلوم والتكنولوجيا Ministry Of Science & Technology</p>	جمهورية العراق وزارة العلوم والتكنولوجيا دائرة الطاقات المتجددة العدد: ط م ٢٠٩ التاريخ: ١٩ / ٤ / ٢٠٢١
<p>إلى/ جامعة كربلاء-كلية الهندسة م/ معايرة أجهزة قياس</p>		
<p>تحية طيبة</p> <p>إشارة إلى كتابكم المرقم بالعدد (د.ع/١١٤٦/٦ في ٢٠٢١/٤/١٥)، بخصوص إبداء المساعدة لطالب الدراسات العليا / الماجستير (محمد محسن جاسم)، تم إجراء المعايرة للأجهزة والمعدات المدرجة تفصيلها في أدناه في مختبراتنا بتاريخ ٢٠٢١/٤/١٩ وهي جاهزة للاستخدام. شاكرين تعاونكم معنا .. مع فائق التقدير</p>		
<p>الأجهزة التي تم معايرتها:</p> <p>١-جهاز قياس شدة الإشعاع الشمسي العدد / ١ ٢-جهاز قياس درجة الحرارة العدد / ١ ٣-جهاز قياس سرعة الرياح العدد / ١ ٤-متحسس درجة الحرارة T/C k طول ١ متر العدد / ١</p>		
		
<p>وزارة العلوم والتكنولوجيا دائرة الطاقات المتجددة</p>		
<p>وزارة العلوم والتكنولوجيا Ministry Of Science & Technology</p>		
<p>د. فلاح إبراهيم العطار ع/المدير العام ٢٠٢١/٤/١٩</p>		
<p>نسخة منه إلى/ مركز تخطيط وإدارة الطاقة مع الأوليات للتفضل بالإطلاع مع التقدير قسم التخطيط والمتابعة للتفضل بالإطلاع مع التقدير</p>		

Table (1) : Comparison between Standard solar Power meter and TES 132 Data Logging Solar power meter Accuracy: (± (10 %) under testing

No.	Time	Solar Power meter W/m ² Standard	TES 132 Solar Power meter W/m ² under testing
1	10:06	648	649
2	10:48	735	733
3	11:30	765	776
4	11:54	795	801
5	12:25	790	784



Appendix- C

Sample of Results

1. Different number of thermoelectric modules

Testing of the thermoelectric modules 24,26, 36, 46,60,70 and 80 items Performance numerically and by data reduction formulas to specify the TEG modules optimal number and distribution in additional to 50 . The obtained results are shown in the table (C.1) and figure (C.1).

Table C-1: The Photovoltaic surface temperature, the output power and the electrical efficiency of the Photovoltaic (PV), Thermoelectric modules and the (PV-TEG) hybrid system with different number of TEG models

Number of TEG modules	Tsc(K)	Ppv (w)	PTEG(w)	η_{pv}	η_{TEG}	P(PV-TEG)(w)	$\eta(PV-TEG)$
80	298.846	19.71347	0.1351	0.059836	4.74692E-06	19.71482	0.05984
70	300.6394	19.56821	0.2218	0.059395	7.97434E-06	19.57042	0.059403
60	300.9477	19.54323	0.2082	0.059319	7.51422E-06	19.54532	0.059327
50		18.5	3	0.0562	0.00409	21.5	0.06
46	302.83	19.39077	0.2578	0.058856	9.53674E-06	19.39335	0.058866
36	306.82	19.06758	0.4254	0.057875	1.66233E-05	19.07183	0.057892
26	307.25	19.03275	0.3282	0.05777	1.29043E-05	19.03603	0.057782
24	305.245	19.19516	0.2182	0.058262	8.33888E-06	19.19734	0.058271

Appendix-C

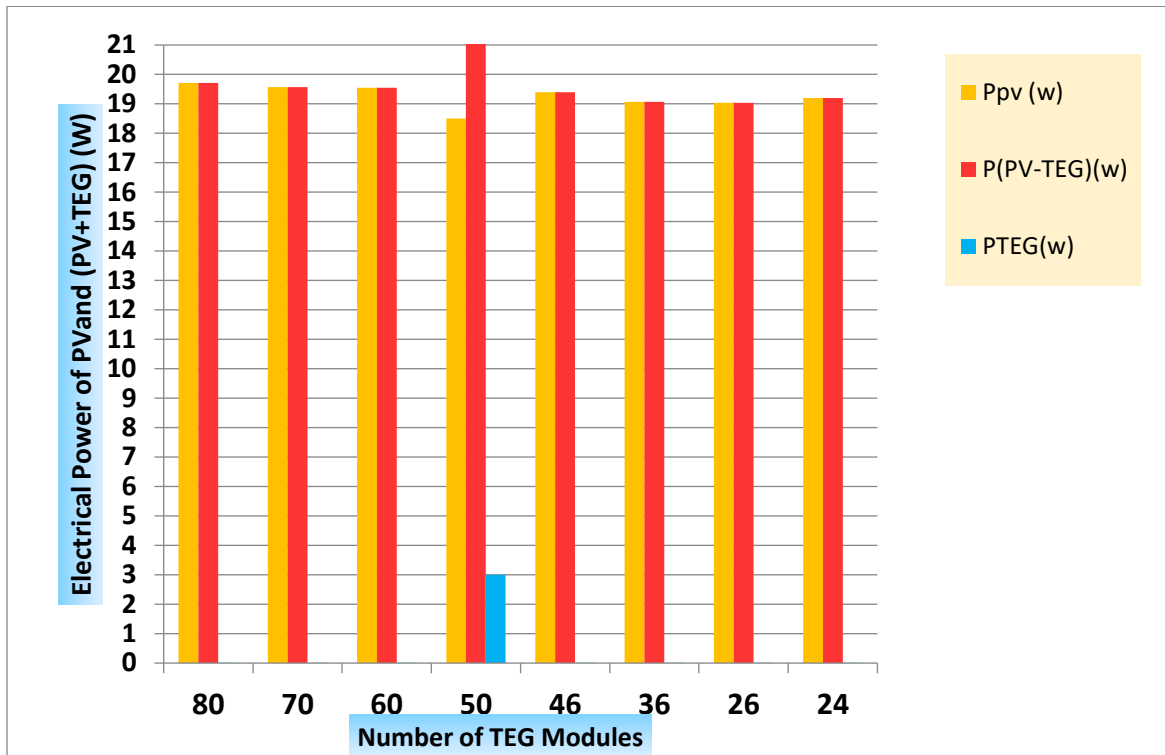


Figure C-1: Relationship between the Electrical Power of PV ,TEG and PV-TEG Hybrid system with Different Number of TEG Modules

Appendix-C

2. Data reduction calculations

Table C-2: The Photovoltaic surface temperature, the output power and the electrical efficiency of the Photovoltaic (PV), Thermoelectric modules, and the all models of (PV -TEG) hybrid system, at 1000 (W/m^2) and other different value of solar radiation as the results of Data Reduction

G(W/m^2)	Tsc(C)	Tcold	Thot	T (C)	T mean	1-(tc/th)	Z	S	ss	Tc/Th	η TEG %	P TEG	η PV%	P PV(W)	η el %	Pel (W)
S1	304.24	293.73	295.98	2.25	294.855	0.0076	0.00228	1.67227	1.2931	0.9924	0.00097	0.23	5.85	19.27	5.95	19.5
S2	308.18	293.864	298.884	5.02	296.374	0.0168	0.00228	1.67573	1.2945	0.9832	0.00217	0.52	5.75	18.95	5.967	19.47
S3	306.767	293.89	298.18	4.29	296.035	0.01439	0.00228	1.67496	1.2942	0.98561	0.00186	0.35	5.78	19.07	5.966	19.42
S4	313.409	294.141	303.613	9.472	298.877	0.0312	0.00228	1.68144	1.2968	0.9688	0.00409	3	5.62	18.5	6	19.62
1250	324	295	312.7	17.7	303.85	0.0566	0.00228	1.69278	1.2968	0.9434	0.0075	3.7	5.88	25	6.6	28.7
1500	331	295.3	321.5	26.2	308.4	0.08149	0.00228	1.70315	1.2968	0.91851	0.01092	4.8	5.7	26.7	6.5	32
1750	337	295.4	326	30.6	310.7	0.09387	0.00228	1.7084	1.2968	0.90613	0.01265	5.9	5.5	30.6	6.4	36
2000	345	295.6	333	37.4	314.3	0.11231	0.00228	1.7166	1.2968	0.88769	0.01526	6.4	5.4	32.4	6.3	39.4

Appendix- D
Uncertainty Calculation

1. Flow meter

The total uncertainty of the cooling water flow rate equal to the uncertainties of the curve fitting and can be calculated by the Root Square Sum equation:

$$U_{F,ov} = \pm\sqrt{(U_{F,c-f})^2}$$

where $U_{F,ov}$ is the overall uncertainty in the flow rate measurement and $U_{F,c-f}$ is curve fitting uncertainty. The statistical calculation of the curve fitting uncertainty is shown in Table (E-1)

Table D-1: Uncertainty in flow rate measurement

Data point	Flow meter reading (L/min)	Measured flow rate (L/min)	Curve fitting equation Y=0.993X+0.27	Deviation squared =(flow rate reading- Y)
1	1	1.2	1.26	0.26
2	2	2.3	2.25	0.25
3	3	3.25	3.24	0.24
4	4	4.3	4.25	0.25
5	5	5.2	5.22	0.22
6	6	6.26	6.21	0.21

Appendix-D

7	7	7.18	7.2	0.18
Sum = 1.61				
Degree of freedom (n-1) = 6				
Standard deviation = $\sqrt{\frac{\sum \text{Deviation squar}}{n-1}} = 0.432$				
$U_{F,c-f} = \pm 0.432 \text{ L/min} = U_{F,ov}$				

To calculate the Repeatability of the experimental results, the following parameter is concerned:

1) The mean value of the variable x calculated as: - $x^{mean} = x_{average} = \frac{\sum^n x_i}{n}$

2) The standard deviation of x , given by: $\sigma = \sqrt{\frac{\sum^n (x_i - \bar{x})^2}{n - 1}}$

2. Output power

While the variable such as output power of photovoltaic in the S4 model hybrid system which are measured at different values of light intensity (G) from 1250 to 2000(W/m^2), their Repeatability are calculated at as shown in the table (D-2) where the value of x_2 is the adopted value in this study.

Table D-2: Standard deviation of power Calculations

G(W/m^2) No.	1250	1500	1750	2000
Reading (1)	26.3	29.7	33.6	37.4
Reading (2)	25.6	29	32.8	36.5
Reading (3)	26	28.7	33.8	37
Standard deviation (σ)	0.286	0.418	0.432	0.368

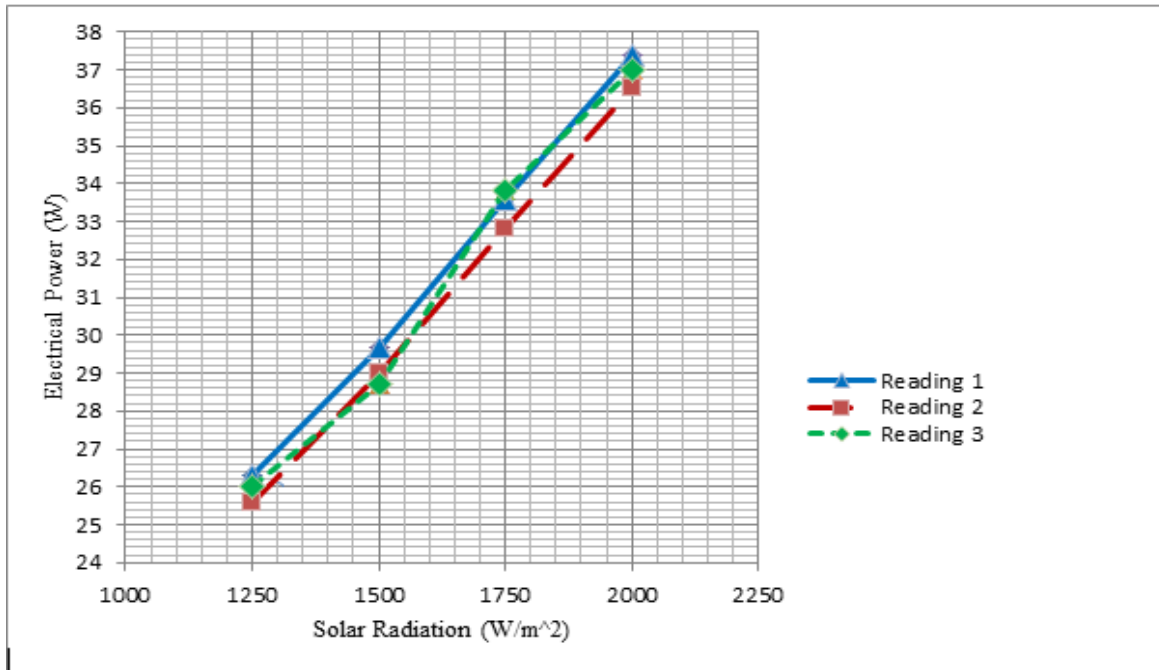


Figure D-1: Repeatability of the output power of the S4 hybrid system reading for light intensity range from 1250 (W/m^2) to 2000 (W/m^2)

Appendix- E

Published Research

4th International Conference on Engineering Sciences (ICES 2020) IOP Publishing
 IOP Conf. Series: Materials Science and Engineering 1067 (2021) 012115 doi:10.1088/1757-899X/1067/1/012115

A Review of Solar Energy Harvesting Utilising a Photovoltaic–Thermoelectric Integrated Hybrid System

M W Aljibury¹, H T Hashim² and W N Abbas¹

¹Mechanical Engineering department, College of Engineering, Kerbala University, Kerbala, Iraq.

²Biomedical Engineering department, College of Engineering, Kerbala University, Kerbala, Iraq.

E-mail: hashim2025@uokerbala.edu.iq

Abstract. Solar energy has the potential to be converted from light to electricity; however, solar cells can only utilise the short-wavelength portion of the solar spectrum to do this directly. In contrast, long-wavelength portions of the spectrum can be converted to heat inside solar cells, and such heat can be harvested and converted into electricity by means of a thermoelectric generator (TEG). The integration of photovoltaic and thermoelectric hybrid systems has thus attracted a great deal of attention due to these offering the ability to utilise solar energy across the full spectrum, including light and heat. This paper reviews the possibility of integrating photovoltaic (PV) and thermoelectric generators (TEG) in a PV-TEG hybrid system based on examining recent efforts in the field of PV-TEG creation. It also examines the efficiency improvement in PV-TEGs and their applications in recent years, offering a valuable guide for researchers and designers.

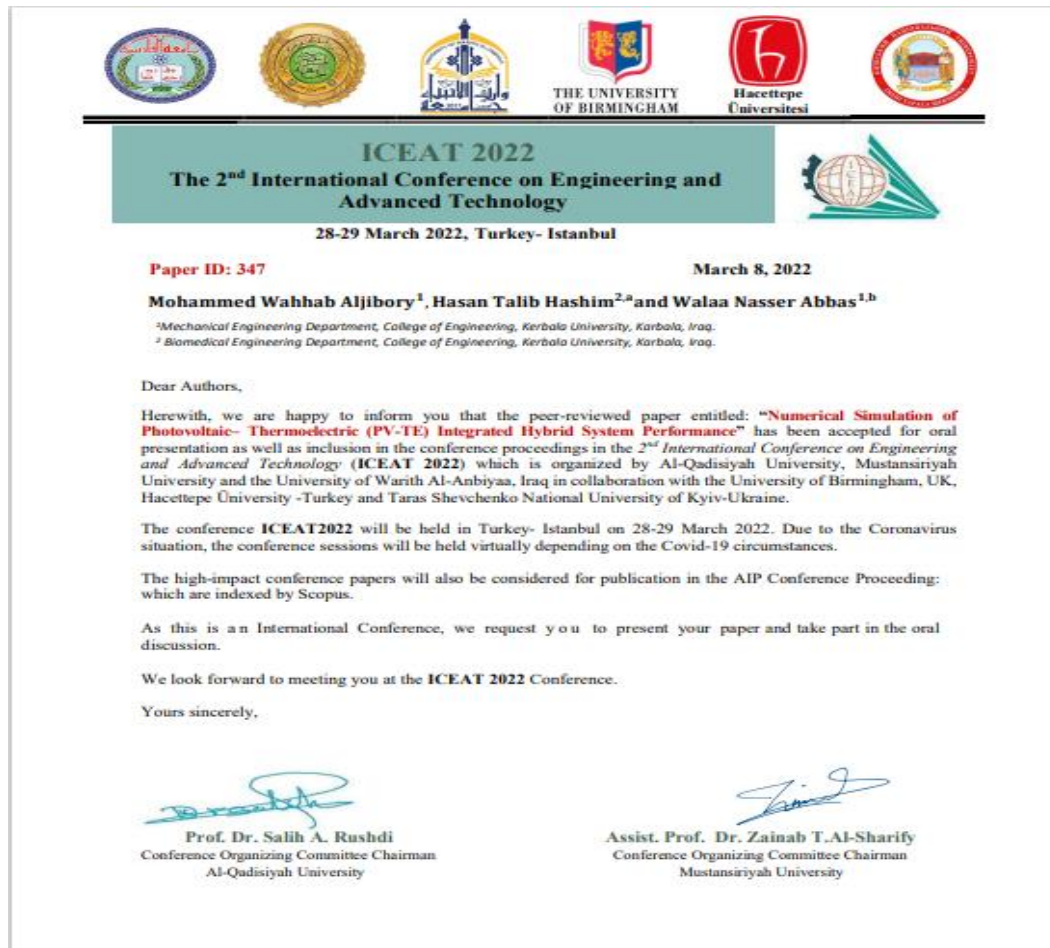
Keywords: Solar energy, Solar cell, Thermoelectric, Solar system harvesting

I. Introduction

Renewable energy is currently attracting a great deal of attention due to climate change and pollution issues which require the immediate limitation of fossil fuel use; sources of energy that are competitive with these traditional sources of electricity are thus in great demand. Most renewable energy originates from the sun, which is the dominant source of thermal energy [1]. The sun offers a continuous source of about 1.2×10^3 terawatts, which is much more than the power consumed globally [2]; however, this solar energy must then be converted into useful forms such as electrical energy or thermal energy.

Photovoltaic devices convert a portion of solar energy into electrical energy, with the rest being transformed into heat inside the photovoltaic cell, reducing the performance of the device; removing heat from photovoltaic cells is thus a crucial issue. A device made from n-type and p-type semiconductors, known as a thermoelectric generator (TEG), can be used to convert the heat to electricity by applying a temperature difference across the cell [3]. TEGs are characterised by being maintenance free, without chemical reactions, having long lifetimes, being reliable, having no emissions or moving parts, and being environmentally friend. TEG use can also reduce the heat in PVs if both are integrated in a hybrid system. Examining the combination of PVs and TEGs to reduce the temperature of photovoltaic cells to thus enhance

 Content from this work may be used under the terms of the [Creative Commons Attribution 3.0 license](https://creativecommons.org/licenses/by/3.0/). Any further distribution of this work must maintain attribution to the author(s) and the title of the work, journal citation and DOI.
 Published under Science by IOP Publishing Ltd





الخلاصة

نظرًا لأن PV و TEG لهما علاقة متعارضة تمامًا مع درجة الحرارة ، فإن دمج المولدين يحتاج إلى دراسة متأنية. تعتمد كفاءة تحويل TEG على الوصول إلى فرق درجات حرارة عالية ، بينما تحتاج الكهروضوئية إلى درجة حرارة منخفضة لإنتاج كفاءة عالية. لذا ، فإن التكامل الصحيح والفعال للخلايا الكهروضوئية مع الوحدات الكهروحرارية هو القضية الرئيسية لتحسين أداء النظام الهجين وزيادة إنتاج الطاقة الكهربائية. طرق تحقيق ذلك: تشمل اعتماد نظام تبريد حراري فعال لضمان الحصول على أقصى درجة حرارة واكتشاف العدد الأمثل والتوزيع المناسب لوحدات TEG التي ستغطي السطح الخلفي للنموذج الكهروضوئي

اشتملت الدراسة الحالية على محاكاة عددية ودراسة تجريبية لفحص أداء نظام هجين (PV-TEG). أولاً ، أجرت الدراسة الحالية دراسة عددية وتحليلية لنماذج النظام الهجين المختلفة بأرقام وتوزيعات مختلفة للعناصر الكهروحرارية عند الإشعاع الشمسي 1000 (واط / م²) ، ودرجة الحرارة المحيطة 28 درجة مئوية ، وسرعة الرياح صفر (م / ث) كظروف تشغيلية. كانت نماذج النظام الهجين الرئيسية أربعة نماذج: S1 نموذج (PV و 204 عنصر من TEG) ، S2 نموذج (PV و 94 عنصر من TEG) ، S3 نموذج (PV و 85 عنصر من TEG) ، و S4 نموذج (PV و 50 عنصر من TEG). وقد أظهرت النتائج أن النظام الهجين S4 كان الأمثل في التوزيع وعدد وحدات TEG. لإظهار درجة موثوقية البرنامج المستخدم في العمل الحالي ودقة النتائج العددية لهذه الرسالة ، تم التحقق من النتائج التحليلية لأداء نظام PV / T. بمقارنة هذه النتائج بنتائج دراسة سابقة في نفس المجال وتحت نفس الظروف تقريبًا ، فإن أقصى فرق لا يزيد عن 4 ٪ وأصغر فرق هو 0,4 ٪ بين النتائج. لذلك ، تم التوصل إلى أن البرنامج قد تم إنشاؤه بشكل صحيح وأعطى نتائج مقبولة إلى حد كبير.

ثانياً ، تم فحص الأداء الأمثل للنظام الهجين للنموذج (S4) في دراسة تجريبية داخلية. تم بعد ذلك وضع أداء النظام الكهروضوئي ونظام PV / T تجريبياً وعددياً للمقارنة مع أداء النظام الهجين طراز S4. وفقاً للنتائج ، أظهرت أن طاقة المتولدة الكهربائية لنموذج (S4) PV-TEG كانت أعلى في ظل ظروف تشغيل متطابقة من تلك اللوحة الكهروضوئية ونظام PV / T ، على التوالي ، بنسبة (36,94 ٪) و (16,8 ٪) عددياً و (31,66 ٪) و (16,5 ٪) تجريبياً. أيضاً ، يمكن ملاحظة أن متوسط السطح الأمامي للوحدة الكهروضوئية في النظام الهجين (S4) PV-TEG كان أعلى بنسبة

(٤,٥ ٪) و (٥,٧ ٪) من نظام PV / T وأقل بنسبة (٢٩ ٪) و (٣٠ ٪) من تلك في اللوح الكهروضوئية ، عددياً وتجريبياً ، على التوالي. بالإضافة إلى الكفاءة الكهربائية (η_{el}) للنظام الهجين PV-TEG كانت حوالي (٦,٢ و ٥,٨٣)٪ في الاختبارات العددية والتجريبية على التوالي وأعلى من تلك الخاصة بالوحدة الكهروضوئية ونظام PV / T.

تمت دراسة تأثير الإشعاع الشمسي على أداء النظام الهجين عند درجة حرارة محيطية ثابتة. أظهرت النتائج زيادة الطاقة الناتجة للنظام الهجين مع زيادة الإشعاع الشمسي. كانت أقصى طاقة تم الحصول عليها للنظام الهجين (٣٩,٤ واط) عند الإشعاع الشمسي ٢٠٠٠ (واط / متر مربع).

وأخيراً تم إجراء مقارنة بين النتائج التجريبية والعددية للدراسة الحالية ولوحظ اتفاق جيد بينهما. أظهرت النتائج أن نسبة الاختلاف في متوسط درجة حرارة السطح الأمامي للوحدة الكهروضوئية (Tsc) في اللوحة الكهروضوئية ، ونظام PV / T ، والنظام الهجين PV -TEG بين النتائج العددية والتجريبية كانت (٢,٩ ، ٤,٥ ، و ٣,٥)٪ على التوالي. في الوقت نفسه ، كانت نسبة الفرق في طاقة المتولدة الكهربائية (E_{el}) بين النتائج العددية والتجريبية في اللوحة الكهروضوئية ، ونظام PV / T ، والنظام الهجين PV -TEG هي (٢,٢ ، ٦,٣ ، و ٦) ٪ على التوالي. تشير نتيجة المقارنة هذه إلى أن العمل الحالي تم وفقاً لما تم التخطيط له وبطريقة تضمن تجنب الأخطاء قدر الإمكان. تسلط النتائج الضوء على أن دمج وحدات TEG مع اللوحة الكهروضوئية كنظام هجين من طراز S4 كان الحل الأفضل لحصاد الإشعاع الشمسي وتحويل الحرارة المهدرة في اللوح الكهروضوئية إلى طاقة كهربائية إضافية.



جمهورية العراق
وزارة التعليم العالي و البحث العلمي
جامعة كربلاء
كلية الهندسة
قسم الهندسة الميكانيكية

حصاد الطاقة الشمسية باستخدام نظام هجين متكامل (كهروضوئي- كهروحراري)

رسالة مقدمة الى مجلس كلية الهندسة / جامعة كربلاء وهي جزء من متطلبات نيل درجة الماجستير في
علوم الهندسة الميكانيكية

من قبل:

ولاء ناصر عباس

باشراف :

أ. م. د. حسن طالب هاشم

أ. م. د. محمد وهاب كاظم